y 3. At 7:
36/13-2

1970
Quarterly
Technical
Progress
Review
Volume 13—2

A publication of the
Division of Technical Information
U.S. Atomic Energy Commission
Prepared in Cooperation
with
The American Nuclear Society.

REACTOR TECHNOLOGY

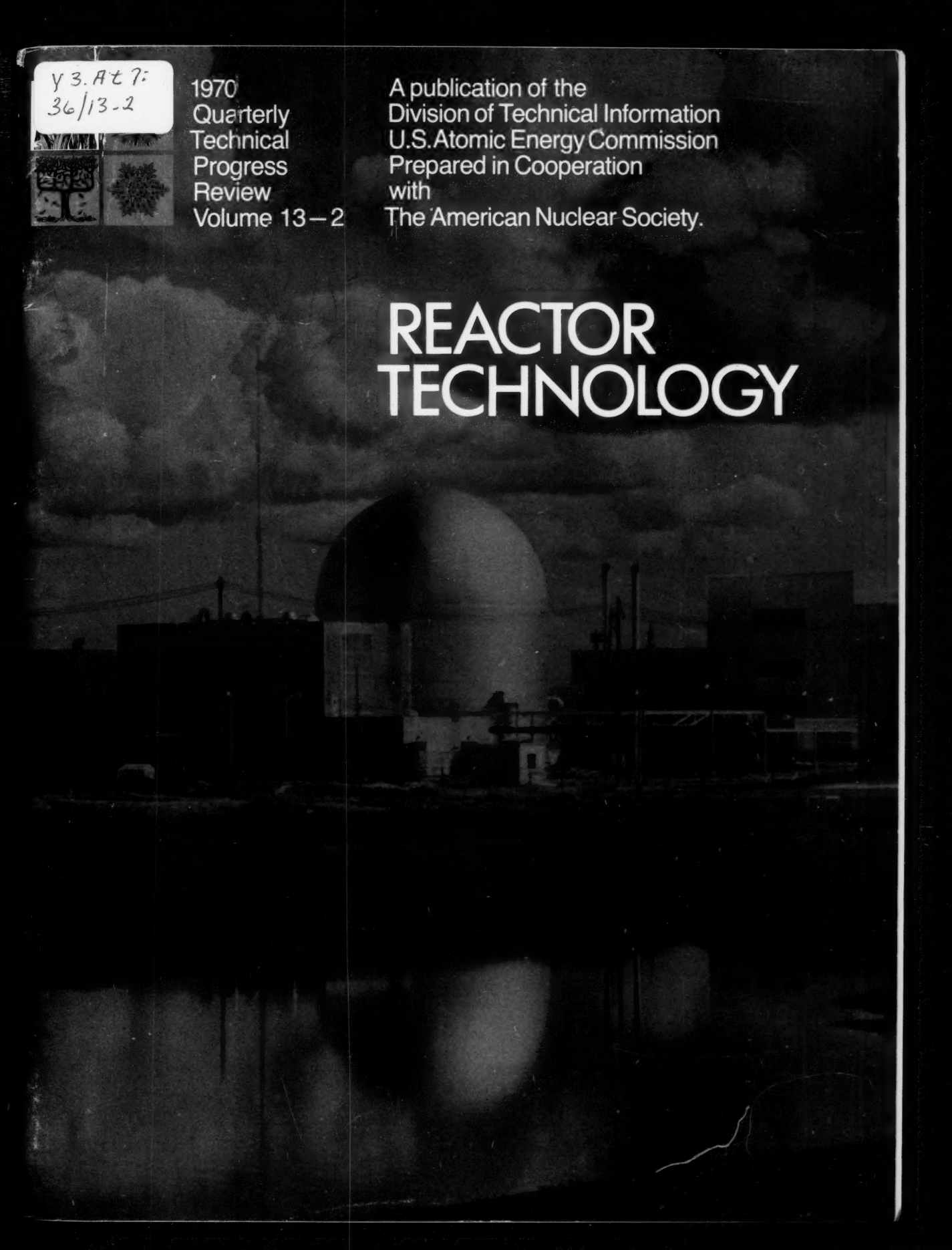

TECHNICAL PROGRESS REVIEWS

The United States Atomic Energy Commission publishes the Technical Progress Reviews to meet the needs of industry and government for concise summaries of current nuclear developments. Each journal digests and evaluates the latest findings in a specific area of nuclear technology and science. *Nuclear Safety* is a bimonthly journal; the other two are quarterly journals.

Isotopes and Radiation Technology
P. S. Baker, A. F. Rupp, and associates
Isotopes Information Center, Oak Ridge National Laboratory

Nuclear Safety
Wm. B. Cottrell, W. H. Jordan, J. P. Blakely, and associates
Nuclear Safety Information Center, Oak Ridge National Laboratory

Reactor Technology
Prepared in cooperation with the American Nuclear Society

All are available from the U. S. Government Printing Office. See the back cover for ordering instructions.

NOTICE

This journal was prepared under the sponsorship of the U. S. Atomic Energy Commission. Neither the United States nor the U. S. Atomic Energy Commission, or any of their employees, contractors, subcontractors, or their employees, makes any warranty, express or implied, or assumes any legal liability or responsibility for the accuracy, completeness, or usefulness of any information, apparatus, product, or process disclosed, or represents that its use would not infringe privately owned rights.

Availability of Reports Cited in This Review

United States Atomic Energy Commission (USAEC) reports are available at certain libraries that maintain collections of these reports. They are also sold by the following governmental and international organizations: (1) Clearinghouse for Federal Scientific and Technical Information (CFSTI), U. S. Department of Commerce, Springfield, Va. 22151 ($3.00 for printed copy and $0.65 for microfiche); (2) International Atomic Energy Agency (IAEA), Vienna, Austria; and (3) National Lending Library, Boston Spa, England.

Other U. S. Government agency reports identified in this journal are generally available from CFSTI.

Reports from other countries are available at some libraries in the United States and from IAEA and the originating country. **United Kingdom Atomic Energy Authority (UKAEA)** reports are sold by Her Majesty's Stationery Office, London. **Atomic Energy of Canada Limited (AECL)** reports are sold by the Scientific Document Distribution Office, Atomic Energy of Canada Limited, Chalk River, Ontario, Canada. UKAEA and AECL reports issued after March 1, 1967, are sold by CFSTI to purchasers in the United States and its territories.

Private-organization reports should be requested from the originator.

The views expressed in this publication do not necessarily represent those of the United States Atomic Energy Commission, its divisions or offices, or of any Commission advisory committee or contractor.

Y 3. At 7:
36/13-2

REACTOR TECHNOLOGY

Vol. 13, No. 2 Spring 1970

Contents

REVIEW ARTICLES

CONTAINMENT ELECTRICAL PENETRATIONS IN THE SAN ONOFRE AND PRAIRIE ISLAND PLANTS
Fred Verber, Argonne National Laboratory 97

RECENT ADVANCES IN THE TECHNOLOGY OF PRESTRESSED-CONCRETE REACTOR PRESSURE VESSELS
Chen Pang Tan, Franklin Institute Research Laboratories 109

AMERICAN NUCLEAR SOCIETY—CRITICAL REVIEWS

INTRODUCTION 123

SOLUBILITIES OF METALLIC ELEMENTS IN LIQUID SODIUM
T. D. Claar, Argonne National Laboratory 124

DEVELOPMENT POTENTIAL OF ZIRCONIUM ALLOYS FOR HIGH-TEMPERATURE APPLICATIONS
C. D. Williams, Atomic Energy of Canada Limited, Chalk River Nuclear Laboratories 147

CURRENT AWARENESS REVIEWS

SODIUM-COOLED REACTORS: EBR-II PHYSICS ASPECTS
Myrna L. Steele, USAEC Division of Technical Information Extension 170

SODIUM-COOLED REACTORS: CURRENT STATUS
Myrna L. Steele, USAEC Division of Technical Information Extension 186

COVER:
Experimental Breeder Reactor II at Argonne National Laboratory's Idaho Division

ILLINOIS STATE LIBRARY
AUG 20 1970
U. S. Dept. of Documents Deposit

Superintendent of Documents, U. S. Government Printing Office, Washington, D. C. 20402, $3.00 per year.

REACTOR TECHNOLOGY

is a quarterly review of progress and developments in the reactor field including the following subject areas:

Economics	Fuel Cycles
Physics	Fluid and Thermal Technology
Mechanics	Fuel Processing
Construction	Components
Fuel Elements	Operating Performance

Prepared for reactor physicists, reactor operators, designers, fuel-cycle specialists, administrators, and others interested in the field, this journal reviews, summarizes, critically evaluates, and interprets the state of the art as reflected in the current literature.

The many reports and publications referenced merit further study, and readers are urged to consult them for additional details.

Qualified authors are invited to contribute review articles for consideration for publication.

U. S. Atomic Energy Commission
Division of Technical Information
Washington, D. C. 20545

Issued quarterly by the U. S. Atomic Energy Commission. Use of funds for printing this publication approved by the Director of the Bureau of the Budget on May 12, 1969.

Containment Electrical Penetrations in the San Onotre and Prairie Island Plants

By Fred Verber*

As is often the case for other kinds of components, the design of gastight electrical penetrations of containment vessels for new nuclear power plants is usually predicated on the best-performing features of previous designs. Even so, it is not unusual for difficulties to arise during construction, startup, or operation of a station, even though components were thought to embody all possible design advantages and virtually no disadvantages. Obviously, knowledge of such experience can prove valuable to engineers designing components or systems for new stations, and it could prevent needs for major revisions in the field. Some information of this nature was included in previous descriptions of experience with electrical penetrations of reactor containment buildings.[1,2]

This article deals with (1) the electrical penetrations for the San Onofre Nuclear Generating Station Unit 1, including a number of problems that developed during installation of the electrical-penetration system and startup and operation of the station, and (2) the design of electrical penetrations for the Prairie Island Nuclear Generating Plant Units 1 and 2.

PENETRATIONS AT SAN ONOFRE

The containment vessel for the San Onofre Nuclear Generating Station (Unit 1) consists of a steel sphere designed for an internal pressure of 46.4 psig. The sphere houses the reactor, steam generator, and various auxiliaries.

*Reactor Engineering Division, Argonne National Laboratory, Argonne, Ill. 60439.

The electrical cables enter the containment vessel through 33 penetration assemblies;[3] they are arranged in groups on the sphere as shown in Fig. 1. The numbers and types of conductors penetrating the containment vessel are listed in Table 1; note that, of a total of 2885 conductors, 816 are available for future circuits or for replacement of existing circuits, if needed.

Although the electrical penetrations for the San Onofre station have performed generally in accordance with the design, several problems developed during the installation of the penetration canisters and during station startup.[3,4]

For Instrument Cables

Eight penetration assemblies (Fig. 1) were installed to accommodate the instrumentation circuits, consisting of shielded twisted pairs and quads, twisted Chromel–Alumel and copper–constantan thermocouple conductors, and coaxial and triaxial conductors.

The design concept for the canisters provides double seals that form a pressure chamber for leak tests. The pin-and-socket arrangement is similar to that of commercially available hermetically sealed pressure connectors; the contacts are crimped, soldered, or welded to wires, and assembled into the plug, which then is inserted into the socket. The socket serves as the end of the penetration assembly.

For Twisted Shielded Pairs and Quads

Figure 2 shows the type of penetration assembly used for twisted shielded pairs and quads. The plug

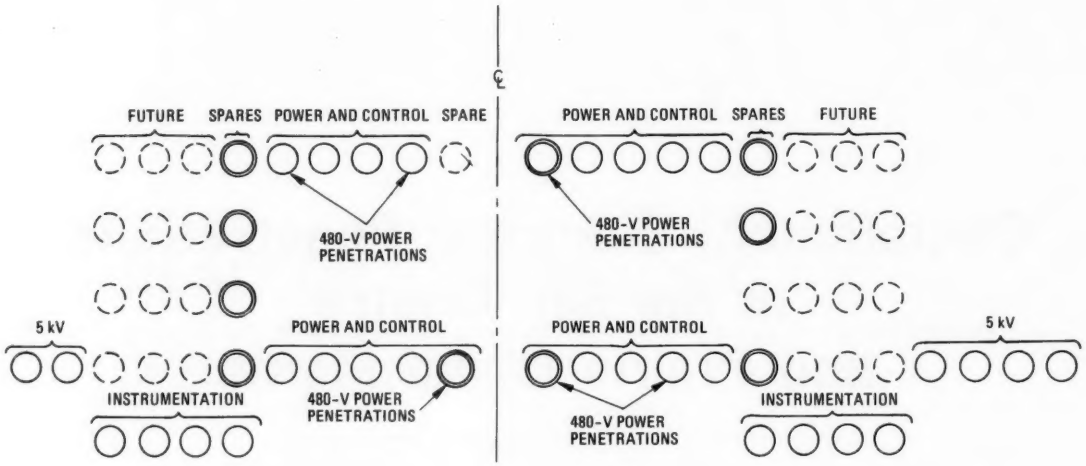

Fig. 1 Arrangement of electrical penetrations on San Onofre containment sphere (outside elevation).[3]

Table 1 Conductors Penetrating the San Onofre Reactor Containment Vessel[3]

Function and cable	Total no. of conductors available	No. of spare conductors
Instrumentation		
Coaxial (40)	80	20
Triaxial (10)	30	3
Copper–constantan thermocouple (60)	120	36
Chromel–Alumel thermocouple (60)	120	22
Shielded and twisted 2/c (160)	320	144
Shielded and twisted 4/c (40)	160	52
125-V d-c and 120-V a-c power and control		
1/c #12 AWG	1400	469
1/c #4 AWG	244	64
1/c #2 AWG	110	6
480-V power and control		
#8 AWG	108	0
#4 AWG	144	0
#2 AWG	13	0
#1/0 AWG	12	0
#4/0 AWG	6	0
5-kV power		
#3/c 500 MCM (6)	18	0
	2885	816

contains 340 contacts that are indexed to the socket with three sets of keys and grooves and are seated in the socket with a screw-on follower ring.

The plug and socket can be mated even with as much as 20 mils' misalignment of the pin contacts in the socket with the female contacts in the plug. Because misalignment exceeded 20 mils on approximately 5% of the contacts, the female contact was ejected when mating was attempted. After a special tool was used for straightening and checking the alignment of the pins, the mating occurred satisfactorily.[3,4]

For Thermocouple Cables

Figure 3 shows the type of penetration assembly used for thermocouple cables. Figure 4 shows a cutaway view of two typical "snap-seal" designs used generally for thermocouple conductors, as well as for instrumentation, low-voltage power, and control conductors. As shown, the pin contact is sealed hermetically into the header plate with a compression-type glass-to-metal seal. A glass-filled thermoplastic insulator (Fig. 4) shrouds the pin contact and receives the silicone-rubber boot on the cable. In terminating a wire the rubber boot is slid onto the wire, insulation is removed from the end of the wire, and the wire is welded to the socket contact. Then the rubber boot is moved over the socket contact. When the pin and socket contacts are mated, the rubber boot locks the mating contacts together and seals the connection from moisture and dust.

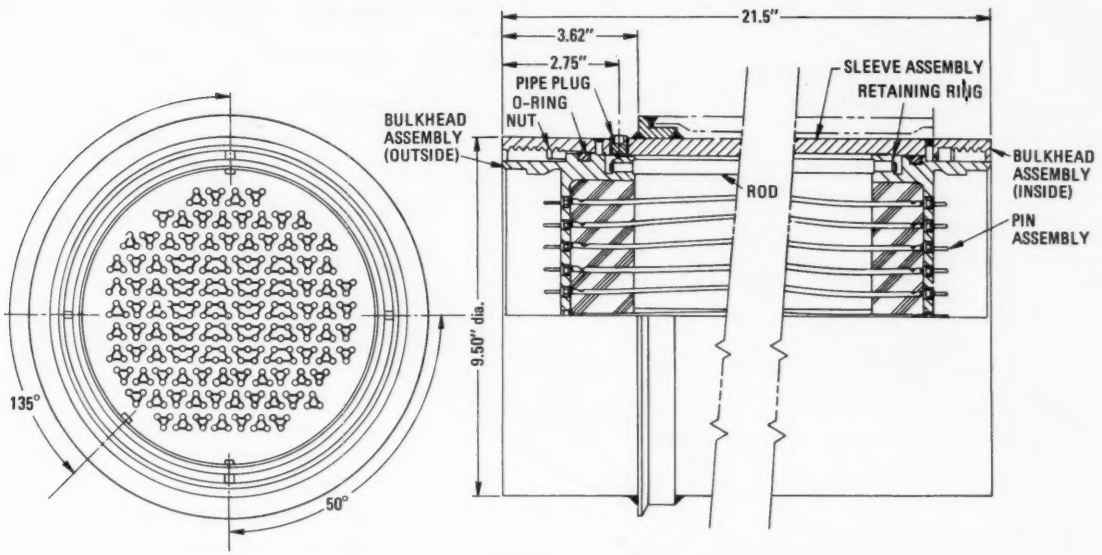

Fig. 2 Penetration assembly for twisted pair and quad instrument cables at San Onofre.[3]

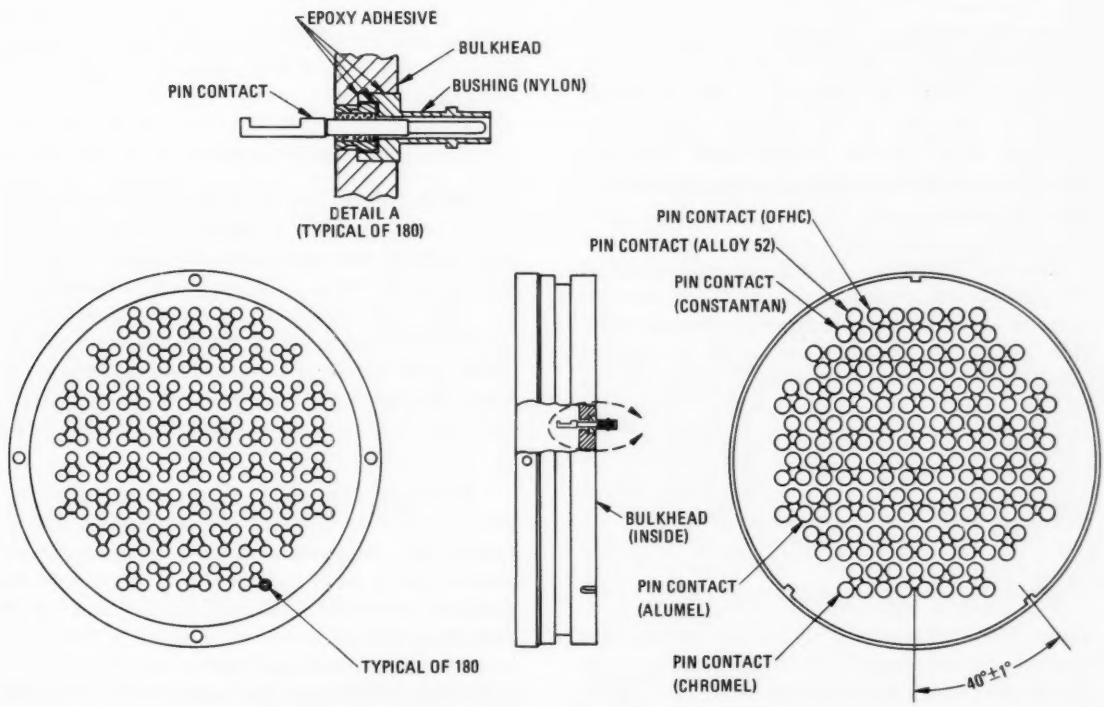

Fig. 3 Penetration assembly for thermocouple cables at San Onofre.[3]

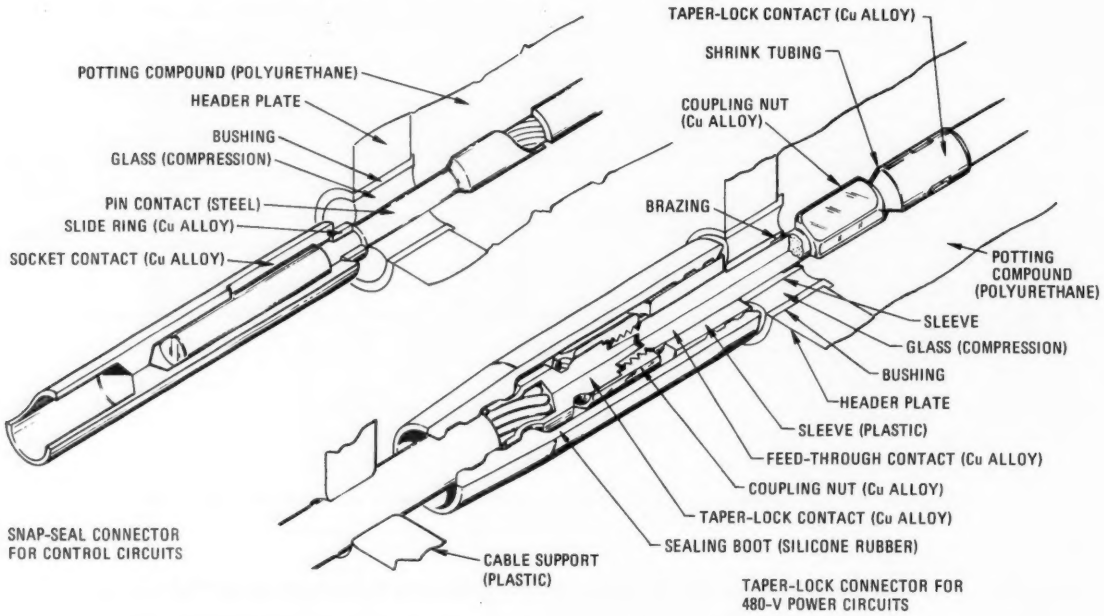

Fig. 4 Typical "snap-seal" connector for control circuits and "taper-lock" connector for 480-V power circuits in San Onofre electrical penetrations.[3]

Each thermocouple conductor through a penetration assembly has 6 connections, for a total of 12 connections in each thermocouple circuit. The female contact is crimped to the external cable and is connected to the pin by a slip-on joint. Inside the assembly the cable is soldered to the hermetically sealed pin.[3,4]

Parasitic Voltages. During the calibration of Chromel–Alumel thermocouples, a ±12°F variation from the reference temperature was observed over a 24-hr period. The variation was caused by parasitic voltages generated at the connections because of the difference between the containment and outside temperatures. However, the largest parasitic voltage was the result of mismatch of the cable and contact material caused by improper annealing of the contacts after machining. The manufacturer erroneously annealed the contacts at 1000°F instead of at the required 1600°F.

The problem was solved by replacing the penetration assemblies with properly matched and annealed Chromel–Alumel material and by spot-welding joints instead of crimping and soldering them. The replacement thermocouple material was so well matched that the parasitic voltage generated across 12 connections was less than 0.1 μV/°F in a test where the temperature difference was 100°F across the length of the penetration assembly.

For Coaxial and Triaxial Cables

Figure 5 shows the penetration assembly used for coaxial and triaxial cables. Figure 6 is a side view of the plug assembly that mates with an end of the penetration assembly shown in Fig. 5. The plug assembly for the coaxial and triaxial cables is similar to that used for twisted and shielded cables. A retaining ring holds the coaxial and triaxial female connector assemblies in place. The seal for the coaxial cables consists of two concentric glass bushings; the triaxial cables are sealed by three concentric glass bushings.[3,4]

Alignment Problem. An alignment difficulty, similar to that encountered with the penetrations for twisted pairs and quads, occurred with the coaxial- and triaxial-cable penetrations. However, because of the elasticity of the shield material, the alignment of the coaxial contacts could not be corrected in the manner used for the twisted pairs and quads. Therefore the plugs were modified so that each coaxial and triaxial connector could be plugged separately into the socket through the rear of the plug.[3,4]

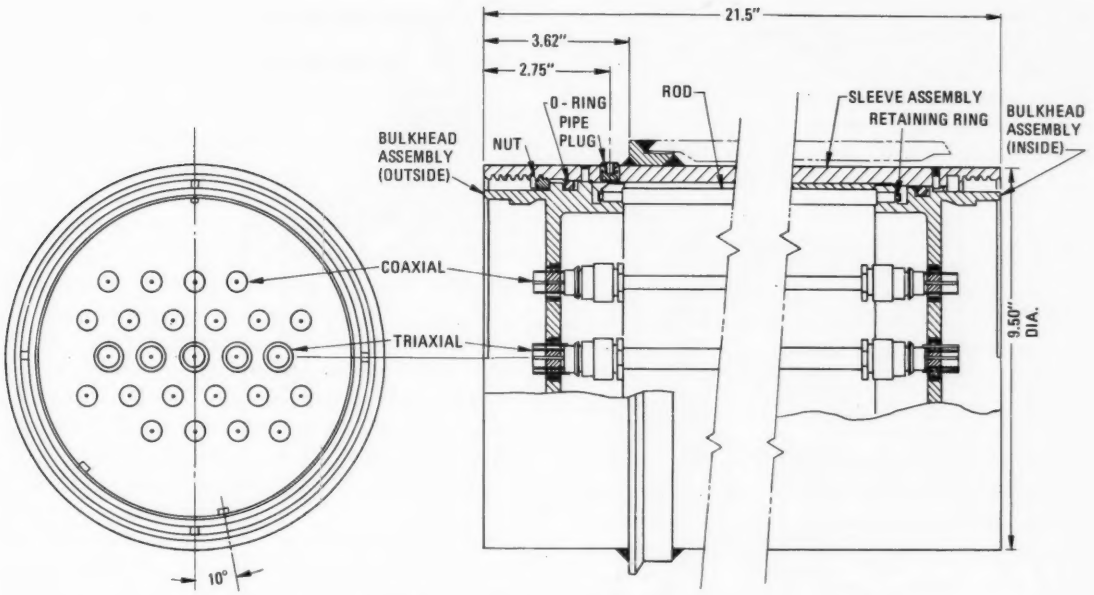

Fig. 5 One of two penetration assemblies for coaxial and triaxial cables at San Onofre.[3]

Insulation Curing Caused Grounding of Shields. Electrical-grade polyurethane potting material inside the ends of the penetration assemblies insulates and supports the connections between the cables and the hermetically sealed pins. The polyurethane had been oven-cured for 7 hr. However, before the circuit connections at the containment vessel were completed, tests of electrical continuity revealed that all the shields were grounded. Investigation disclosed that the polyurethane had continued to cure, and that the associated shrinkage of the polyurethane had moved the internal cable shield contacts of the penetration assembly against the header plate of the penetration assembly. This condition was remedied by enclosing the shield contacts in a nylon sleeve; the sleeve isolates the contacts from the polyurethane and prevents the contacts from spreading.[4]

For Low-Voltage Power and Control Cables

A total of 19 penetration assemblies (Fig. 1) were installed to accommodate low-voltage power and control circuits.[3] These have single conductors ranging in size from No. 12 AWG to No. 4/0 AWG. The penetration design eliminated the use of the large plug and allowed each conductor socket contact to plug directly onto the pins of the penetration assembly.[1,4] Thirteen of the penetration assemblies are used for 125-V-dc and 120-V-ac circuits. As shown in Fig. 4, the pins in these are steel and have "snap-seal" connectors.

The other six penetration assemblies are used for 480-V circuits. As shown in Fig. 4, the pins in these are copper and have "taper-lock" connectors.[3]

For 5-kV Power Cables

Six penetration assemblies for 5-kV power cables (Fig. 1) were installed in the containment vessel. Through-type, 15-kV class, 600-A bushings are used on both ends of the penetration assembly.[1,4]

Welding Distorted Nozzles

The operation of welding nozzles into the containment sphere distorted nearly every nozzle. This made it necessary to machine and fit each penetration assembly or canister weld ring to its respective nozzle before a cold weld could be made to join the ring to the nozzle. After that was done, all installed penetration assemblies were tested by being pressurized to 46 psig with dry helium; they showed leakage of $<1 \times 10^{-6}$ cm^3/sec when checked with a mass-spectrometer leak detector.[4]

Tieup of Equipment

During tests of equipment before startup, it became evident that the use of multiconductor cables and

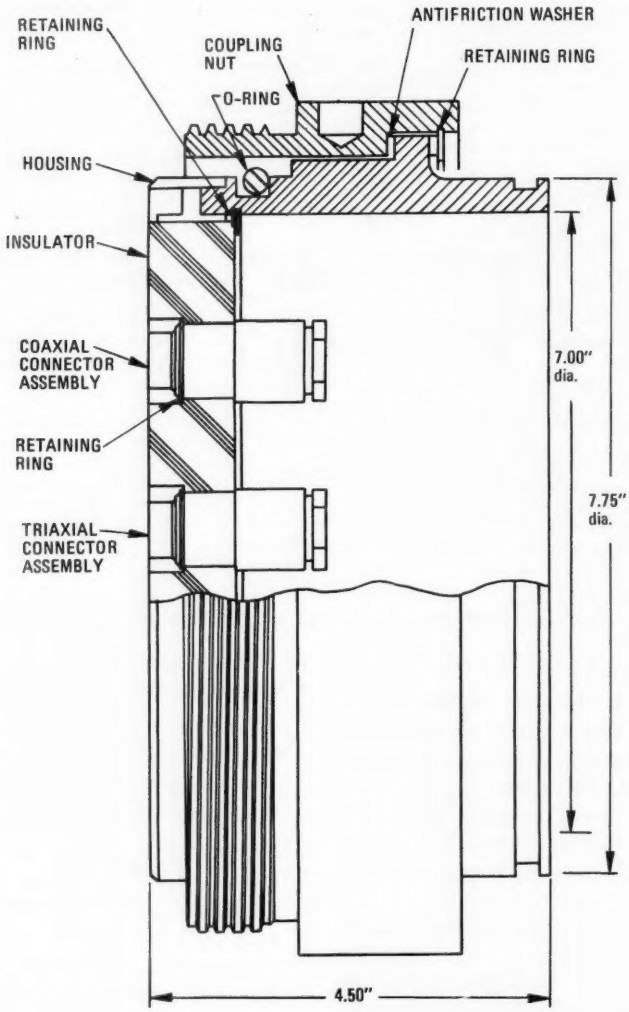

Fig. 6 Side view of plug that mates with penetration assembly (Fig. 5) inside San Onofre containment sphere.[3]

multicircuit plugs to serve several different pieces of equipment was very undesirable because it often tied up equipment that was not directly involved with the specific test of immediate interest.[4]

Future Specifications

The specifications for future penetrations will be essentially the same as for those described above. However, to avoid the difficulties experienced:

- Each multiconductor cable will provide only a single service to a piece of equipment.
- Chromel–Alumel thermocouples will be specified both as to accuracy class and as to matching of deviations from platinum-27.
- Chromel–Alumel materials will be connected only by spot-welded and mechanical joints.
- Slip-on neoprene insulation, similar to that used at the termination of ignition cable on automobile spark plugs, will be used for the cable contact insulation.
- Production control of the penetration canisters will use a quality-control chart technique.[4]

Circuit Protection

The various circuits to the equipment in the sphere of the San Onofre station are protected against loss of service caused by fires external to the system. A brief description of these methods is of interest.

The high-voltage cables have butyl-rubber insulation, a neoprene-rubber jacket, and are covered overall with aluminum interlocked armor. Cable trays are used both inside and outside the sphere up to the sphere penetrations, where conduit and junction boxes protect the connections.

The low-voltage general power and control conductors inside the sphere are insulated with cross-linked polyethylene. Outside the sphere the conductors have butyl-rubber insulation and a neoprene-rubber jacket. The extensions from the cable trays to the penetration assemblies and the terminations are protected by metal weather covers.[4]

The shielded twisted pairs and quads, thermocouple cables, and special instrumentation cables are insulated with polyethylene and have polyvinylchloride jackets. Foamed-polyethylene insulation and high-density-polyethylene jackets are used on the coaxial and triaxial cables for nuclear instrumentation. These cables are supported in trays, both inside and outside the sphere. Tray covers are provided on all exterior horizontal runs and on interior horizontal runs beneath gratings. The cables are protected at the penetrations by metal weather covers that extend to the trays.[4]

Fire in Cowling of a Power Penetration

On Feb. 7, 1968, a cable failure occurred within the weather protective cowling of a 480-V power penetration on the exterior of the containment.[3] The failure resulted in a fire.

This penetration had 65 conductors, ranging in size from No. 1/0 AWG to No. 6 AWG copper wire. At the time of the failure, each of the 45 No. 6 AWG conductors supplying the pressurizer heaters had been loaded at approximately 46 A for 96 hr.

The most probable cause of the failure in the cowling was the use of No. 6 AWG copper wire in the pressurizer-heater cables, which were grouped in bundles that restricted ventilation. Power losses in these conductors under the cowling heated the conductors above the 90°C rating of the insulation, which accelerated its aging. Other factors that could have contributed to the failure were:

1. Lack of supports allowed the conductors to bear heavily against each other, thus contributing to a phase-to-phase fault.

2. The exterior face and the areas between the conducting pins in these penetrations were filled with an RTV (room-temperature vulcanizing) silicone rubber, which could have permitted moisture to enter. The moisture could have allowed tracking currents to develop and, subsequently, fault current to flow between 480-V pins on the exterior face of the penetration.

3. Circuit protection for the pressurizer heaters consisted of fused disconnect switches for the 30 three-phase circuits. The use of individual fuses to clear faults on the three-phase 480-V circuits involved in the fire resulted in single-phase operation. Thus low-level fault current continued to flow, causing additional faults and heat generation at the outside face of the penetration.

4. Heat from the fire traveled through the pins to the inside of the canister, where it decomposed the insulating materials, forming gases whose pressure expelled the outside bulkhead from the canister.[3]

Fire in Cable Trays

On Mar. 12, 1968, a cable failure occurred; the resulting fire damaged three cable trays.[3] As in the February 7 incident, all the pressurizer heaters had been in service, with each of the 45 No. 6 AWG conductors serving these heaters loaded at approximately 46 A. In this case the heaters had been in service about 9 hr before the failure. The pressurizer-heater cables were in the lower tray.

Again, the most probable cause of the failure was the use of No. 6 AWG copper wire in the 45 pressurizer-heater conductors in a cable tray so heavily filled that ventilation was restricted, causing overheating. Other factors that could have contributed to the failure were:

1. Cables filled the tray to a level above the side rails, physically loading the lower cables and possibly deforming the insulation. This deformation or other mechanical damage, combined with the thermal overload, contributed to a phase-to-phase fault condition between two 480-V circuits, setting the insulation afire in the tray.

2. The cable might have been defective or have been damaged during installation.

3. Although the large initial short-circuit current was cleared by the fuses in the faulted phases, the current in the unaffected phases was below the continuous rating of the fuse. Subsequently, current was back-fed through the pressurizer heaters into the short-circuited cables, supporting the combustion of adjacent cable insulation.

4. Lack of three-phase clearing permitted low-level fault current to continue to flow and sustain the fire, causing additional faults and heat generation in the tray.[3]

Steps taken at San Onofre to prevent future failures due to these causes included:

1. For more orderly arrangement of the cable in the trays (and to tend to keep related conductors in a single circuit adjacent to each other), the butyl-rubber-insulated neoprene-jacketed single-conductor No. 6 AWG cables in the pressurizer-heater circuits were replaced with No. 4 AWG three-conductor cable.

2. To reduce both the number of circuits and the total resistive heat load in each 480-V penetration, and to provide for the larger conductors, three canisters were modified and three spare penetrations were equipped with new canisters. All 480-V circuits entering the containment use these modified penetrations. Supports were installed at the penetrations so the cables will not be supported by their terminals.

3. All penetrations were equipped with weather-proof enclosures to prevent moisture from entering through the face of the low-voltage power and control penetrations. All exterior enclosures were provided with thermostatically controlled heaters to maintain the temperature above the dewpoint.

4. For short-circuit and overload protection, the fuses were replaced by three-phase circuit breakers on all 480-V circuits, including the pressurizer-heater circuits; this type of breaker has several modes of protection, each of which provides three-phase tripping.

5. Some of the cables were relocated to new trays to reduce physical loading in cable trays. This relocation, together with the use of larger conductors, where required, also reduced the thermal loading in the cable trays throughout the plant. The pressurizer-heater cables were relocated to new separate trays.[3]

PENETRATIONS AT PRAIRIE ISLAND

The steel containment cylinders for Prairie Island Nuclear Generating Plant Units 1 and 2 are being designed for an internal pressure of 45 psig. Concentric with each steel containment cylinder, and providing a 5-ft annulus, there will be a secondary concrete containment building for biological shielding. The atmosphere in the annulus will be maintained at slightly negative pressure to prevent the egress of gas to the outdoor atmosphere. Operation of Unit 1, with an electrical capability of 550 MW(e), is scheduled to begin[5,6] in the spring of 1972.

At the time of this writing, a procurement package for the electrical-penetration assemblies is being prepared. Selection of specific penetration assemblies will be made after evaluation of the assemblies offered by several prospective suppliers. Therefore the details of the actual penetration assemblies that will be installed might differ appreciably from those depicted in this article.

Electrical Penetrations

A maximum of 10-in.-diameter nozzles will be provided in the steel containment cylinder to accommodate the 55 presently estimated electrical-penetration assemblies.[6] Cartridge- or canister-type penetration assemblies (Fig. 7), to be obtained from a commercial source, will be used for all electrical conductors entering the steel containment vessel. The planned penetration assembly consists of a hollow cylinder closed by plates at both ends. The assembly is provided with a port so that the penetration can be pressurized for leak-rate tests. The method to be used to seal the joint between the end plate of the assembly and the cable conductor, and to seal hermetically the cable interstices, will depend on the type of cable involved.[5,6]

For monitoring leakage, the atmosphere (probably nitrogen gas) inside the penetration assemblies will be pressurized at a fraction (yet to be established) of the design pressure of the containment vessel.

Figure 8 shows details of the canister header insert being considered for high-voltage (4160-V) power circuits. These penetrations will consist of single-conductor compound-insulated cables. A double seal will be provided by alumina insulating bushings at each end of the assembly.

Figure 9 shows basic details of a typical canister header insert for 600-V and lower power circuits.

The header insert of the type shown in Fig. 10 will be used for 600-V and lower power, control, and instrumentation circuits; it will be composed of single- or multiconductor compound-insulated cable. The cable conductors will be joined to fused-glass-sealed connectors at each end of the penetration assembly, thus providing a double barrier.

Penetrations for thermocouple extension leads will be as shown in Fig. 11. These will be copper conductors.

Figure 12 shows the basic details of the canister header insert to be used for coaxial and triaxial cables.

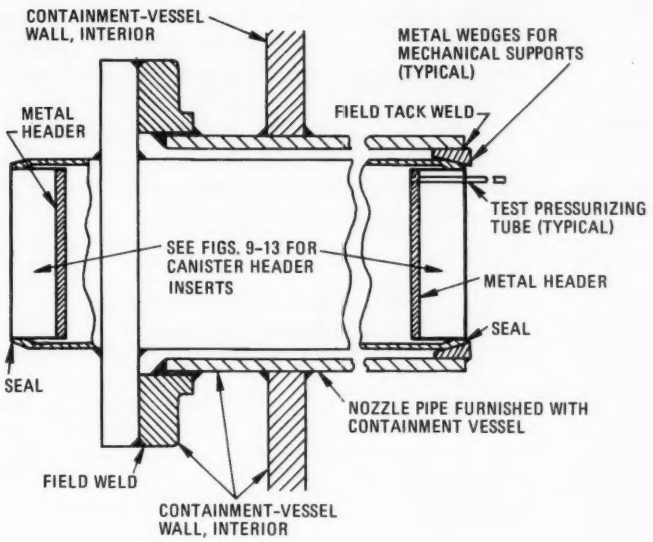

Fig. 7 Typical electrical-penetration assembly for Prairie Island Nuclear Generating Plant.[6]

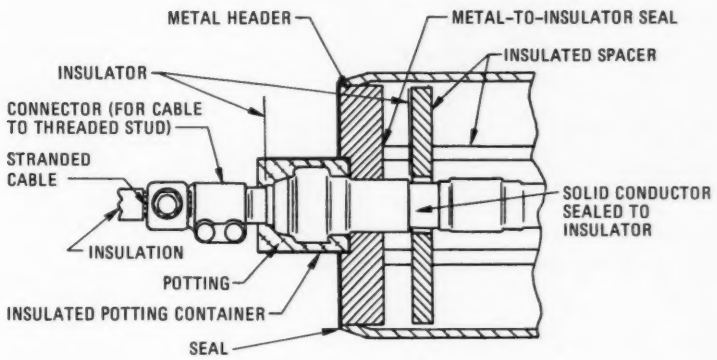

Fig. 8 Canister header insert for 4160-V power cables at Prairie Island.[5]

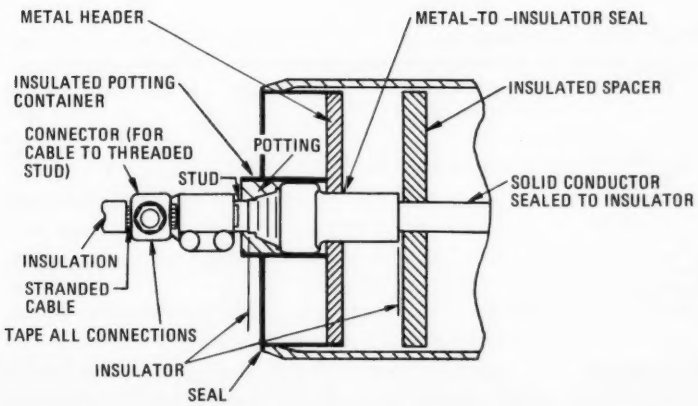

Fig. 9 Prairie Island canister insert for 600-V and lower power circuits.[6]

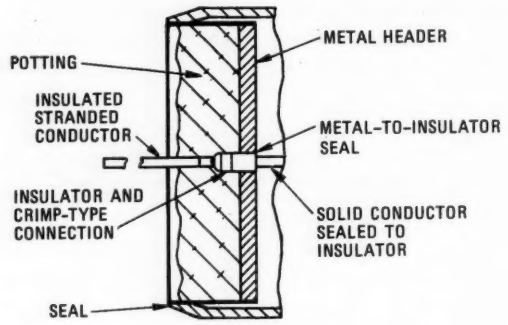

Fig. 10 Canister header insert for Prairie Island 600-V and lower power and control cables.[6]

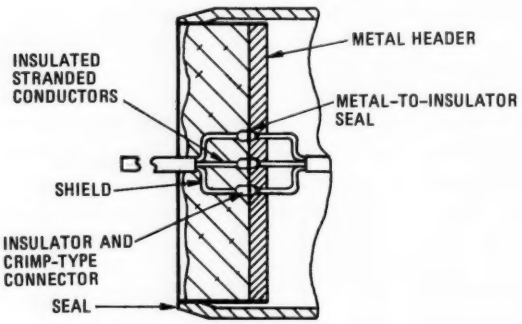

Fig. 11 Canister header insert for thermocouple extension leads.[6]

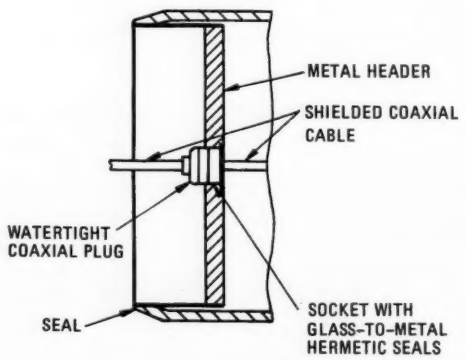

Fig. 12 Canister header insert for Prairie Island coaxial and triaxial cables.[6]

Special fused-glass-sealed fittings will be used at the ends of the penetration assembly to provide a double seal; the coaxial and triaxial cables will be connected to these fittings.[5,6]

Table 2 lists the conductor sizes and maximum practical number of conductors per penetration in a 7.5-in. (working diameter) canister header for each of the penetrations shown in Figs. 8 to 12.

Table 2 Conductors for Penetration Assemblies at Prairie Island[6] *

Conductor size	Tentative maximum no. of conductors per penetration	See Fig. no.
4160-V power		8
500 MCM	3	
750 MCM	3	
600-V and lower power		9
#1/0 AWG	42	
#2/0 AWG	30	
#4/0 AWG	30	
250 MCM	3	
350 MCM	3	
600-V and lower power and control		10
#16 AWG	180	
#14 AWG	180	
#12 AWG	180	
#10 AWG	180	
#8 AWG	60	
#6 AWG	60	
#4 AWG	60	
#3 AWG	60	
#2 AWG	42	
Thermocouples		11
Sixty #16 shielded pair copper cables 600 V a-c	180	
Sixty #16 shielded pair thermocouple cables	180	
Coaxial–triaxial	18	12

*10-in.-diameter pipe nozzle; 7.5-in. canister-header working diameter.

To provide for segregation of sensitive circuits and for more direct routing of cables to equipment and controls, the penetration assemblies will be installed on the containment cylinder in two similar but separated groups of 36 each. This arrangement is shown in the partial plan and section views of Fig. 13.

The electrical cables that penetrate the concrete containment wall will pass through ducts buried in the

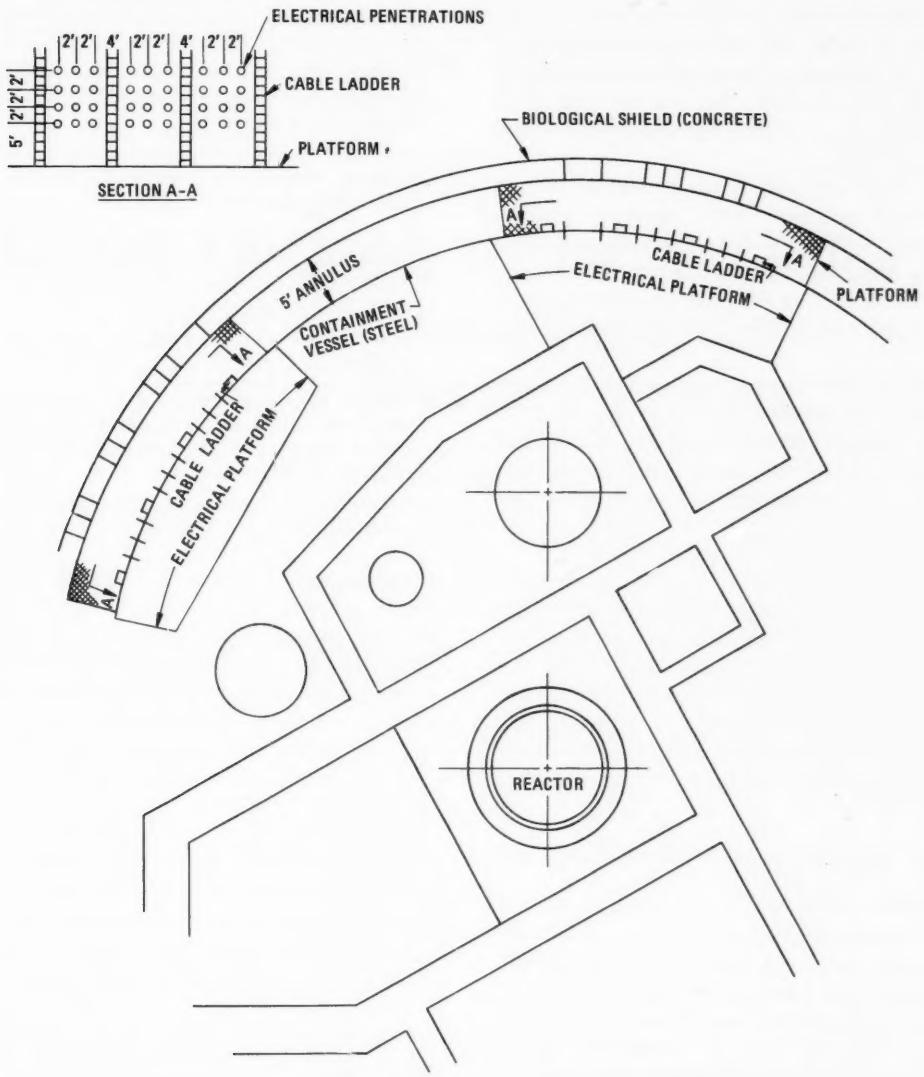

Fig. 13 Arrangement of electrical penetrations at Prairie Island (preliminary design). Note two separated groups of 36 penetrations each for segregation of sensitive circuits and for more direct routing of cables.[6]

wall. Glands or soft sealing materials will be used around these cables.

Cable-Tray System and Fire Safeguard Criteria

The preliminary criteria and fire safeguards being considered for incorporation in the electrical design of the cable-tray system for the Prairie Island station include:

- Power cables shall be installed in their own cable trays. There shall be no mixing of power and control cables.
- When power and control trays are located in the same tier, the power trays shall be located in the top level of the tier.
- Cables for redundant devices for engineered safeguards will be routed and separated so that any one incident will not impair both systems.

• All cable entrances into the control room, or into the cable room under the control room, shall be sealed to prevent the entrance of smoke generated by outside sources. (Both the control room and the cable room will be maintained at a slightly higher pressure than the surrounding areas.)

• The 4160- and 480-V power sources will be wye-connected grounded neutral systems. Instantaneous tripping will be provided for all fault conditions.

• Cable trays shall be routed to provide adequate separation from or shall be otherwise protected from any special fire hazards such as oil storage rooms and oil tanks.

• Cables in vertical trays shall be provided with fire stops at each floor elevation.

• Smoke and fire detectors shall be provided in all areas where electrical switchgear, motor control centers, and containment-building penetrations are located.

REFERENCES

1. F. Verber, Electrical Penetrations of Reactor Containment Buildings, *Power Reactor Technol. Reactor Fuel Process.*, **10**(2): 122-135 (Spring 1967).

2. F. Verber, Further Developments in Containment-Building Electrical Penetrations, *Reactor Fuel-Process. Technol.*, **11**(1): 5-12 (Winter 1967–1968).

3. B. R. Laverty, Southern California Edison Co., personal communication, Mar. 22 and July 24, 1968; also, K. P. Baskin, Southern California Edison Co., personal communication, Dec. 11, 1969.

4. J. B. Moore, Southern California Edison Co., personal communication, Dec. 26, 1967.

5. Northern States Power Co., Prairie Island Nuclear Generating Plant Units 1 and 2, Facility Description and Safety Analysis Report, U. S. Atomic Energy Commission, Volume 1, Docket 50-306.

6. L. Latourette, Pioneer Service and Engineering Co., personal communication, July 3, 1968 and Nov. 14, 1969.

Recent Advances in the Technology of Prestressed-Concrete Reactor Pressure Vessels

By Chen Pang Tan*

Significant advances in techniques and concepts for the utilization of prestressed-concrete pressure vessels (PCRV's) in nuclear reactors were presented at the Second Conference on PCRV's and Their Thermal Insulation, held November 1969, in Brussels, under the auspices of the Commission of the European Communities. The first such conference within the community was held about 2 years ago. In contrast with the first conference, the second conference was attended by participants from nine nonmember states in addition to those from the six member states. This reflects the realization that significant advances in scientific and technological research require cooperation between member states and nonmember states, especially those in Europe. The number of participants was more than 300.

The purpose of this article is to summarize the wealth of knowledge and ideas presented at the conference, indicating general approaches to the complex problems encountered in PCRV technology.

From the number of participants and the number of countries represented at the conference, one obtains a measure of the great interest in PCRV technology and the important role it is playing in the application of nuclear energy to civilian power generation. Compared to that of steel pressure vessels, the technology of PCRV's is still young. For a youthful technology in which safety is emphasized much more than it is in conventional concrete structures, designers and constructors of PCRV's are faced with unprecedented challenges. Potential applications of PCRV's are now far beyond the graphite/gas family of reactors which first used them. The application of PCRV's to high-temperature gas-cooled reactors is already a reality. The potential of applying PCRV's to boiling-water reactors is under serious consideration. As a result, new methods and new concepts are evolving.

*The Franklin Institute Research Laboratories, Philadelphia, Pa. 19103.

RESEARCH AND DEVELOPMENT

The advancement of the PCRV technology has relied heavily on research and development programs, without which it would be almost impossible for anyone to design and construct such complex structures. The United States and West German programs are described below.

In the United States, emphasis has been centered on the development of light-water-cooled reactors; and, because of the advanced state of the technology developed for the steel vessels used in water-reactor systems, the U. S. entry into the field of PCRV technology was belated. Besides the research and development effort exerted by Gulf General Atomic in support of the design and construction of the first PCRV for the high-temperature gas-cooled reactor of the Fort St. Vrain Nuclear Station, Oak Ridge National Laboratory (ORNL) has been managing a program of research and development for AEC for the last 3 years. A paper presented by Nephew (on behalf of Whitman)[1] of ORNL summarized the program. The program was organized around four major areas:

literature surveys and state-of-the-art reviews, analytical methods development, materials investigations, and model studies. It was pointed out that, even though only one PCRV is under construction in the United States, prestressed-concrete containment vessels are being widely used in light-water-cooled nuclear reactors. Significant results obtained from the AEC program to date include:

1. The development of analytical methods based on finite-element, as well as on lumped-parameter, concepts.
2. The demonstration, with small mortar models, that the shear failure in the end slab of a cylindrical vessel can be avoided.
3. The demonstration that failure processes in PCRV's can be detected and monitored through the use of stress-wave emission techniques.

The program also includes an effort to obtain valuable data on creep and moisture movement in concrete.

The research and development program planned for the next 4 years in West Germany was reported by Jaeger[2] of the West German Institute for Material Testing. The West German program lays emphasis on basic research, so that the results will have broad application either to gas-cooled or water-cooled power reactors or other types of reactors. In essence, the West German program is aimed at broad applicability and maximum flexibility so as to accommodate the PCRV technology to the continuous evolution of reactor types. The basic research will consist of:

1. Safety and economy evaluation.
2. Study of the material properties of concrete, such as microstructure, creep, shrinkage, thermal properties, and the effect of moisture movement on the properties of concrete.
3. Computer-oriented numerical analysis to correlate the theoretical and experimental results and to optimize the design, taking into consideration problems in construction and operation.
4. Study of the liner for both gas-cooled and water-cooled reactors, including all details at penetrations, shear connectors, and other pertinent design features.

The emphasis of the West German program is on computer-oriented analysis. Instead of devoting their effort to model testing, they will correlate the experimental results obtained by Britain, the United States, and other countries. Obviously, international cooperation and coordination will be vital to the West German program. It was mentioned that contacts had been made with groups in Britain, Sweden, Austria, and the United States aimed toward possible cooperation.

PRACTICAL EXPERIENCES WITH PCRV'S

Since the inception of the two vessels at Marcoule, France, in 1956, the technology of PCRV's has been developing rapidly. There are now nearly 20 PCRV's, including those commissioned or under construction. Experience gained from the construction and, especially, the operation of these complex structures is of great value in improving the design of later PCRV's and in enhancing the economy and safety of these structures.

The construction of the PCRV of the Spanish Vandellos Nuclear Power Station was described by the members of the French construction group.[3] Basically, the PCRV of Vandellos is a replica, with some modifications and improvements, of the two vessels in EDF-4 and St. Laurent 2. The major differences are: (1) In EDF-4 the hoop tendons in the cylindrical portion traverse one-third of the circumference, whereas in the Vandellos they traverse two-thirds of the circumference. Thus the number of end anchorages needed in the cylindrical portion of Vandellos is reduced to half the number used in EDF-4. The tendons are tensioned from both ends instead of one, as is done in the EDF-4. (2) In EDF-4 the Société d'Études et d'Equipments d'Entreprises (SEEE) prestressing system is used, whereas the Freyssinet system, with Y2T15 strands, is used in Vandellos. (3) Oil is used to reduce the friction loss of the tendons at the time of tensioning. (4) Cables in the bottom slab are perpendicular to the cylinder wall surfaces at the ends, instead of at a skewed angle, as they are in EDF-4. (5) Seawater is used in the primary cooling circuit. It was pointed out that the improvements and new solutions outlined above were made feasible by the experience gained in the design and construction of EDF-4.

A paper presented by Costaz,[4] of Service Génie Civil of France, described the first results obtained from the commissioning of the St. Laurent 1 PCRV. Construction of this PCRV was started in the autumn of 1964, prestressing was accomplished in the summer of 1966, and pressure testing was completed in April 1968. After a series of startups and shutdowns, the station was expected to reach full power by the end of 1969. The paper presented the principal phases of construction of the PCRV involving the concreting and prestressing of the structure. The cycles of temperature

and pressure loadings to which the PCRV was subjected from January 1968 to April 1969 were depicted. A radioactive tracer was used to study the flow of water in the 1-in. primary cooling pipes. Of 430 pipes studied, none were found to be clogged.

The cooling of the steel liner was also studied. It was found that there were no apparent hot spots in the liner and that the heat flux removed by the cooling circuit was slightly higher than expected. The problems that arose during the period of initial startup, up to the date of the electric-power run-up, were described in detail. To keep the steel liner and the adjacent concrete at a suitable temperature, irrespective of variations in heat flux impinging on them, the operators used special maneuvers to regulate the flow of natural cooling water while maintaining a constant flow of demineralized water. There were difficulties in obtaining correct readings from thermocouples mounted on the liner and in the concrete. Consequently there was little information on thermal stresses. On the other hand, good response of the structure to pressure stresses was obtained from dynamometers on prestressed tendons. These experiences led to modifications in the operational monitoring techniques used in the St. Laurent 2 PCRV.

An outline of the interaction that exists between the design and construction of PCRV's was presented in a paper coauthored by Burrow of Taylor Woodrow Construction Limited, and Tate and Williams of British Nuclear Design and Construction Limited.[5] The paper discussed the evolution of the principles of construction of the Wylfa and Hartlepool PCRV's, which involved extensive prefabrication and parallel construction work in the various parts of the plant. In Wylfa a Goliath crane with a lifting capacity of 400 tons and a traveling span of 200 ft was used to move major prefabricated mechanical components. In addition, four Peine cranes and two derricks, each of 10-ton capacity, were used to carry out construction work involving lighter components. Time was lost as a result of difficulties encountered in welding the liner and in installing the reactor equipment. The steam generators and the reactor core were installed in parallel. Maintenance of temporary access routes into the vessel, the need for early manufacture of steam-generator modules, necessity of a great deal of in-situ welding, and the irreversibility of the process of erection were cited as drawbacks of the method of steam-generator installation. The adoption of the design of a spherical internal cavity with a stepped cylindrical shape on the outside for the Wylfa PCRV was mainly the result of considerations of construction. It was pointed out that the behavior of the structure will be largely dictated by the spherical shape of the pressure boundary and that wide variations in the external shape would have relatively little effect. By designing the outside of the vessel as a series of flat surfaces, it was possible to arrange for all tendons to approach and terminate normal to the concrete surfaces; and the congestion of the tendons was alleviated.

In the case of the most recent Hartlepool PCRV's, the principle of prefabrication and testing in shops, to minimize the extent of site activities, has been emphasized even more because of the compactness of an advanced gas-cooled-reactor station compared with one having uranium–Magnox reactors. The turbine hall and reactor building are integrated. Instead of using a Goliath crane, a gantry crane with a capacity of 260 tons is used. The crane tracks are carried by six large towers that were constructed at the beginning of the program using slip-form techniques. Cranes of less than 10-ton capacity are used to carry out the construction. The modular steam-generator concept was used, whereby shop-assembled and -tested units are fitted into vertical, cylindrical "pods" in the walls of the PCRV. It is expected that the temperature in the liners of the pods will be nearly the same as that in the main vessel liner. The steam generators can be readily removed for maintenance or replacement, and their location within the walls of the vessel facilitates the new prestressing concept of wire winding in the circumferential direction. A Cable Covers Limited (CCL) prestressing system is used for the vertical prestressing; each tendon consists of 28 strands 0.7 in. in diameter, giving a guaranteed ultimate strength of 1040 tons and a working load of 780 tons. The wire-winding arrangement is based on the use of concentrated bands of wire, wound under tension into preformed channels in the vessel walls. The wire winding is accomplished by a machine working from a steel platform, traction being obtained from a continuous chain encircling the vessel. There are devices to monitor the tensioning load in the wire.

The construction of the top cap of PCRV's presents a number of problems. The area is crowded with standpipes, which are so closely spaced that placement of concrete is very difficult. In Wylfa the 1-in.-thick top cap of the spherical steel liner supported the wet concrete. The total standpipe load of 800 tons was carried by a support structure, and constant-load devices were provided to connect the standpipes to the support structure so as to ensure that the standpipe and concreting loads were suitably distributed between the liner and the support.

At Hartlepool the support structure must carry both standpipes and wet concrete. Concrete is placed in strips comprising two or three rows of standpipes in lifts not exceeding 4 ft. After a curing period the strips become self-supporting. To minimize the deflections of the support structure as a result of the strip method of construction, the structures will be preloaded with kentledge, which is removed progressively as the standpipe and concrete loads are added.

The practical experience with the world's first two PCRV's, G-2 and G-3, was contained in a paper prepared by Dupay,[6] of CEA France. The paper contains information on the compression in the concrete cellular floor of G-2 and G-3, on the behavior of the new tendons as determined through the use of dynamometers, and on the thermal gradients across the vessel walls.

PROPERTIES OF MATERIALS

In a nuclear reactor-vessel application, concrete is subjected to nuclear radiation, heat, and pressure, which produce a range of combined mechanical and thermal stresses, and may change the properties of the concrete. In view of the fact that the technology of PCRV's is relatively new, there is virtually no information on the behavior of concrete under such conditions; and there is general concern in this regard. The nine papers concerned with the various properties of concrete were contributed by authors from The Netherlands, Italy, the United Kingdom, France, and West Germany, illustrating the deep and widespread interest in this subject.

The paper presented by Houben and van der Schaaf,[7] of The Netherlands, was concerned with the effect of irradiation and temperature on mortar specimens with different kinds of fine aggregates. The mortar specimens were subjected to a total irradiation dosage of 0.3 to 0.8 x 10^{20} neutrons/cm^2, a temperature gradient obtained by having opposite ends of the specimens at 270 and 125°C, and a uniform temperature of 400°C. From the results of these tests, it was concluded that the moduli of elasticity, both static and dynamic, and the ultimate strength of the mortars are reduced as a result of irradiation and heating to high temperature.

The behavior of concrete under the effects of temperature and irradiation was also studied by Crispino, Granata, and Risoluti of Italy.[8] Various types of cement and aggregates were considered in their study. The kinds of concrete adopted in the study were first optimized by comparing the parameters that affect the strength of concrete, such as cement content, water–cement ratio, and the form of the aggregates. The concretes were subjected to thermal cycles between ambient temperature and a maximum temperature of 300 to 350°C. The study led to the discovery of factors responsible for the deterioration of mechanical properties of ordinary concrete under thermal cycling. The most important result of the study was the development of a high-temperature concrete, called BHT concrete, which was reported to be capable of withstanding temperatures as high as 500°C. The properties of BHT concrete were studied, including compressive and tensile strengths, modulus of elasticity, Poisson's ratio, creep properties, thermal conductivity, and thermal expansion.

The BHT concrete was subjected to irradiation in the Galileo Galilei swimming-pool reactor, using two capsules inserted into the element grid at various distances from the reactor core. The integrated thermal neutron flux was 10^{20} neutrons/cm^2 for the capsule nearest the core and 10^{19} neutrons/cm^2 for the other one. The mean temperatures attained were 280°C and 130°C, respectively. In order to differentiate between thermal and irradiational effects, a similar series of samples was kept in an environment having the same conditions of temperature and humidity as those under irradiation. As examination of the irradiated samples had not been completed at the time of the conference, the results of this part of the study were not available. It was concluded that the BHT concrete could be considered suitable for use at high temperature and for thermal cycling, but not necessarily as the optimum solution.

The results of a detailed study of the effects of reactor radiation on concrete were presented in a paper by Kelly et al. of the United Kingdom.[9] Two high-strength concretes typical of those employed to construct PCRV's were exposed to reactor radiation. Similar concrete samples were also subjected to X-ray irradiation from spent reactor fuel elements to attempt a separation of neutron and X-ray damage effects. The significant results of their study are: (1) in the range of neutron dosage of 10^{18} to 4 x 10^{19} neutrons/cm^2, pronounced changes occur in both concrete and aggregates; (2) dimensional changes of the aggregate compared with those of the concrete and cement paste are slightly less, and there is evidence of cracking due to differential strains between the cement paste and aggregates; (3) changes in thermal conductivity/diffusivity are smaller in concrete than in aggregates, (4) neutron irradiation causes a marked decrease in the strength and Young's modulus of the aggregate and

concrete; (5) a wide difference was observed in the behavior of aggregates, even of the same basic type, particularly in dimensional changes; (6) strain gradients due to neutron flux may be as important as those due to temperature; (7) corrosion occurred at the ends of the steel-rod samples in contact with water under irradiation, but there was no reaction in other parts of the samples; however, the hydrogen content of the rods increased slightly; and (8) there was a very considerable volume of gas generated by both types of irradiation, and a relatively large concrete weight loss occurred.

Results of a study of the properties of concrete, particularly creep, were presented in a paper by Ausangee et al. of France.[10] They performed uniaxial creep tests at various temperatures on small sample blocks having dimensions of 7 by 7 by 28 cm. The test conditions were chosen so that the results could be applied to a scaled-down vessel model, which was the subject of the second part of the paper. The vessel model is of $\frac{1}{25}$ scale; and it has a cylindrical shape with an inside diameter of 80 cm, a wall thickness of 40 cm, and a height of 150 cm. It is prestressed. The test data were automatically recorded through use of a CDC 6600 computer. The experimental results were compared with theory by the use of two computer programs: ELVIS for the analysis of an infinite cylinder and BOOBLV for the analysis of short cylinders. The ELVIS program gives thermal and viscoelastic solutions for an infinite cylinder, whereas the BOOBLV is adapted to the simulation of a simple geometry, processed at a high speed. Actually, BOOBLV was used essentially for isothermal analysis. The test program included mechanical, rheological, and thermal tests. The mechanical tests consisted of both rapid and slow tests. The model was also tested for the onset of cracking at different temperatures. In interpreting the test results, various factors were evaluated, such as the effect of vibrating the concrete in the block specimens and the small-scale ring model, the effect of creep and shrinkage on deformation, the nonlinearity of creep, and the effect of different temperature gradients on the block specimens and the ring model.

Another French paper by Dubois and Noel[11] was concerned with the determination of the modulus of thermal rigidity of an insulating concrete subjected to thermal and mechanical stresses. The precise characteristics of the material were determined by applying constant moment loading to a prismatic beam of uniform cross section, which was subjected throughout its length to a temperature differential between its hot and cold sides. By applying a constant bending moment to this beam, so that the location of the neutral plane remained horizontal, without changing the thermal stress, a mechanical effect equal and opposite to the thermal effect was produced on the distortion of the beam. With the help of simple, strength-of-materials-type equations, the relation $\sigma = KE_d\alpha\Delta T$ was obtained.* A description of the testing machine, its controls, and other apparatus was given.

Test results on an expanded clay-based insulating concrete showed a very slight drop in the modulus of thermal rigidity ($E_d\alpha$) when tested at temperatures in the vicinity of 320°C; the concrete also showed excellent mechanical and insulating properties.

Irving and Goodall,[12] of Berkeley Nuclear Laboratories of the British Central Electricity Generating Board, presented their study of the creep behavior of a circular concrete slab containing a symmetrical array of penetrations with steel sleeves. This problem was chosen because considerable cracking had been found in concrete between the steel sleeves of test models of an elastically designed standpipe zone after the models were subjected to a sustained load. By using the Maxwell model with time replacement and an iterative time-step technique of numerical solution, a theoretical analysis was made which showed that considerable changes in stress and strain occur in a heated, reinforced-concrete structure, with a tendency for tensile stresses to be produced in the concrete on cooling and unloading. This phenomenon was attributed to the presence of residual creep strain. From this analysis it was inferred that, in penetrated regions of PCRV's, tensile cracking could also be caused by cooling during the reactor shutdown cycle.

A study of the moisture movement in mass concrete, such as occurs in PCRV's, was presented in a paper by Hornby of the United Kingdom.[13] Moisture in concrete has an important influence on many factors, such as shrinkage strains, creep stresses, thermal conductivity, strength, and elastic moduli, all of which affect the design of a PCRV. The method used is based on the measurement of the electrical conductivity of the concrete between two electrodes. Moisture losses observed in a 2-m-diameter block of concrete, in the first 5 years, showed that concrete loses moisture at a slow rate under ambient-temperature conditions. At a depth of 150 mm, the loss is only 16% of the total

*α is the coefficient of thermal expansion, σ is the stress in the beam, E_d is the global modulus of elasticity, K is a constant, and ΔT is the temperature difference between the hot and cold sides of the beam.

available evaporable water. Bars of concrete, 130 mm in diameter and 2.7 m long, were subjected to a temperature gradient (end faces at 150 and 25°C), the bars being sealed against moisture along their length. It was found that, as the high-temperature end dries out, a "front" is formed, which slowly changes slope. During a discussion period, R. D. Browne, also of the United Kingdom, presented some results of concrete testing which correlated quite well with those of Hornby. C. R. Lee, of Building Research Station, recounted his experience in the use of electric moisture gauges. It was pointed out that unless control gauges are used the interpretation of the gauge readings cannot be precise. There is considerable drying behind the liner, and the rate of drying decreases as time proceeds.

An investigation of the rupture behavior of concrete in the multiaxial stress state was reported by Bremer of West Germany.[14] A loading device was first developed for producing any desired compressive stresses, initially along only two or three axes; this was later modified so that tensile stress could also be applied along at least one axis. The strength was measured along two or three axes as a function of the stress ratio and type and then compared with the uniaxial strength. It was indicated that, with the capability of determining the actual strength of concrete in the multiaxial stress field, it would become possible to perform more exact design calculations for a PCRV.

NEW TYPES OF VESSEL DESIGN AND MODEL TESTING

Two concepts of prestressing PCRV's were presented by Muhe of West Germany:[15,16] one for circumferential prestressing, the other for axial prestressing. The circumferential prestressing tendon consisted of cables whose individual wires are arranged between clamping plates. The ends of each cable, which are initially not in contact with each other, are drawn together by means of a jack and then coupled together through use of a coupling device. The wires can be wrapped either with or without separators between layers. When the cable ends are coupled, the auxiliary clamping plates can be removed and used for prestressing the next cable. The prestressing tendon profile in the horizontal section can be circular or polygonal. In the latter case the prestressing force is transmitted to the concrete cylinder as concentrated loads through direction-change bars. The prestressing tendons are exposed on the outside of the vessel.

The axial prestressing system consisted of tendons with breaking strengths of 1500 mp, and a large clamp anchorage. The tendon consists of 240 diagonally ribbed, oval prestressing wires of grade ST 145/160 steel, bunched together without spacers. A long-term corrosion inhibitor is to be used. The tendon is tensioned through use of a hydraulic jack that works against the standard clamp anchorage on the other end of the large tendon.

In a discussion from the floor, questions were raised concerning protection against corrosion of the prestressing system, conceived by Muhe,[15] especially at points of contact with clamps. Questions were also raised concerning the coefficient of friction and stresses at points of change in direction.

Another concept of prestressing concrete pressure vessels by external hoops was presented by Puyo et al. of France.[17] Instead of wire or strand tendons, this group investigated the use of steel strips of high tensile strength. The strip steel was wrapped around the vessel in several layers to form external hoops of high unit strength, which were tensioned by radial jacks bearing on the vessel wall. Test results led to a favorable evaluation of this prestressing system. In discussion from the floor, doubt was expressed concerning the economy of leaving hydraulic jacks in the structure as required by this prestressing system.

The technique of constructing a PCRV from prefabricated parts was presented by Rissler of West Germany.[18] A ¼-scale model was built for a pressure vessel with an internal pressure of 100 atm. A prestressed prefabricated hoop resembling a ring section of the cylindrical vessel was made to clarify design questions. Each complete prefabricated ring consisted of 16 sectors. A hollow cylinder is formed by stacking the rings one above the other. Then vertical prestressing is accomplished by passing prestressing tendons through holes in the ring sectors and tensioning these tendons. Horizontal prestressing is attained by wire winding. Following completion of prestressing, the grooves between ring sectors are filled with grout, and the circumferential prestressing tendons are enclosed in a layer of cast-in-place concrete. A ring section with a piping penetration was included in the study.

The concept of multilayer vessel design has been pursued by Friedrich Krupp Universalbau of West Germany for quite some time. In such a design, each layer has a separate function. Starting from the central cavity, a first layer of special, high-temperature concrete serves as a support for heat-resistant refractory concrete made of clay or expanded ceramic material

which can be easily mounted on site. These first two layers are surrounded by a film of cold water at the same pressure as the reactor coolant. The PCRV is thus protected from thermal stresses, and its design is thereby simplified. Schrage, of Friedrich Krupp Universalbau, gave an account of their studies on a $\frac{1}{5}$-scale model,[19] using France's Bugey 1 reactor as a reference.

The United States' experience in the design, construction, and testing of a small PCRV was reported by Northup of Gulf General Atomic.[20] The small PCRV is approximately a one-quarter scale of the Fort St. Vrain PCRV under construction in Colorado. This is the first U. S. PCRV for a high-temperature gas-cooled reactor. The model was tested for short-term loadings, such as prestressing, pressurization, vessel heating, hydraulic and pneumatic overpressures, permeation, concrete moisture loss rate, pressure-cycle effects, and creep. It was concluded from this model testing that the design, construction, instrumentation, evaluation, and analysis methods were quite adequate for use on larger, similar vessels; also, the behavior of the vessel could be predicted with reasonable accuracy.

The application of PCRV's to water-cooled reactors was advocated in two French papers. In one presented by Arathoon and Peuchmaur of Socia (Société pour l'Industrie Atomique) of France,[21] the reactor considered was of the boiling-heavy-water type. A cylindrical vessel 10.3 m in diameter was designed for a pressure of 125 bars. Specified as requirements for this vessel were (1) a primary circuit of heavy water and a secondary circuit of light water, with the heat exchangers to be enclosed in the reactor vessel; (2) heat exchangers that would be replaceable following an accident. A removable head would be needed to meet the second requirement, so that the vessel could be opened completely. However, such a solution would require loosening of the axial prestressing steel. In order to overcome this inconvenience, there are two alternatives: (1) the cover can be separated from the rest of the vessel, which becomes an open structure taking the reaction from the cover, and (2) the end structure can be arranged so that it can be separated from the rest of the vessel, but so that the vessel and the cover act together as a monolithic structure when in service. The second alternative was adopted (Fig. 1). The cover is in the form of a dome, prestressed throughout its thickness. It is solidly attached to a metal ring that is of the same thickness and rigidity as the concrete it replaces. The ring, composed of plates and spacers, has deep slots that enable the cover to be fixed onto the vessel with removable bolts. With such a construction, the cover does not slip in relation to the body of the vessel under the effect of pressure, thus

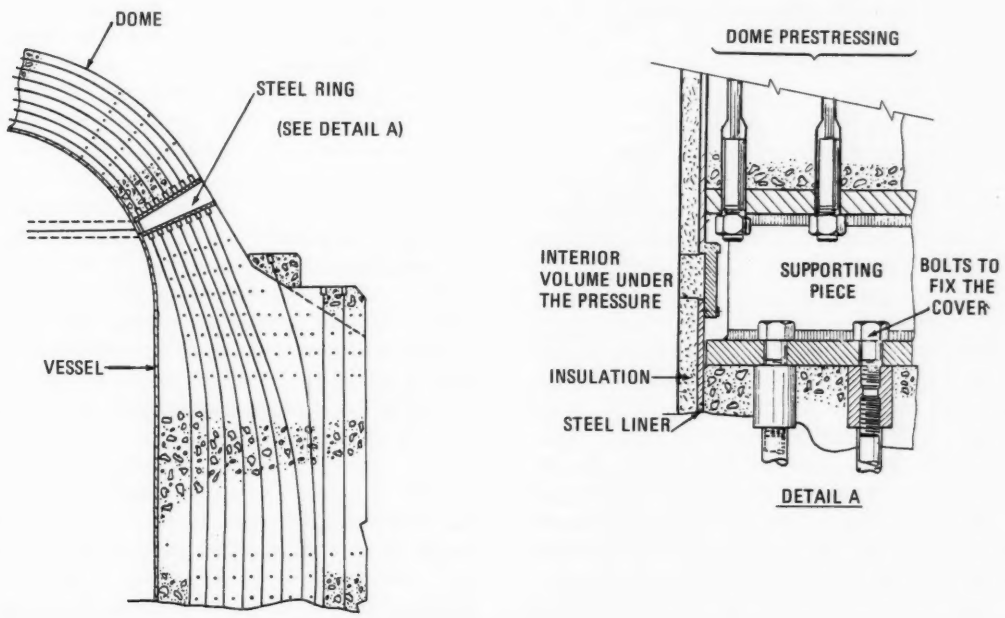

Fig. 1 Conceptual design of a PCRV for a BWR.

enhancing heat insulation and leaktightness. Arathoon and Peuchmaur also studied PCRV's for high-temperature, helium-cooled reactors. Two types of PCRV's were considered: one designed with a removable end slab and the other with modular heat exchangers, i.e., the heat exchangers were housed in pods in the vessel wall. The latter type was considered to be more economical than the former.

Another paper devoted solely to the development of a PCRV for a boiling-water reactor was presented by Merot and Languille of France.[22] The configuration of the PCRV is a vertical cylinder with top and bottom slabs. The cylinder wall thickness is 3.60 m, and the slabs are 4.50 m thick. The principal elements of the vessel and their arrangements are basically the same as those in PCRV's for gas-cooled reactors. The inside diameter is 7.10 m, compared with 5.30 m for a steel reactor vessel having the same generating capacity of 600 MW(e). The thermal insulation is designed on a so-called "hot-wall" principle. The hot-wall construction includes, from inside to outside, the steel liner, a layer of high-temperature concrete, the cooling circuits, and the concrete vessel wall, on which the strength of the whole structure depends. This type of thermal insulation was adopted because it was realized that the problem of the two-phase, water-vapor system could not be resolved by other types of insulation. The properties required of the steel liner, high-temperature concrete, cooling circuit, and the concrete vessel were discussed. The main advantages of such a PCRV are economy and safety. However, the internals are not readily accessible.

METHODS OF ANALYSIS

Among the developments in the technology of PCRV's, that of theoretical analysis can be regarded as the most rapid and impressive. Four papers were presented, two of which were devoted to the finite-element method, one to the dynamic-relaxation method, and the fourth to a comparison of the advantages and disadvantages of the various analytical methods.

A paper by Zienkiewicz, Owen, and Phillips, of the University of Wales, reviewed the history of the application of finite-element methods to structures of linear elasticity and to nonlinear and nonhomogeneous ones.[23] The elements used in the mathematical model include shapes ranging from the simplest plane triangular element to sophisticated solid tetrahedrons. The numerical analysis can predict the true behavior of the structure only if the constitutive laws for the materials concerned are known completely. This presents difficulties for concrete structures because tensile cracking, compressive failure, and time-dependent creep cannot be accounted for properly in the constitutive law of concrete. Zienkiewicz gave some indication of the relation between accuracy and the size and number of finite elements. He also showed how variation in axial prestressing in a PCRV may be represented in Fourier form by a series of even harmonics, and the solution may be obtained by an extension of the axisymmetric method of solution. The treatment of nonlinear material behavior through the assumptions of small strains and displacements was discussed. Solutions can be obtained through any one of three approaches: (1) variable elasticity approach, (2) initial stress approach, or (3) initial strain approach. Idealizations applicable to PCRV analysis include: (1) no tension in concrete, (2) limited tension in concrete, (3) limited tension and nonlinear compression in concrete, (4) steel as an elastoplastic material, and (5) the constant-volume-plasticity approximation. It was suggested that concrete creep can be represented by a number of Kelvin models in series. A viscoelastic solution using Zadoian's creep function may also be sufficiently accurate for general-purpose use.

The analysis of three-dimensional structures, such as PCRV's, based on the matrix-displacement approach of the finite-element method, was discussed in a paper by Argyris and Grieger, of the University of Stuttgart, West Germany.[24] The structure is represented by three-dimensional, tetrahedron elements, with straight or curved edges. The nodal points can be placed not only at the edges but also at the centroids of the four faces. Conditions under which a general hexahedronal element is introduced were also indicated. For axisymmetrical structures, ring elements with either straight or curved edges can be used conveniently for the analysis. Membrane shell elements for the analysis of axisymmetric boundaries with symmetric or harmonically distributed loading and section elements with axisymmetric geometry and unsymmetric loading can be conveniently used in the analysis of shell structures. A number of applications, including PCRV's, were described.

The dynamic-relaxation method has been used generally to analyze the overall behavior of PCRV's as an axisymmetric structure. The stress conditions around large openings are usually analyzed by the finite-element method. In the paper presented by Schnellenbach,[25] of Ruhr University, West Germany, it was demonstrated that the dynamic-relaxation method can be used to determine the spatial stress and

deformation state and also the stress conditions around holes. Some two-dimensional examples were worked out, and the results can be compared favorably with those of other analytical solutions or model tests. Some results of a three-dimensional analysis around a hole in a cylinder wall, using the dynamic-relaxation method, were also given.

A survey of the numerical methods used in the analysis of PCRV's was given by Brandes[26] of West Germany. He discussed the advantages and drawbacks of the finite-element and dynamic-relaxation methods, which are those most commonly used.

THERMAL INSULATION

There were 10 papers related to this subject, 8 from French sources and 2 from British sources.

A paper by Furber and Davidson,[27] of the Nuclear Power Group Ltd., was concerned with the development of thermal-insulation systems capable of working in high-pressure gas environments, such as in AGR (advanced gas-cooled-reactor) and HTR (high-temperature reactor) systems. Materials suitable for insulation of such systems are porous, of a fibrous or granular structure, so that gas movement can occur through them. In high-pressure gas systems, any movement of gas within the insulation can lead to a deterioration of thermal insulation and the possible generation of hot spots on the steel liner. In order to develop insulations having isotropic, or nearly isotropic, thermal performance in high-pressure systems, experimental and theoretical work related to the insulation of vertical surfaces was carried out. The amount of natural-convection circulation and the influence of pressure gradients imposed within an insulating panel are limited by the resistance to gas flow within the material. Since this flow resistance is dependent on the permeability of the insulant, the factors influencing the permeability of insulants were considered in detail, and theoretical and experimental work to establish the values of permeability for several insulants under reactor conditions was described. The gas movement through a porous insulant is shown to obey Darcy's equation under the conditions likely to arise in reactor operation. In the theoretical analysis, two mathematical models were considered.

The first considers a high-aspect-ratio rectangular panel with sealed boundaries; the second, a more realistic model, involves a porous hot face. The influence of surface-pressure gradients was also considered for the second model. Heat transfer through forced convection, as well as natural convection along an open hot face and a closed hot face, was studied theoretically. The data presented showed close correspondence between theoretical and experimental results. An investigation of the insulation problem in a helium-cooled reactor was also reported to be in progress.

The performance of thermal insulation immersed in helium was the subject of a paper presented by Kinkead and Pitchford[28] of the Dragon HTR project. The study was confined to the multilayer, metallic-foil type of insulation, using an approximate, semiempirical analysis. It was assumed that global circulation could be neglected within the thickness of the multifoil insulator; and, consequently, the insulator permeability was not taken into consideration. The height of the insulating panel used in experiments was only 2 m. In view of the various simplifications in the analysis and tests, the study can be regarded as being exploratory only.

A paper[29] by Grossin et al., of Société Bertin et Cie, and Klarsfeld, of Compagnie de Saint-Gobain, dealt with heat transfer by natural convection in a porous medium. The theoretical and experimental model that they studied consisted of a homogeneous solid bathed by an interstitial fluid and contained in a leaktight parallelepiped panel, the two opposite faces of which were raised to different temperatures. On the basis of such a model and other simplifying assumptions, a system of differential equations expressing the conservation of mass, energy, and motion of an elementary volume of interstitial fluid was derived. Computer solutions of the differential equations showed the possible existence of two types of convective flow when the heated walls are vertical. One is the "adjacent boundary layer" type, and the other is the "separate boundary layer" type. Numerous experiments substantiated the theoretical findings.

In gas-cooled reactors the coolant is carbonic gas under pressure, kept in motion by blowers. As the gas flows through the space inside the vessel, the flow may be disturbed by various causes, resulting in vibration of various components inside the vessel. The results of a study on the behavior of a thermal insulant under cyclical forces of aerodynamic origin were presented in a paper by Roure, of the Société Bertin et Cie of France.[30] The thermal insulation studied was of metallic gauze, known as CAFL metalysol, enclosed in a casing. The nature and magnitude of the stresses, as well as the dynamic behavior of the thermal insulation, were studied theoretically and experimentally. The study was conducted primarily for the insulation of the Bugey 1 PCRV.

The general design and construction of the thermal insulation by metallic gauze and sheet metal of Bugey 1 were detailed in another paper by DeLort, Lecour, and Soulier.[31] The basic design concept was cited as follows:

The insulation is applied on the inside face of the steel liner in contact with the coolant and bathed by it. Cooling circuits are placed on the other face of the liner, which is in contact with the prestressed concrete. The use of the metallic gauze between the heat source (the gas coolant) and the heat sink (the liner) introduces a great obstacle to natural convection, which is the essential form of heat transfer. In addition, this structure is highly opaque to radiation, and it has a very low conductivity as a result of the numerous contact resistances.

Prior to installation in the vessel, the CAFL metalysol insulation was subjected to a series of large-scale thermal and mechanical tests. The major features of the metalysol insulation are efficiency, reliability, cleanliness, resistance to shock, high static and dynamic strength, and ease and rapidity of installation.

A paper on the development of new types of heat-insulating concrete for PCRV's was presented by Dubois et al. of Commissariat à l'Énergie Atomique.[32] The main advantages of these types of concrete were cited to be ease of installation, economy, and capability for perfect adaptation to any vessel geometry. The principal heat-resistant aggregates that they investigated were pumice, pozzolan, vermiculite, pearlite, expanded clays, and oxide globules. Among these, expanded clays were chosen by reason of their good mechanical properties. Two heat-insulating concretes made with expanded clays were tested at various temperatures under CO_2 pressure, outside the reactor and then inside the reactor. One such concrete was subjected to a temperature of 350°C and the other to 450°C under CO_2 pressure. It was found that, to a large extent, the CO_2 became chemically fixed on the concrete, particularly under pressure. The physical properties are considerably degraded at elevated temperature as compared to ambient temperature. However, regardless of the CO_2 pressure used, there is practically no difference in the mechanical properties obtained at elevated temperature compared with those obtained in air at the same temperature. Under irradiation to an integrated flux of 10^{19} neutrons/cm^2, $E > 1$ MeV, in CO_2 atmosphere at a temperature between 200°C and 450°C, the two concretes behaved well with only slight change in their physical characteristics. It appears that these heat-insulating concretes, prepared with an aluminate base cement and expanded clay aggregate, are particularly suitable for PCRV's. They have low cost, a compressive strength of 100 bars at 450°C, and a thermal conductivity lower than 0.40 W/(m)(°C) at 250°C.

A concept of insulation by gas circulation screens was described by Freour, of the Société pour l'Industrie Atomique, and Wurdig, of Deutsche Babcock and Wilcox.[33] In this concept the cooling fluid in the "gas screens" is a cold gas of the same kind, and at the same pressure, as the gas in the primary circuit of the reactor. Also, the cooling-circuit heat exchangers and blowers, which circulate the gas in panels, are integrated into the vessel. The solution possesses the following advantages: (1) It eliminates the presence of water in the interior of the vessel structure, which can be very harmful in case of an accident. (2) The pressure in the interior of the tubes and collectors is equal to that in the interior of the reactor. (3) Because of this pressure equality, the thickness of the insulating structure can be less than it is in the case of the water cooling system; this considerably simplifies the problem of thermal expansion and reduces the weight of the insulation panels. (4) For the same reason, there is practically no possibility of ruptures in the collectors and cooling pipes, and there is no need to provide two parallel independent cooling circuits. This permits a material simplification of the cooling-pipe network. The purpose of the reported study was to determine the effectiveness of the insulation in the rectilinear portion of the vessels around the penetrations for the standpipes and tubing at the top and bottom of the vessel. From the test results it was concluded that the thermal insulation in these regions is very efficient.

The problems of thermal insulation in PCRV's for HTR's were investigated and reported by Naudin of the Société Bertin et Cie.[34] In HTR's the coolant is helium, and its important physical characteristics from the point of view of heat transfer are its specific mass, its thermal conductivity, its specific heat, and its radiation-absorption properties. The physical characteristics of helium as compared with those of CO_2 were set forth: (1) the specific mass is 11 times less than that of CO_2, and heat exchange by natural convection is therefore less serious; (2) since its thermal conductivity is about 10 times that of CO_2, thicker insulation is needed; (3) since its specific heat is about five times that of CO_2, the circulation of helium in the interior of the insulation needs careful examination; and (4) since helium is transparent to thermal radiation, there is less heat transfer through radiation. The temperature and pressure to which the thermal insulation is to be

subjected are, respectively, in the ranges 300 to 400°C and 40 to 50 bars. The methods of heating, the helium-circulating device, and the sensors for local heat-flux density measurements were described. The vessel in which the tests were conducted was a cylinder 1.2 m in diameter, 2.5 m in height, and closed by two hemispherical heads. It was capable of withstanding pressures to 50 bars. The results of tests with this model showed that the thermal insulation was satisfactory; its performance under full-scale applications could be easily extrapolated.

Two concepts of insulating PCRV's for water-cooled reactors were presented by Freour of the Société pour l'Industrie Atomique.[35] In a water-cooled PCRV, the liner must be protected against a high-temperature water–steam atmosphere. Therefore an insulating structure must be provided next to the liner. This insulant can lie either in the atmosphere of the inner cavity of the pressure vessel or in a specially created gaseous atmosphere adjacent to the vessel wall. The first insulating concept presented by Freour includes an inner, balanced-pressure casing separating the water–steam mixture from a layer of nitrogen. Counting from the concrete toward the inside of the vessel, the constituents of the cooling and insulation system are the liner cooling circuit, the liner, the metallic insulation, the nitrogen layer, the nitrogen casing, and the water–steam mixture. With such a system it is necessary to have an exterior circuit of nitrogen and a central nitrogen supply. There are three problems that need careful consideration: (1) disposition of the supports of the internal structure, (2) differential thermal expansion at transverse outlets, and (3) in the case of heavy-water reactors, reduction of the thickness of the nitrogen layer in order to balance the pressure on the two sides of the casing. The second insulating concept presented by Freour was the wet thermal insulant, i.e., insulation immersed in water. Although this solution is more attractive than the first concept, it will be more expensive due to the cost of heavy water, the greater thickness of insulant, and the considerable thermal losses; and it also introduces problems of structural disposition inside the vessel. The realization of this concept has not been studied in detail.

The possibility of applying corrugated metal sheets, which are used as thermal insulation in the EL-4 reactor tubes, to other reactor types was investigated by DuPont of Sud Aviation.[36] Insulation of the liquid-layer type is obtained very easily by simple superposition of corrugated metal sheets on two faces of flat sheets. Freedom in choosing the number of layers and the corrugation depth (and hence the thickness of the layers) from over a very wide range renders such insulation easily adaptable to all working conditions. Such insulation has been used successfully in the stainless-steel pressure vessel of the Phenix fast reactor. Application of such insulation is also envisaged for gas-cooled reactors, AGR's, HTGR's, and light- or heavy-water-cooled reactors using PCRV's.

Another concept of thermal insulation for PCRV's used for BWR's was presented during a discussion period by Menon of Sweden. In some respects the idea resembles the one presented by Freour.[35] The PCRV is of cylindrical shape, with the steel liner and its cooling circuit anchored to the inside of the cylinder. The thermal insulation is contained in a removable casing which encloses the reactor, the water, and the steam. The top head of the vessel is also removable and is held in position by a series of hydraulic jacks resting against a ledge near the top of the cylinder. The stainless-foil thermal insulation covers the side and the top of the casing on the inside. With the removable casing, it is possible to examine the insulation at the time of reactor shutdown. The gap between the casing and the steel liner can be filled either with gas or water, which is at the same pressure as the pressure inside the casing. Means are provided to balance the pressure inside and outside the casing. The bottom of the cylinder cavity is insulated through the hot-skin concept. Therefore the insulation at the bottom is not removable. The practicality of this concept was tested under a pressure of 95 bars on a model having an inside diameter of 4 m and a height of 7 m.

CONCLUSION

The chairman of the conference, P. Fernet, summed up the results of the conference and made some general comments on the various topics presented. He foresaw the increasing importance of nuclear energy. The use of HTGR's, large water-cooled reactors, and other advanced types of reactors has led to the consideration of PCRV's and has posed new technological challenges. From the papers presented, it was observed that numerous tests had been conducted. He felt that standards for tests must be established so that a systematic synthesis of the test results can be made and the test results correlated. Models are useful, but they are expensive and cannot be used for all variables. There is an urgent need to develop new materials to meet the requirements of the new types of reactor systems. Several more years may be required for the development of a practical and economical

insulation for PCRV's using these advanced types of reactors.

The advent of computers has helped the technology to meet the challenge. The imagination and ingenuity of scientists and engineers have progressively reduced the complexity of the problem from the technical level to the economical level and finally to the psychological level.

The development of nuclear energy has encountered much public resistance based on concern for safety. Mr. Fernet advised the participants not to engage in the senseless fight, but, instead, to devote themselves to the many technical problems that must be resolved in order to assure safety.

Finally, Mr. Fernet emphasized the cooperation between researchers and practicing engineers and between nations. The problems are not national, but rather international. In view of the fact that the Commission of the European Communities is not nationalistic, it can play its role freely and independently. He hoped that a specialist group on the technology could be formed within the next 2 years.

REFERENCES

The following are preprints of papers at the Second Conference on PCRV's and Their Thermal Insulation (to be published). Reference 37 is not cited in this article.

1. G. D. Whitman, Oak Ridge National Laboratory, Summary of a Program of Research and Development for Prestressed-Concrete Nuclear Pressure Vessels.
2. T. Jaeger, Bundesanstalt für Materialprufung, Berlin, The Conception of the Basic German Research and Development Programme for Prestressed-Concrete Reactor Pressure Vessels.
3. J. P. Arathoon and F. LeCars, Société pour l'Industrie Atomique, Paris; J. Muller and Ph. Moreau, Campenon Bernard, Paris, The Prestressed-Concrete Vessel of Vandellos Nuclear Power Plant.
4. J. L. Costaz, Electricité de France, First Results of the Commissioning of St. Laurent Prestressed-Concrete Pressure Vessel.
5. A. J. Williams and L. A. Tate, British Nuclear Design and Construction Limited; R. E. D. Burrow, Taylor Woodrow Construction Limited, The Interaction Between the Design and Construction of Prestressed-Concrete Pressure Vessels for Nuclear Reactors.
6. F. Dupay, The Practical Result Obtained on Our Prestressed-Concrete Vessels at the End of Eleven Years of Use.
7. J. A. Houben, R. C. N.–Petten; C. F. van der Schaaf, Bredero, Utrecht, The Irradiation of Mortar Samples in The Netherlands Reactor Center.
8. E. Crispino, S. Granata, and P. Risoluti, Agip Nucleare, Milano, Behavior of Concrete Under the Effect of Temperature and Radiation.
9. B. T. Kelly, J. Brocklehurst, D. Mottershead, and S. McNerney, United Kingdom Atomic Energy Authority; I. Davidson, United Kingdom Atomic Energy Authority, Risley, The Effect of Reactor Radiation on Concrete.
10. R. Ausangee, M. Boisserie, J. Corbel, S. Licheron, and M. Lida, Électricité de France, Paris, Study of the Properties of Concrete, Particularly Creep, Under the Effect of Temperature.
11. F. Dubois, Commissariat à l'Énergie Atomique; G. Noel, Centre d'Études et de Recherches du Batiment et des Travaux Publics, Paris, Determination of the Modulus of Thermal Rigidity $E_d\alpha$ of an Insulating Concrete Subjected to Thermal and Mechanical Stresses.
12. J. Irving and I. W. Goodall, Central Electricity Generating Board, Berkeley, Creep Behavior of Prestressed-Concrete Slabs with Reinforced Holes.
13. I. W. Hornby, Central Electricity Generating Board, Leatherhead, Moisture Measurements in Mass Concrete.
14. F. Bremer, Fried. Krupp GmbH Universalbau, Essen, Rupture Behavior of Concrete in the Multiaxial Stress State.
15. L. Muhe, Philipp Holzmann AG, Frankfurt/Main, Wire-Wound Circumferential Prestressing System with Several Secondary Anchorages for the Pretensioning Tendons (Prisma System).
16. L. Muhe, Philipp Holzmann AG, Individual Tendons for Vertical Prestressing with Breaking Strains over 1500 mp.
17. A. Puyo and J. Picaut, Coyne and Bellier, Paris, Experiment of Hoop Prestressing with High Tensile Steel Strip.
18. P. Rissler, Siemens AG, Erlangen, Reactor Pressure Vessels Made from Prefabricated Parts—Part Model for Testing Design Improvements.
19. H. P. Schrage, Fried. Krupp GmbH Universalbau, Essen, Results of Model Tests on Multilayer Pressure Vessels.
20. T. E. Northup, Gulf General Atomic, San Diego, Pressure and Temperature Tests and Evaluation of a Model Pressure Vessel.
21. J. P. Arathoon and A. Peuchmaur, Société pour l'Industrie Atomique, Paris, Pressure Vessels for Water and Gas Reactors.
22. J. P. Merot and M. Languille, Société d'Études et d'Equipments d'Entreprises, Paris, Prestressed Concrete BWR Pressure Vessels.
23. O. C. Zienkiewicz, R. Owen, and D. Phillips, University of Wales, Swansea, Nonlinear Analysis of Pressure-Vessel Behavior Including Cracking.
24. J. H. Argyris and I. Grieger, Three-Dimensional Elastic and Elastoplastic Analysis of Reactor Pressure Vessels.
25. G. Schnellenbach, Ruhr-Universitat Bochum, Institut für Konstruktiven Ingenieurbau, Dynamic Relaxation as a Practical Method for the 3-Dimensional Calculation of Prestressed-Concrete Pressure Vessels.
26. K. Brandes, Bundesanstalt für Materialprufung, Berlin, Numerical Methods for Calculating Prestressed-Concrete Reactor Pressure Vessels.
27. B. N. Furber and J. Davidson, Nuclear Power Group Ltd., Knutsford, The Thermal Performance of Porous Insulants in a High Pressure Gas Environment.
28. A. N. Kinkead and B. E. Pitchford, OECD Dragon Project Office, Dorchester, Performance of Thermal Insulation Immersed in Helium.
29. R. Grossin, M. Jannot, P. Micheau, and A. Pirovano, Société

Bertin et Cie, Paris; S. Klarsfeld, Cie de Saint-Gobain, Paris, Heat Exchange of Natural Convection in a Porous Medium.
30. L. Roure, Société Bertin et Cie, Paris, Behavior of a Thermal Insulant Under Cyclical Stresses of Aerodynamic Origin.
31. G. DeLort and Y. Lecour, Compagnie des Ateliers et Forges de la Loire, Firminy; Soulier of EDF-3, Thermal Insulation by Metallic Gauze and Sheet Metal—Industrial Application to the Prestressed-Concrete Vessel of the Bugey-I Reactor.
32. F. Dubois, P. Mauny, A. Bernard, and Mf. F. Elleuch, Commissariat à l'Énergie Atomique, Saclay, New Types of Heat Insulating Concretes for Nuclear Reactors.
33. A. Freour, Société pour l'Industrie Atomique, Paris, Insulation by Gas Circulation Screens.
34. P. Naudin, Société Bertin et Cie, Paris, Methods of Testing Thermal Insulants for HTR.
35. A. Freour, Société pour l'Industrie Atomique, Paris, Thermal Insulation for Water-Cooled Reactors.
36. J. DuPont, Sud Aviation, Suresnes, Thermal Insulating of Nuclear Reactor Vessels and Structures by Means of Corrugated Metal Sheets.
37. W. Muller and G. Zeitschel, Allgemeine Elektricitats-Gesellschaft-Telefunken, Frankfurt, Integration of a Prestressed Concrete Pressure Vessel into a Nuclear Power Plant and Comparison with a Plant with a Steel Vessel.

AMERICAN NUCLEAR SOCIETY—CRITICAL REVIEWS

Beginning with this issue the Atomic Energy Commission has contracted with the American Nuclear Society (ANS) to prepare for publication a series of detailed Critical Review articles written by experts selected from the ANS membership and reviewed by an advisory committee of top leaders and scientists in the field. In this issue the articles are on pages 124–169.

Members of the Critical Review Advisory Committee are:

Sidney Siegel, *Chairman*	*Atomics International*
Jack Chernick	*Brookhaven National Laboratory*
William Chittenden	*Sargent & Lundy Engineers*
Paul Lottes	*Argonne National Laboratory*
Peter Murray	*Westinghouse Electric Corporation*
David Okrent	*Argonne National Laboratory*
Herbert Parker	*Battelle–Northwest*
Joseph Prestele	*New York Consolidated Edison*
W. C. Redman	*Argonne National Laboratory*
Charles Stevenson	*Argonne National Laboratory*
Bertram Wolfe	*Battelle–Northwest*

ANS Critical Review Editor, *Norman H. Jacobson*

ANS Officers:

President, *Louis H. Roddis, Jr.*

Vice President, *N. J. Palladino*

Treasurer, *James R. Lilienthal*

Executive Secretary, *Octave J. Du Temple*

Comments on the articles should be communicated directly to the ANS Critical Review Committee or Editor, 244 E. Ogden Avenue, Hinsdale, Ill. 60521.

A Critical Review from the American Nuclear Society

Solubilities of Metallic Elements in Liquid Sodium

By T. D. Claar*

Abstract: *Solubility data have been collected and evaluated for metallic elements in sodium. The reliability of the data for the systems studied has been assessed on the basis of experimental techniques and internal consistency. On the basis of this evaluation, the most reliable data have been used to recommend a solubility–temperature relation for each system that has been well characterized.*

Industrial and government research laboratories have been actively investigating the solubilities of metallic elements in sodium ever since the alkali metal was first proposed as a coolant for nuclear reactors. The earliest sodium solubility work was reviewed in the *Liquid-Metals Handbook: Sodium–NaK Supplement*[1] in 1955. However, much of that work has limited value owing to the lack of adequate sodium purification, sampling, and analytical techniques. This is especially true in the case of the transition metals, whose solubilities are extremely small and are often greatly influenced by the presence of oxygen in the sodium.

Anthrop[2] conducted a literature review of the solubilities of transition metals in liquid alkali and alkaline-earth metals in 1967. Only the solubility data for Co, Fe, Ni, and Ta in Na available at that time were presented and evaluated. More recently, Walker[3] presented a partial literature survey as a portion of his doctoral thesis.

This article represents an effort to collect the available data for sodium–metal systems, evaluate them in the light of recent advances in techniques, and, if possible, recommend a preferred solubility expression for the various elements. This search was undertaken to aid in the evaluation of the performance of materials in the EBR-II reactor, utilizing analyses of its sodium coolant.

Much of the solubility information reported[1] in 1955 is not discussed, since so many conditions now known to affect solubility results were not fully realized at that time. With these exceptions the literature available as of December 1969 has been thoroughly reviewed and discussed.

Recommended solubility expressions have been calculated by least-squares analysis for those elements which have been studied well enough to yield reliable data. These calculated expressions can be compared with the relations obtained by the individual experimenters in Appendix A. Arrhenius-type behavior of the solutes was assumed in the analysis of the data. Under this condition the solubility–temperature relation can be expressed mathematically as

$$S^\circ = A \exp(-Q/RT)$$

where S° is the solubility at temperature $T(^\circ\text{K})$, Q(cal/gram mole) is the activation energy for the solution process, R is the gas constant (1.987 cal/(gram mole)(°K), and A is a constant. The assumption of Arrhenius behavior, which is valid at low concentrations where solute–solute interactions are unimportant, leads to the $\log S^\circ$ vs. $1/T(^\circ\text{K})$ solubility plots shown in the figures. The slope of this plot reflects the magnitude of the activation energy of solution.

In all instances except bismuth and tin, the term *solubility* refers to the concentration of element in solution in sodium in equilibrium with the solid element. The equilibria of bismuth and tin with sodium are described in the appropriate sections.

*Argonne National Laboratory, 9700 South Cass Ave., Argonne, Ill. 60439.

The solubilities of some elements are not known well enough to establish a solubility expression. The data available for these elements are presented in the appropriate graphs and can be analyzed to obtain a general idea of that element's solubility in sodium at temperatures of interest. However, the problems described for each element in the text should be considered to avoid the indiscriminate application of the data for conditions vastly different from those of the particular solubility experiment.

The first seven elements discussed are of practical interest because they are constituents of stainless steels and other alloys used in reactor systems. Most of the remaining elements included are present as impurities in reactor sodium.

LITERATURE SURVEY

Iron

One of the earliest sodium solubility studies was conducted by Epstein[4] on the Na–Fe system. He measured iron solubilities over the temperature range 231 to 483°C using sodium equilibrated with an iron container under an argon atmosphere. The liquid metal was sampled at temperature and dissolved in alcohol. The iron content was then determined by spectrophotometric techniques. Epstein calculated the least-squares fit to his data but did not report his experimentally measured values. Solubilities calculated from his expression range from 4.5 ppM at 200°C to 13.5 ppM at 500°C. In addition to the lack of original data, no mention was made of any attempt to control the oxygen content of the sodium. This lack of experimental information makes it difficult to interpret Epstein's results.

Baus et al.[5] investigated the solubility of iron in systems of varying oxygen activity: (1) sodium containing 30 ppM oxygen,[2] (2) sodium saturated with Na_2O, and (3) sodium containing Na_2O and NaOH. (No mention was made of actual oxygen analyses of the sodium.) Sodium in a stainless-steel container was vacuum distilled onto a previously irradiated ^{59}Fe specimen in another stainless-steel receiver. After an equilibrium period of 2 hr, a sodium sample was forced by nitrogen or argon pressure through a nickel filter into a crucible. The sample was then removed from the system for weighing and radiochemical analysis. After the sodium metal was reacted with alcohol and water, the iron was recovered by converting it to Fe_2O_3. The radioactivity in the Fe_2O_3 was then measured and the iron solubility calculated.

These workers found, as have others, that the apparent solubility of iron increased with increasing oxygen activity in the sodium. The apparent iron solubility increased more than fourfold upon saturating the original sodium (containing 30 ppM oxygen) with Na_2O. A further addition of NaOH increased the solubility by about 10-fold over that in the sodium having 30 ppM oxygen. This effect of oxygen content on iron solubility was observed over the 230 to 544°C experimental temperature range.

The use of the nickel filter may have introduced some uncertainty into the solubility measurements, since metals dissolved in liquid sodium have been shown by Weeks[6] to adsorb onto dissimilar metal surfaces. If such a phenomenon occurred in these experiments, the measured values may be lower than those at true equilibrium with pure iron.

Rodgers et al.[7] studied the iron solubility in sodium in both static and circulating systems constructed from stainless steel. The circulating loop system contained a cold trap to control oxygen activity. The sodium was sampled with nickel buckets after an equilibration period at the test temperature. The thiocyanate method was used to analyze the sodium for iron.

Solubility values in the circulating system ranged from 6 ppM at 213°C to 13 ppM at 518°C. The cold-trap temperature during these tests varied from 165 to 190°C, and the oxygen level was stated to have been 20 ppM.

Measured solubilities in the static system varied from 5 ppM at 218°C to 14 ppM at 521°C. The average iron concentration at 538°C was 9 ppM, at oxygen levels reported to range from 30 to 100 ppM.

They observed no increase in iron solubility when the supposed oxygen level in the sodium was increased from 20 to 450 ppM, although the corrosion rate of an iron specimen in the sodium increased 100-fold. Indications are that the sodium was not actually analyzed for oxygen but that calculations from literature values for Na_2O solubility were used in reporting oxygen concentrations. There was no mention of any steps taken to purify the sodium before experimentation.

Their results for iron solubility nearly coincide with those obtained by Epstein. It is interesting that these two studies, in which the oxygen activity was apparently neither controlled by special techniques nor confirmed by chemical analysis, yielded almost the same results.

Eichelberger and McKisson[8,9] have investigated iron solubility in liquid sodium purified by gettering

and fractional distillation. After purification, the sodium was exposed only to ion-pumped high vacuum. Major sodium impurities were carbon (8 ppM) and oxygen (2 ppM). Much effort was taken to preserve this purity during the equilibration and sampling steps. Their solute material was electron-beam floating-zone refined iron (99.996% purity). This material was formed into a solute crucible, which was equilibrated with sodium at temperature for 6 hr. After equilibration, the crucible was inverted to drain the sodium from the solute-metal vessel into a sample collector. The sodium was analyzed for iron concentration by atomic absorption spectrometry measurements using the lanthanum-carrier precipitation method. (A complete description of their analytical techniques is presented by Bingham et al.[10]) Their results showed a considerable amount of scatter and varied from 7 to 99 ppM over the experimental temperature range 500 to 1000°C.

Thorley and Tyzack,[11] in a report dealing with the corrosion of stainless steel in liquid sodium, mentioned an iron solubility of 7 ppM at 650°C in sodium containing 10 ppM oxygen, measured at the Reactor Materials Laboratory in Culcheth, United Kingdom.

Weeks and Singer[6,12,38] have studied the solubilities of many elements in liquid sodium, one of which is iron. Iron crucibles were prepared from electron-beam zone-refined material typically containing 22 ppM total oxygen, nitrogen, and carbon impurities. The crucibles were irradiated for periods up to 1 month before use in the solubility experiments. After extensive leak-checking and hydrogen-firing treatments, the solute crucible and molybdenum sampling cups were sealed into a 347 stainless-steel solubility chamber lined with molybdenum. The system was pressurized with an "ultrapure" grade of helium after a 24-hr, high-temperature outgassing.

Sodium, vacuum-distilled at 500°C, drained into the radioactive crucible after being condensed in a Nb–1% Zr tube at 200°C. The system was heated to the test temperature and allowed to equilibrate for periods up to 24 hr.

After equilibration, duplicate samples were taken at temperature in the molybdenum sampling cups and prepared for oxygen and iron analyses. The samples were analyzed for ^{59}Fe by activation analysis. Oxygen analysis was done by amalgamation.

In their first experiment, measured iron solubilities ranged from 0.1 ppM at 370°C to 1.0 ppM at 540°C. However, scatter of the data prevented the establishment of a solubility–temperature relation.

In further studies, Weeks et al. observed the effect of increasing oxygen activity on the apparent solubility of iron in sodium. In 482°C sodium containing 50 ppM oxygen, iron solubility was 0.3 ppM, whereas in sodium containing 460 ppM oxygen at 486°C, the solubility was determined to be 1.6 ppM. Thus, with about a ninefold oxygen increase, the apparent iron solubility increased by a factor of about 6.

More recently, a technique has been developed by this same group for continuously varying the oxygen content of sodium by means of oxygen additions in the form of Na_2O or Na_2O_2, followed by uranium gettering.[39] The results of radiochemical analyses of sodium samples taken from radioactive iron crucibles show that the iron content varies directly as the oxygen content of the sodium when the oxygen activity is above ~0.2 (i.e., when the oxygen concentration is >20% of the solubility at the temperature of interest). This is the most conclusive evidence yet that iron solubility in sodium is a function of the oxygen content.

By measuring iron solubility as a function of oxygen content at constant temperature, they have found it possible to extrapolate back to zero oxygen activity, and thus obtain what they feel is the true iron solubility at three temperatures—0.3 ppM at 486°C, 0.85 ppM at 550°C, and 1.65 ppM at 600°C.

The wide range of data obtained by the different experimenters makes choosing an iron-solubility curve a very difficult task. The observed discrepancies may be caused by interactions of the iron solute with sodium impurities, by solute interactions with container materials, or by the presence of particulate iron due to thermal cycling of the melt. At any rate the iron-solubility work of Weeks et al., involving oxygen doping and gettering of sodium, although limited, appears to have produced the most consistent and reliable data.

The least-squares fit to their "zero oxygen" data can be expressed as

$$\log S^{\circ}_{Fe}\,(\text{ppM}) = 5.16 - \frac{4310}{T(^{\circ}\text{K})}$$

This relation predicts a solubility of 3.1 ppM at 650°C, in relatively good agreement with the 7 ppM value reported by Thorley and Tyzack. This expression yields extrapolated values that are also consistent with the range of higher-temperature data of McKisson and Eichelberger. At 550°C the work of Weeks et al. produced iron-solubility results about 85 times higher

than those of Baus et al. and a factor of about 15 lower than the results of both Rodgers et al. and Epstein.

All the iron-solubility data, plus the recommended solubility expression, are presented in Fig. 1.

Chromium

Eichelberger and McKisson,[8] by their previously described techniques, measured chromium solubilities in the temperature range 700 to 1000°C. In their first series of experiments, 99.996% pure halide-purified chromium rods were equilibrated with sodium containing about 2 ppM oxygen. The chromium solubility was 2 to 3 ppM in the 700 to 1000°C range, with the temperature dependence being less than the uncertainty of the atomic absorption spectrometry (AAS) techniques used.

In later experiments the same solute rods were irradiated to ^{51}Cr and equilibrated with sodium as before. The solubility results measured by radiochemical techniques were generally higher than those obtained by AAS and showed a considerable amount of scatter (Fig. 2).

Singer et al.[38] have investigated the solubility of chromium in sodium that was gettered with uranium to less than 1 ppM oxygen. Problems were encountered with chromium precipitation in the melt during temperature cycling. Segregation of these metallic particles at the sodium/cover-gas interface was considered to be a possible problem. However, on the basis of 61 experimental runs, they indicated that the solubility of chromium in sodium at 650°C was 0.41 ppM (see Fig. 2).

Singer et al.[38] calculated a tentative chromium-solubility relation of $\log S^{\circ}_{Cr} = 9.35 - 9010/T(^{\circ}K)$, using both their data and those of Eichelberger and McKisson. The continued work of these two groups of investigators should reduce the uncertainties in the Na–Cr system as the sampling and analytical techniques are improved.

Nickel

Rodgers et al.[7] studied the solubility of nickel in static and dynamic sodium systems. Liquid-sodium samples were taken in stainless-steel cups and analyzed for nickel by the dimethylglyoxime wet chemical method.

In a nickel pot containing static sodium with 110 ppM oxygen, measured solubilities ranged from 4 ppM at 204°C to 10 ppM at 538°C. In the nickel system containing circulating sodium, only the solubility at 538°C was reported—10 ppM nickel in sodium whose oxygen content varied from 50 to 650 ppM. The investigators concluded that nickel solubility was independent of oxygen activity in the sodium. Again, a cold trap was used to control the oxygen content, but actual analyses for oxygen were not reported.

Kovacina and Miller[13] investigated nickel solubility in liquid sodium using a radiochemical technique with ^{63}Ni as the tracer.

The sodium was prepared by vacuum distillation from a nickel crucible into a Pyrex-glass container fitted with a sintered-glass filter. The sodium was then filtered into a radioactive ^{63}Ni equilibration crucible, which was contained in a stainless-steel vessel under an argon-gas blanket.

After equilibration, the sodium was sampled with a nickel crucible for oxygen and nickel analyses. The sodium was analyzed for oxygen using the mercury amalgamation technique; the nickel content of the sodium was determined by counting the weak beta emission of ^{63}Ni.

The experimenters obtained solubility measurements at six temperatures in sodium containing 20 to 50 ppM oxygen. The measured solubilities ranged from 0.005 ppM at 200°C to 0.012 ppM at 600°C.

The values obtained by Kovacina and Miller are generally lower than those of subsequent work by several orders of magnitude.

Lee and Berkey[14] equilibrated a nickel crucible (99.997% purity) with sodium containing <50 ppM oxygen at three temperatures over the range 297 to 449°C. The sodium was not further purified after it was received from the supplier.

A tantalum crucible covered the nickel-solute crucible so that the assembly could be inverted and the sodium sample collected after a 4- to 25-hr equilibration period. The collected sodium was quenched in the tantalum crucible by spraying liquid nitrogen onto the chamber. After complete solidification, the sodium sample was transferred to an argon glove box, where sodium rods were produced by suction and extrusion and submitted for analysis.

The sodium samples were analyzed by spark-source mass spectrography. The scatter of the data indicates that segregation of the solute during solidification may have presented a significant problem with respect to sample homogeneity.

Work has also been done on the Na–Ni system by Singer and Weeks[12] using the same experimental techniques as described for their work on iron solubility in sodium.

The nickel-solute crucible was fabricated from zone-refined ½-in.-diameter rod containing 58 ppM

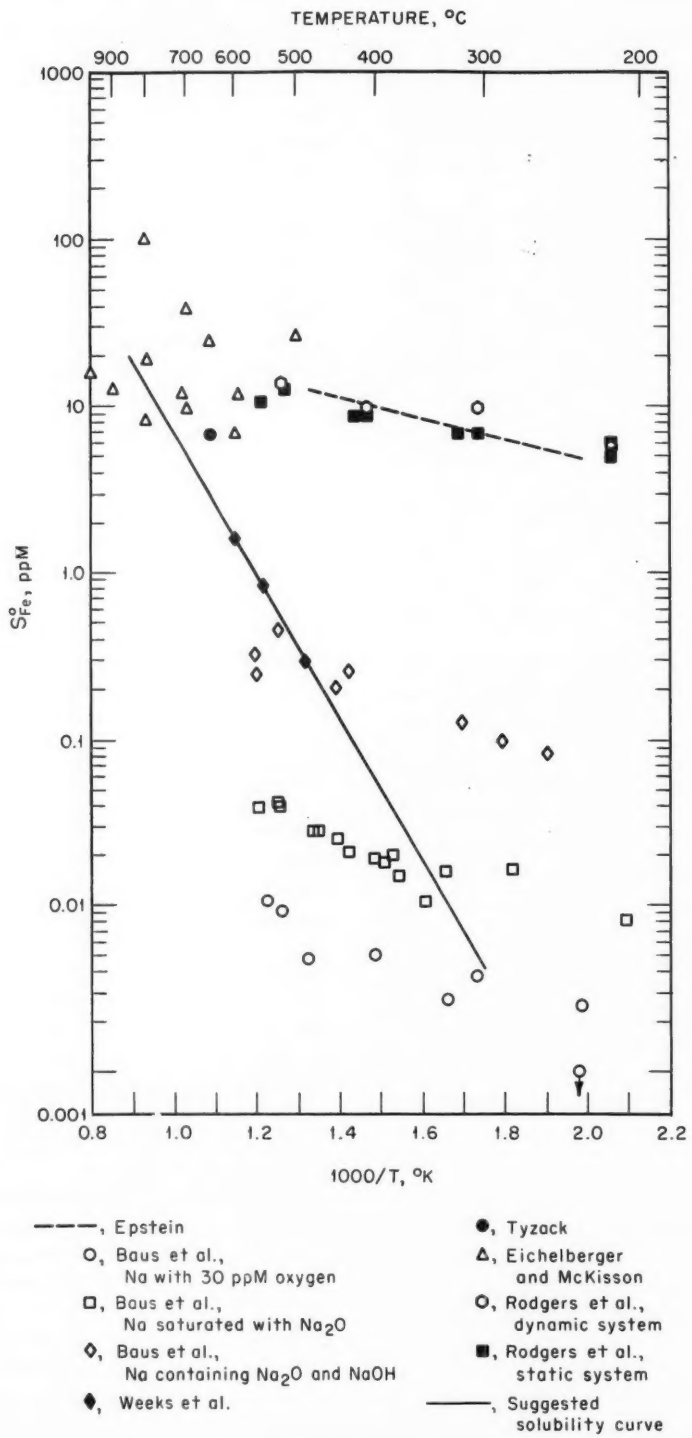

Fig. 1 Solubility of iron in sodium.

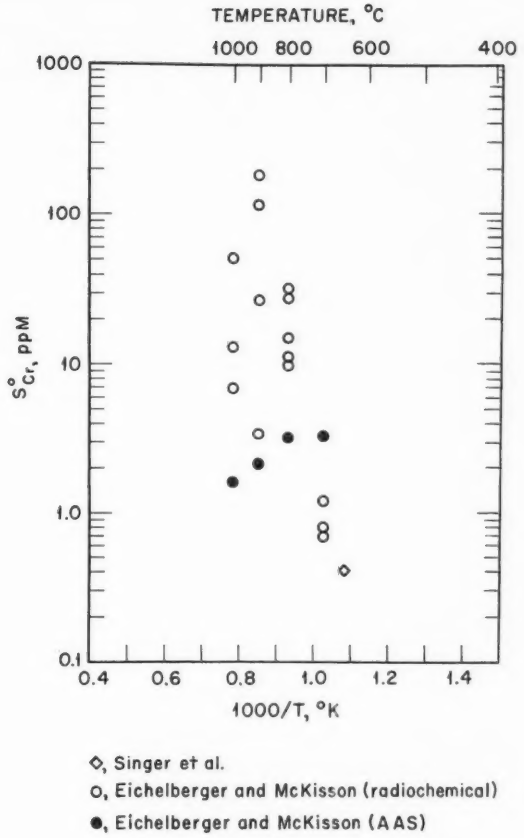

Fig. 2 Solubility of chromium in sodium.

total oxygen, carbon, and nitrogen impurities and 16 ppM total metallic impurities.

Their first nickel-solubility experiments were conducted in the temperature range 340 to 420°C. The data from these tests showed much scatter, which the experimenters attributed to two causes: (1) alternate cooling and heating about the equilibration temperature may have resulted in the formation of particulate matter in the sodium, and (2) the nickel content of the analytical blank used was of nearly the same magnitude as the nickel solubility.

In a second set of experiments, solubility measurements were made in the temperature range 446 to 600°C in sodium containing 20 to 50 ppM oxygen. In these tests, measures were taken to prevent thermal cycling of the melt, and replicate analytical samples were taken at each equilibration temperature. The solubility values measured in this second series of experiments ranged from 0.67 ppM at 446°C to 1.84 ppM at 600°C.

Eichelberger and McKisson,[8] using the same techniques as described for their iron-solubility work, determined nickel-solubility values ranging from 3.0 ppM at 700°C to 4.9 ppM at 900°C.

Kovacina and Miller[15] have reinvestigated this system with particular emphasis on the influence of oxygen content on the solubility of nickel in sodium. The equilibration apparatus included a hermetically sealed chamber connected with a sodium still. Sodium was purified by vacuum distillation from the still into a Pyrex-glass receiver. The distilled and solidified sodium was heated to a temperature just above the melting point and then filtered through a sintered-glass frit into a molybdenum crucible contained in the reaction chamber. This chamber was finally disconnected from the still assembly by flame-sealing the glass line between them.

In the first set of experiments, the sodium in the molybdenum crucible was equilibrated with varying amounts of pelletized NiO at 400°C. The NiO additions reacted with the excess sodium to form metallic nickel and Na_2O, thus establishing the oxygen activity of the sodium. After each of seven Na–NiO equilibrations, the nickel content of a filtered sample was determined by thermal-neutron-activation analysis. The nickel concentrations in sodium at 400°C were found to increase with increasing oxygen content up to the saturation level of Na_2O in sodium. At the 2.1 ppM oxygen level, 0.29 ppM nickel was measured, whereas at 127.8 ppM oxygen, the nickel concentration was found to be 11.6 ppM. The reported oxygen levels were calculated on the basis of the NiO additions to the 20-g sodium samples, rather than by actual analysis.

These investigators postulated the formation of a compound Na_2NiO_2 under the experimental conditions described. However, analysis of the reaction residue recovered from an experiment in which sodium supersaturated with oxygen (as NiO) was held at 400°C for several days showed it to be mainly reduced nickel, with no more than trace amounts of Na_2NiO_2.

The same procedures were used to determine the nickel concentration of sodium saturated with respect to Na_2O as a function of temperature. Measurements were made at three temperatures. The actual measured values were 8.5 ppM nickel at 300°C, 31.7 ppM nickel at 400°C, and 49.5 ppM nickel at 500°C. Again, Na_2NiO_2 was proposed as the soluble species.

Kovacina and Miller's latest work is the most demonstrative yet in showing the influence of oxygen

on nickel solubility in liquid sodium, although the mechanism of the interaction has not been conclusively defined.

The most reliable nickel-solubility work in low-oxygen sodium appears to have been done by Weeks et al., who covered the range 446 to 600°C, and by Eichelberger and McKisson, whose work was in the 700 to 900°C temperature range.

The data of these two investigations were pooled to establish the nickel-solubility relation

$$\log S^{\circ}_{Ni}\,(\text{ppM}) = 2.07 - \frac{1570}{T(^{\circ}\text{K})}$$

Kovacina and Miller's[15] measured value of 0.29 ppM nickel in 400°C sodium containing 2 ppM oxygen (calculated from NiO addition) agrees fairly well with this solubility curve, shown in Fig. 3 with all the nickel-solubility data.

Manganese

The solubility of manganese in ultrapure sodium is being measured at Atomics International[16] and Brookhaven,[6] but no results have been reported.

The mass transfer of manganese in sodium-cooled-reactor systems has been observed and studied[16] by tracing the movement of the radioisotope ^{54}Mn. That such a phenomenon exists implies that manganese does have a measurable solubility.

Cobalt

Grand et al.[17] measured cobalt solubilities at three temperatures from 365 to 525°C by equilibrating distilled and filtered sodium with a cobalt crucible. After the melt was maintained at the testing temperature for 24 hr under an argon atmosphere, a sodium sample was taken with a quartz pipette. The sodium sample and analytical standards were then irradiated, and the cobalt content was determined by radiochemical analysis. The measured solubilities ranged from 0.028 ppM at 365°C to 1.0 ppM at 525°C.

The presence of radioactive metallic impurities in the Na, particularly Fe, Cd, Sn, and Zn (totaling 1 to 10 ppM compared to the small cobalt concentration in the sodium) casts some doubt on the reliability of the data, since these impurities may have interfered with the cobalt counting procedure.

Lee and Berkey,[14] by the same techniques used in their nickel-solubility study, investigated the Na–Co system. Their solubility results, as determined by spark-source mass spectrography, exhibited an extreme amount of scatter, presumably due to segregation within the solidified sodium sample. Measured concentrations ranged from 0.07 to 14.4 ppM within the 289 to 544°C temperature span.

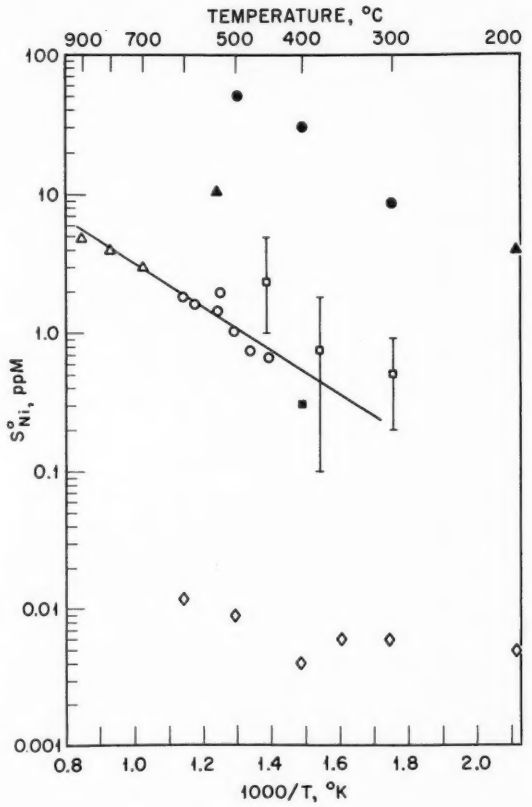

▲, Rodgers et al.
■, Kovacina and Miller (1969) low O–Na
●, Kovacina and Miller (1969) high O–Na
◇, Kovacina and Miller (1961)
△, Eichelberger and McKisson
○, Weeks et al.
I, Lee and Berkey (□, av. value)
—, Suggested solubility curve

Fig. 3 Solubility of nickel in sodium.

No cobalt-solubility relation can be established owing to the inconsistencies in the limited data that are available (Fig. 4).

Molybdenum

Eichelberger and McKisson[8] have also investigated the Na–Mo system using their previously described

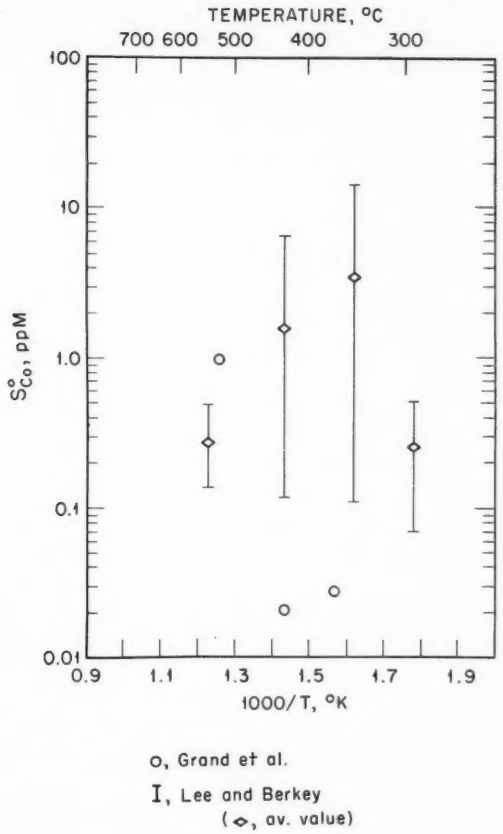

Fig. 4 Solubility of cobalt in sodium.

techniques. Molybdenum of 99.992% purity in the shape of a crucible was equilibrated with liquid sodium at five temperatures from 800 to 1000°C. Their results ranged from 0.5 ppM at 850°C to 1.3 ppM at 1000°C, and the least-squares fit to the data (neglecting the 800°C datum point) was calculated to be

$$\log S^{\circ}_{Mo}\,(\text{ppM}) = 3.27 - \frac{3962}{T(^{\circ}\text{K})}$$

Since all the data were obtained at temperatures above 800°C, discretion should be used in extrapolating to lower temperatures. (See Fig. 5.)

Copper

The Na–Cu system has been studied very extensively. Koenig et al.[18] measured copper solubilities at temperatures from 120 to 500°C by equilibrating a

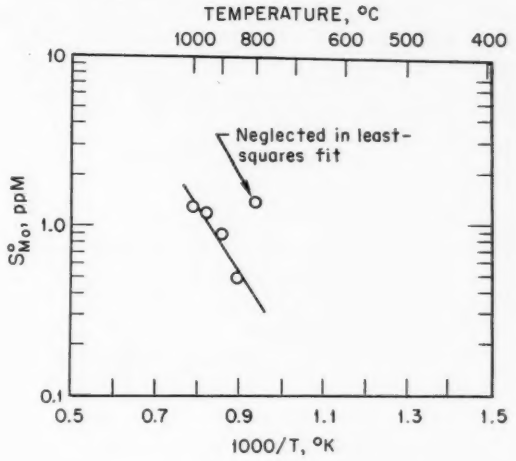

Fig. 5 Solubility of molybdenum in sodium. ○, Eichelberger and McKisson. ——, suggested solubility curve.

small sodium sample with a thick-walled copper crucible. To provide temperature control, he suspended the copper crucible in a thermostatted sodium bath within a stainless-steel pot. The sodium inside the crucible was filled separately so that it was never in contact with the stainless-steel surfaces. After equilibration, the sodium was sampled through a port under a flow of purified argon and analyzed for copper by a wet chemical method, probably colorimetry. Apparently, no special measures were taken to control or measure the oxygen content of the sodium.

The average solubilities measured at five temperatures are shown in Fig. 6.

Singer and Weeks[12] have studied this system over the 255 to 547°C temperature range using the same techniques as in their iron- and nickel-solubility studies. The equilibration crucibles were made from zone-refined 99.999% pure copper sheet (2 ppM total oxygen + carbon + nitrogen impurities). Duplicate samples were taken in two molybdenum sampling buckets mounted on the same rod, one above the other.

In the first of two runs, considerable data scatter was evident at temperatures below 300°C. During this run it was found that the lower of two sampling buckets often contained about 10 times as much copper as the upper bucket. The experimenters attributed this behavior to the precipitation of copper particles during cooling from previously higher test temperatures.

In the second run the same crucible was equilibrated at 550°C, cooled to about 250°C for 24 hr, and

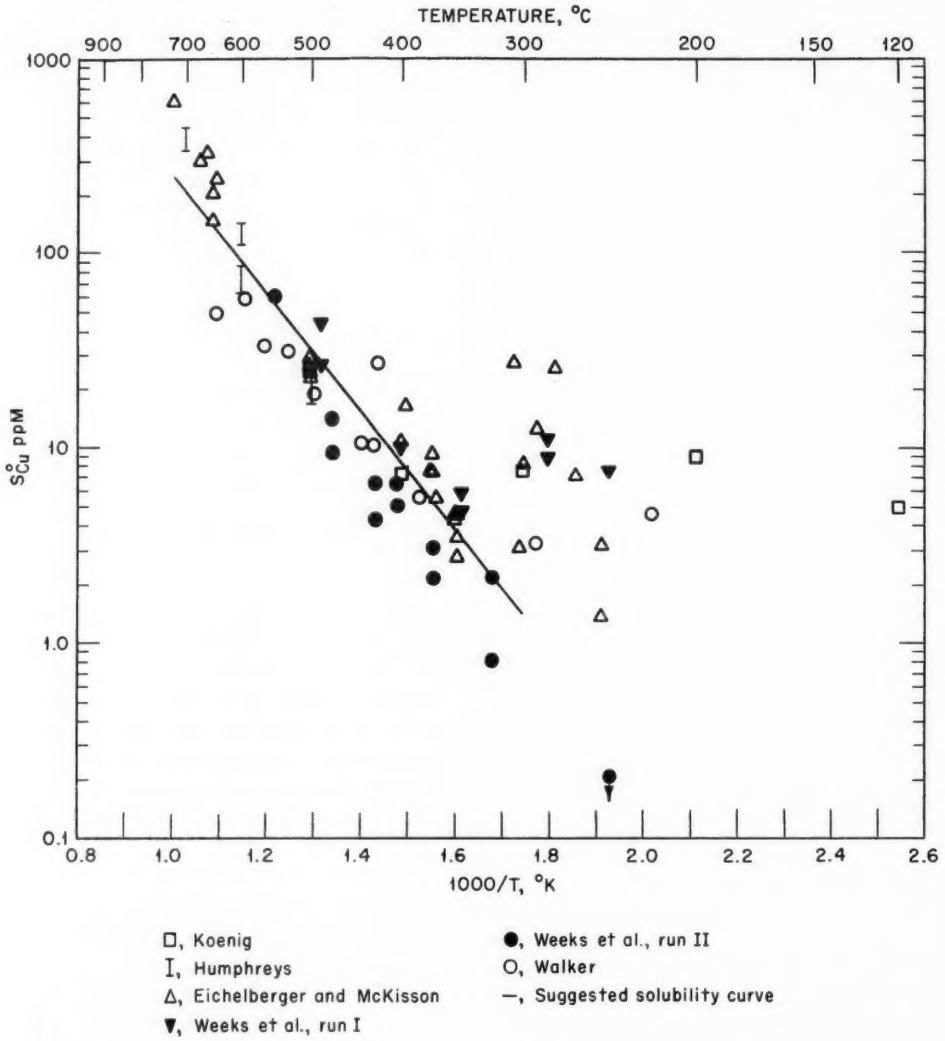

Fig. 6 Solubility of copper in sodium.

the melt sampled after the temperature had finally been raised to the equilibration temperature. This revised procedure produced data displaying less scatter than that obtained in the first run.

During both runs the oxygen content of the sodium did not exceed 15 ppM, as determined by the mercury amalgamation technique. Atomic absorption spectroscopy was used to analyze the sodium samples for copper concentration.

The copper-solubility values determined from the second run ranged from <0.2 ppM (below detection limits) at 245°C to 60 ppM at 547°C.

Eichelberger and McKisson,[8,19] by previously described techniques, obtained copper-solubility values showing fair agreement with those determined by other experimenters.

Their solute material was oxygen-free high-conductivity copper (99.95% purity) in the form of rods and crucibles, which were hydrogen fired at 600°C for 1 hr to reduce surface oxides that may have been present. The oxygen content of the sodium was maintained at about 2 ppM.

Solubilities were measured at temperatures ranging from 250 to 726°C. As in the work of other ex-

perimenters, considerable data scatter was evident at temperatures below 350°C, suggesting that particulate copper prevented the measurement of true solubility at these temperatures.

Humphreys,[20] in his copper-solubility work, equilibrated neutron-activated copper foils with sodium contained in stainless-steel capsules. Zirconium foils were used to hot-getter oxygen from the sodium. After gettering, the activated copper foils were exposed to the sodium for at least 17 hr before the sodium was analyzed for copper.

Solubilities measured at four temperatures were found to increase from 25 ppM at 500°C to ~400 ppM at 700°C.

Walker[3,21] equilibrated distilled sodium (16 ppM oxygen) and high-purity copper wire (10 ppM total impurity level) at various temperatures in a nickel crucible under an atmosphere of purified argon (99.999% purity with <2 ppM oxygen by volume). The entire solubility apparatus was contained in an argon dry box.

The sodium was heated in the nickel crucible at 650°C for 24 hr and stirred to facilitate equilibrium. It was then cooled to the first testing temperature and equilibrated there for 12 hr before sampling. Since particulate copper was observed to precipitate on the nickel-crucible surface at the sodium-vapor interface, stirring was discontinued during the last hour before sampling to allow copper particles to settle from the solution. The sodium bath was cooled to the next equilibrium temperature after each sample was taken. It was then reequilibrated, while being stirred, for 12 hr before the next sampling. Sodium samples were taken at 11 temperatures between 640 and 222°C.

Each sodium sample was dissolved in absolute alcohol in preparation for the chemical analysis for copper. The sodium diethyldithiocarbonate method was used to measure the copper concentration colorimetrically.

A Debye–Scherrer powder-diffraction analysis identified the deposit on the nickel crucible as face-centered cubic copper, indicating that the equilibrium was between virtually pure copper and the liquid-sodium alloy. The author concluded that there are no stable intermediate phases in the Na–Cu system, in agreement with some earlier studies conducted by Kienast.[22]

All copper-solubility results are presented in Fig. 6. At temperatures lower than 350°C, the data exhibit too much scatter to be meaningful. In the 350 to 500°C temperature range, fairly good agreement exists between the results of the various experimenters. The values at 600°C and above show a deviation from the rather linear behavior in the 350 to 500°C range. A least-squares analysis of all data above 300°C produced a solubility expression of the form

$$\log S^{\circ}_{Cu}\ (\text{ppM}) = 5.45 - \frac{3055}{T(^{\circ}\text{K})}$$

No investigators have reported any dependence of copper solubility on oxygen content of the sodium. This is in agreement with the fact that sodium oxide is much more stable than any of the copper oxides. In addition, there is no evidence of the existence of Na–Cu double oxides.[8]

Aluminum

The solubility of aluminum in sodium was measured by Brush[23] as part of a materials compatibility study between the two metals. The experimental procedure involved immersing 99.95% pure aluminum strips in a stainless-steel pot containing sodium that had been passed through a 5-μ filter; the entire system was under an argon atmosphere.

The melt was sampled at various temperatures ranging from 150 to 500°C after equilibration periods of 1 and 24 hr. One-gram sodium samples were taken in evacuated glass sampling bulbs and analyzed by wet chemical methods.

Brush questioned the reliability of the solubility results, since the sodium contained iron, nickel, and chromium that had been dissolved from the stainless-steel pot. These other solutes may have interacted with the aluminum in sodium to form Fe–Al or other such compounds. The greatest criticism of the work was that the oxygen content of the sodium was not determined. It is doubtful that the oxygen level was very low, since only minimal purification techniques (filtering) were employed. Since Al_2O_3 is more stable than Na_2O at the temperatures investigated, it is doubtful that the true aluminum solubility was determined. However, the values may present some idea of the type of solution behavior to expect when aluminum is exposed to high-oxygen sodium. Brush's data, which are plotted in Fig. 7, do not show enough variation with temperature to allow determination of a solubility relation.

Tantalum

Grand et al.[17] also investigated the solubility of tantalum using the same procedures as used in studying cobalt solubilities. As in their cobalt work, interference

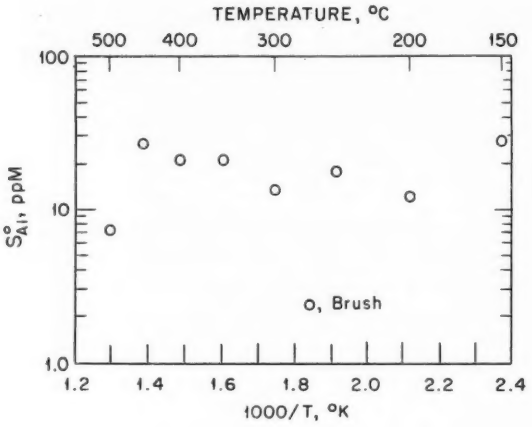

Fig. 7 Solubility of aluminum in sodium.

from other radioactive impurities in the sodium may have affected the reliability of the results. Their measured values ranged from 0.032 ppM at 325°C to 2.9 ppM at 525°C.

Humphreys[24] measured tantalum solubilities in zirconium-gettered sodium contained in tantalum capsules. Neutron-activated tantalum foils were placed in the capsules and equilibrated for at least 180 hr at the testing temperature. Radioactive counting techniques yielded solubility values ranging from 0.02 ppM at 650°C to 0.09 ppM at 791°C. It was concluded that systematic errors were larger than the true solubilities, and thus the data had little more than "order-of-magnitude" value.

The data from these two investigations are given in Fig. 8. In these studies, interference of impurities with radioactive counting and the production of fine tantalum oxide particles reduced the reliability of the results.

Niobium

Eichelberger and McKisson[8] investigated the Na–Nb system in the same manner as several other systems. Niobium of 99.983% purity was equilibrated with sodium at four temperatures in the 600 to 900°C range, with the measured solubilities ranging from 28 to 88 ppM.

Kovacina and Miller[25] measured the niobium solubility between 803 and 1380°C using a Nb–1% Zr alloy as the solute source and determining equilibrium concentrations in sodium by means of activation analysis. They used the same apparatus and techniques as described for their work on the Na–Ni system. The oxygen concentration in the sodium was not reported. Over the experimental temperature range, solubilities increased from 17.9 to 243 ppM.

Klueh[26] has investigated the effect of oxygen on the Na–Nb interaction at 600°C. He used zirconium foils to hot-getter the sodium and adjusted the oxygen content by means of weighed additions of Na_2O. The sodium and a niobium tab were contained in a niobium capsule under argon gas. After a 500-hr equilibration period, the capsule was quenched in liquid nitrogen. The sodium was then dissolved in isopropyl alcohol and precipitated as the chloride, the solution being analyzed spectrographically for niobium.

In Klueh's study, niobium solubility in sodium was found to vary greatly with the oxygen content of the liquid. At 600°C the solubility varied from about 35 ppM niobium with 100 ppM oxygen to about 2000 ppM niobium when the oxygen level was increased to 1000 ppM oxygen. An extrapolation to 1 ppM oxygen

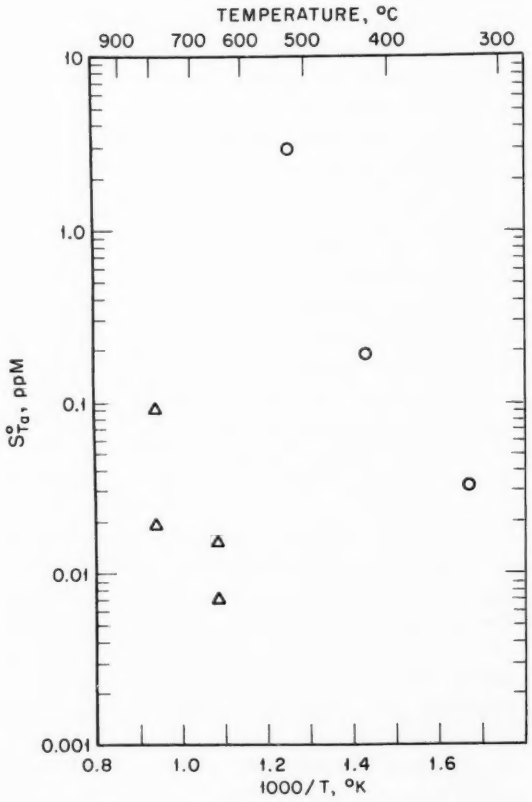

Fig. 8 Solubility of tantalum in sodium. ○, Grand et al. △, Humphreys.

yields a niobium solubility of about 10 ppM. This value is plotted in Fig. 9, along with the data of other experimenters. The strong oxygen effect observed by Klueh suggests that oxygen contamination may have been responsible for the scatter of all the niobium-solubility data. No relation between niobium solubility and temperature can be established on the basis of the data presently available.

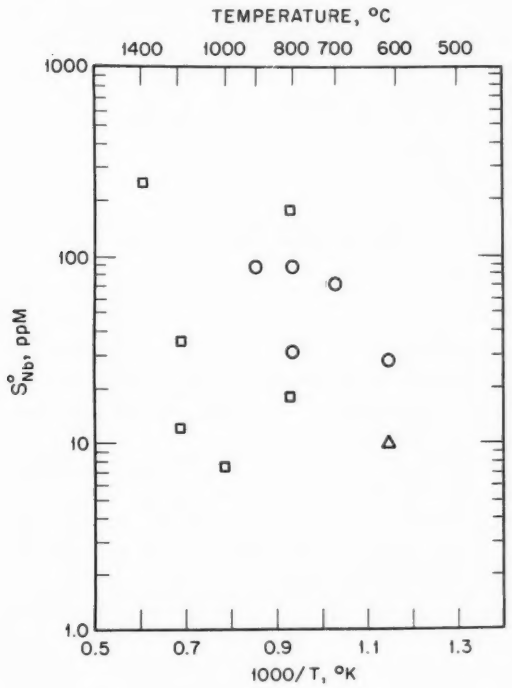

Fig. 9 Solubility of niobium in sodium.

Zirconium

Kovacina and Miller[25] also measured zirconium solubilities in the same experiments in which niobium was investigated. The results at six temperatures ranged from 0.77 ppM at 803°C to 3.60 ppM at 1380. The degree of scatter can be seen from Fig. 10. In this study the sodium impurity levels were not well established, and the use of a low-zirconium alloy (Nb–1% Zr) raises some doubt as to whether or not equilibrium was actually attained.

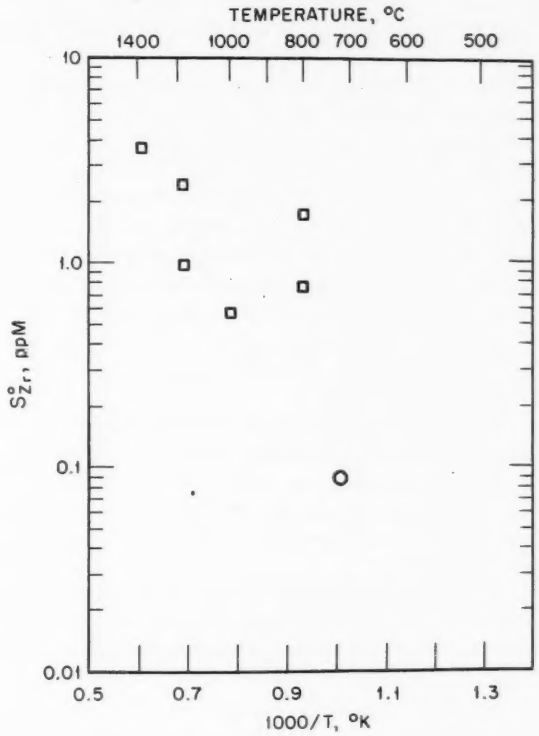

Fig. 10 Solubility of zirconium in sodium. □, Kovacina and Miller. ○, Humphreys.

Humphreys,[24] using neutron-activated zirconium foils under the same experimental conditions as in his copper work, determined a single zirconium-solubility value of 0.09 ppM at 722°C. Interference from other sodium impurities during the activity measurement caused Humphreys to conclude that this value was probably larger than the true solubility at 722°C.

Bismuth

Of all the systems studied in sodium-solubility work, Na–Bi is one of the best characterized. Bismuth exists in sodium not in elemental form, but rather as the compound Na_3Bi,* as determined by Walker[3] using X-ray diffraction analysis of the material precipitated during cooling of the melt. He investigated the solubility of bismuth in sodium at 10 temperatures from 253 to 563°C by equilibrating Grade I bismuth (total impurity <7 ppM) with sodium containing 16

*As used here, the "solubility" of bismuth in sodium refers to the bismuth content of sodium, present as Na_3Bi.

ppM oxygen in an electroformed nickel crucible. The experiment was conducted in an argon-atmosphere dry box.

The Na–Bi mixture was heated, while stirring, to a temperature above the first testing temperature for a 24-hr period. The melt was then cooled to the first sampling temperature (563°C), where it was equilibrated for an additional 12 hr. During the final hour of equilibration, the melt was not stirred, and any insoluble bismuth could precipitate before sampling. The solution was sampled in another nickel crucible and then allowed to cool to the next sampling temperature for a 12-hr equilibration period. This cooling–equilibrating–sampling cycle was repeated for each of the sampling temperatures.

The samples were removed from the dry box in bottles and weighed. Following weighing, the sodium was dissolved in alcohol in preparation for bismuth chemical analysis, which showed that the solubility ranged from 84 ppM bismuth at 253°C to 7.7 wt.% bismuth at 563°C.

Gehri and Sullivan[27] studied bismuth solubilities in the temperature range 200 to 650°C. The compound Na_3Bi was prepared in a high-vacuum system from high-purity bismuth and sodium (<22 ppM total impurities) that had been hot gettered and distilled. The Na_3Bi, used as the solute, was transferred to an argon glove box where it was placed into a stainless-steel solubility capsule. The capsule was then moved to a high-vacuum chamber where the argon was pumped out and the high-purity sodium added. The loaded capsules were equilibrated for a 20-hr period at the desired temperature.

After equilibration, the capsules were inverted at temperature to allow the 150- to 300-μ screen within the capsule to separate the still undissolved Na_3Bi from the solution. The sodium was analyzed for bismuth content by dissolving it first in alcohol, water, and finally dilute nitric acid. Measuring the bismuth in this solution by means of atomic absorption spectroscopy showed that the solubility ranged from 38 ppM bismuth at 203°C to 13.04 wt.% bismuth at 648.5°C.

Johnson[28] conducted thermal-analysis experiments to obtain information about the Na–Bi phase diagram. The breaks in the solubility curve or the halts in the peritectic and eutectic reactions were measured at six fixed compositions ranging from 32.4 wt.% bismuth to 75.3 wt.% bismuth. His measured solubilities ranged from 32.4 wt.% bismuth at 650°C to 75.2 wt.% bismuth at 848°C.

Brown et al.[29] measured low-temperature bismuth solubilities by equilibrating bismuth metal with reagent-grade sodium within an argon glove box. The solution was continuously stirred during the 4- to 24-hr equilibration period. The solution was finally filtered through a fine-porosity glass frit, and the bismuth content was determined by means of atomic absorption spectroscopy. Their results ranged from 6.4 ppM bismuth at 125°C to 207 ppM bismuth at 250°C.

Considering the data of all experimenters shown in Fig. 11, the solubility curve appears to break at about 290°C. A least-squares analysis of the data points above and below 290°C yields the following two equations: In the range 290 to 650°C

$$\log S^{\circ}_{Bi}\,(\text{ppM}) = 5.67 - \frac{4038}{T(^{\circ}\text{K})}$$

and from 125 to 290°C

$$\log S^{\circ}_{Bi}\,(\text{ppM}) = 2.15 - \frac{2103}{T(^{\circ}\text{K})}$$

Indium

Lamprecht[30] et al.[31-33] have investigated the solubilities of In, Ag, Zn, Sb, Sn, Pb, and Ce in liquid sodium using generally the same experimental techniques for each solute.

Commercial sodium, with a 0.028% maximum-impurity specification, was purified by three-stage filtration (5-μ porosity final filter) to yield a solvent containing 11 ± 2 ppM oxygen, as determined by vacuum distillation analysis.

Spectroscopically pure metals were irradiated in a thermal-neutron flux to produce radioactive solute tracers. Each radioactive solute was equilibrated with the purified sodium for 6 hr in a flask constructed from either glass (low-temperature tests) or stainless steel (high-temperature tests). Purified helium was bubbled through the melt to promote equilibration of the system.

When equilibration had been completed, the liquid alloy was separated from the undissolved metal solute by increasing the helium pressure and forcing the liquid through a capillary tube into a receiving vessel. A sodium iodide detector placed beneath this vessel was used to measure the activity of the alloy, which was subsequently correlated with the liquid-alloy composition. Following the activity measurement, the sodium alloy was forced back into the first flask where the above steps were repeated to measure solubilities at higher temperatures.

Lamprecht employed a closed experimental system in an attempt to overcome the problems associated

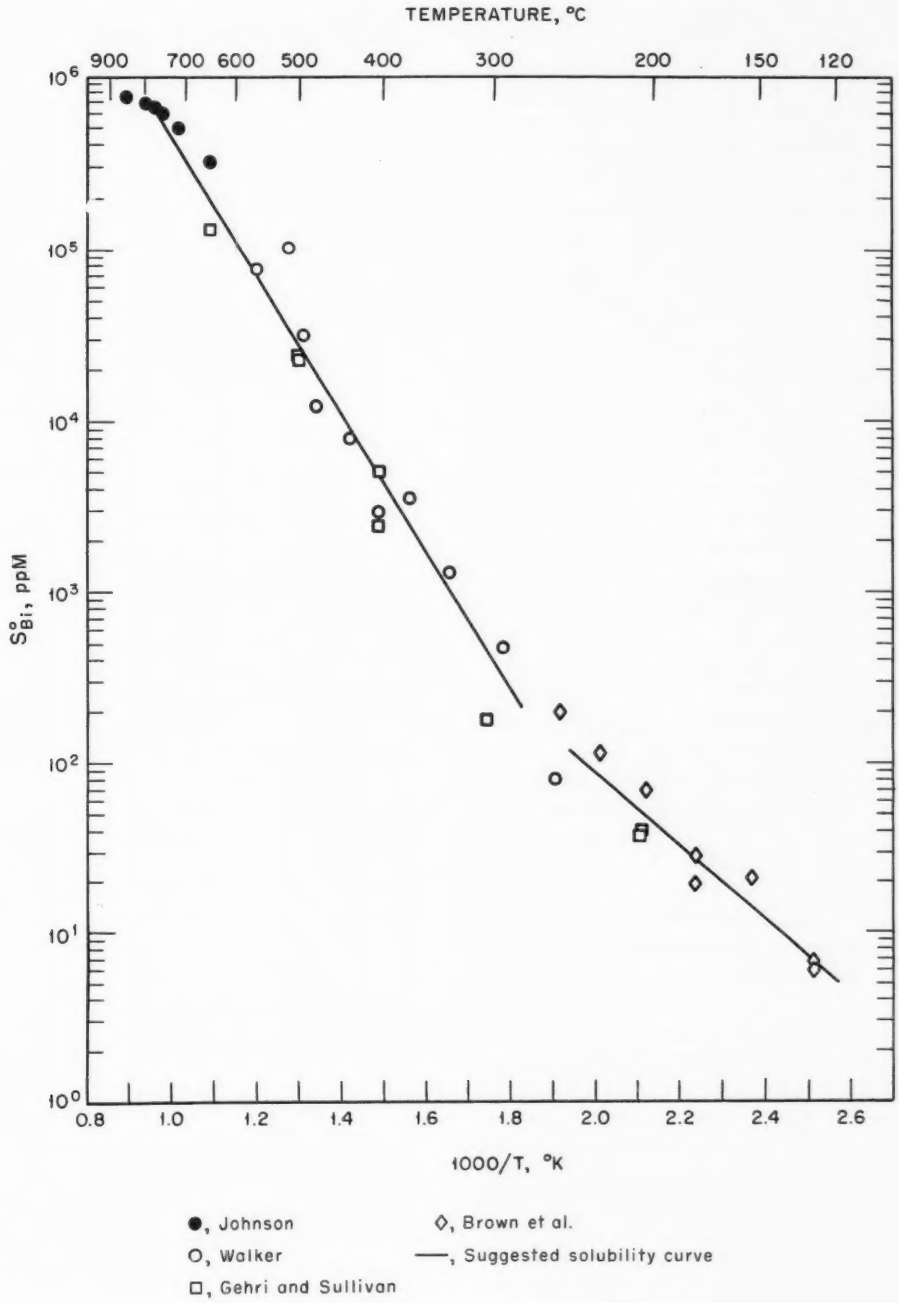

Fig. 11 Solubility of bismuth in sodium.

with oxygen contamination and inhomogeneities in sampling. The self-consistency of his data shows that he was fairly successful in his efforts.

Lamprecht's results for indium solubility ranged from 3.33 wt.% at 116°C to 21.45 wt.% at 221°C.

Weeks and Davies[6,34] investigated the solubility of indium in liquid sodium over the temperature range 102 to 269°C. The 99.9(8)% pure sodium was purified by hot-gettering it with a 50% Ti–50% Zr alloy. The Na–In alloy melt was equilibrated in a zirconium crucible contained within a stainless-steel furnace chamber. To prevent vaporization loss of sodium or indium, these investigators maintained a purified helium atmosphere (2 to 5 psig) over the system.

The melt was held at a temperature well above the first sampling temperature for 48 hr, then cooled to ~270°C, and maintained there for 24 hr before sampling with a stainless-steel cup. The sampling cups were fitted with a stainless-steel filter through which the samples were forced by increasing the helium pressure in the system to about 15 psig. After the first sampling the alloy was cooled to the next testing temperature and held there for 24 hr before withdrawing the next sample.

The sodium samples were dissolved in ethanol, and the solution was analyzed by wet chemical methods for indium. The measured solubilities ranged from 1.85 wt.% at 102°C to 36.9 wt.% at 269°C.

The data of Lamprecht and of Weeks and Davies (Fig. 12) were combined to yield a least-squares fit for indium solubility of $\log S^{\circ}_{In}$ (wt.%) = 4.48 – 1562/T(°K), over the range 100 to 300°C.

The experimental procedures employed in Weeks's indium study were also used by him to measure Cd, Ag, Sn, and Sb solubilities in liquid sodium.

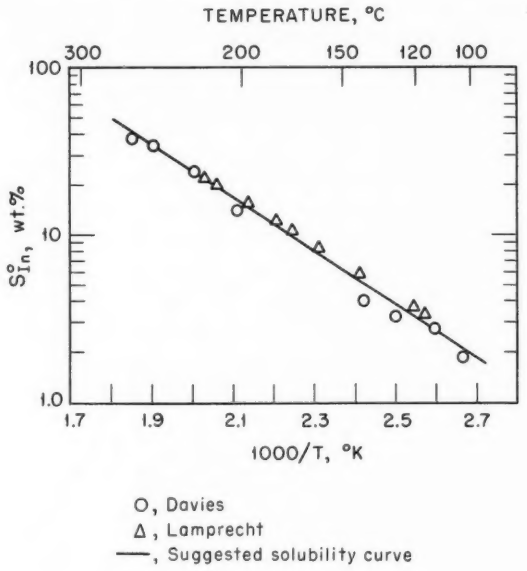

Fig. 12 Solubility of indium in sodium.

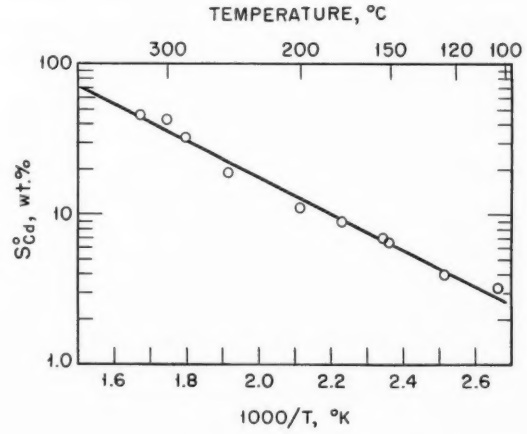

Fig. 13 Solubility of cadmium in sodium. ○, Weeks and Davies. ——, suggested solubility curve.

Cadmium

Weeks and Davies[6,35] measured cadmium solubilities ranging from 3.22 wt.% at 102°C to 46.2 wt.% at 326°C. Their data, shown in Fig. 13, appear to be reliable, with very little scatter. A least-squares fit to the experimental values was calculated to be $\log S^{\circ}_{Cd}$ (wt.%) = 3.67 – 1209/T(°K).

Silver

Weeks[6,36] obtained silver-solubility values that increased from 0.21 wt.% at 104°C to 21.5 wt.% at 518°C. Lamprecht investigated mainly low-temperature solubilities and found values of 0.35 wt.% at 136°C to 3.09 wt.% at 260°C.

The data from these two studies are seen to agree very well in Fig. 14. Pooling the data and calculating a least-squares fit yielded a solubility expression of $\log S^{\circ}_{Ag}$ (wt.%) = 3.22 – 1479/T(°K).

Zinc

Lamprecht's data for the Na–Zn system are shown in Fig. 15. The solubility of zinc was found to vary

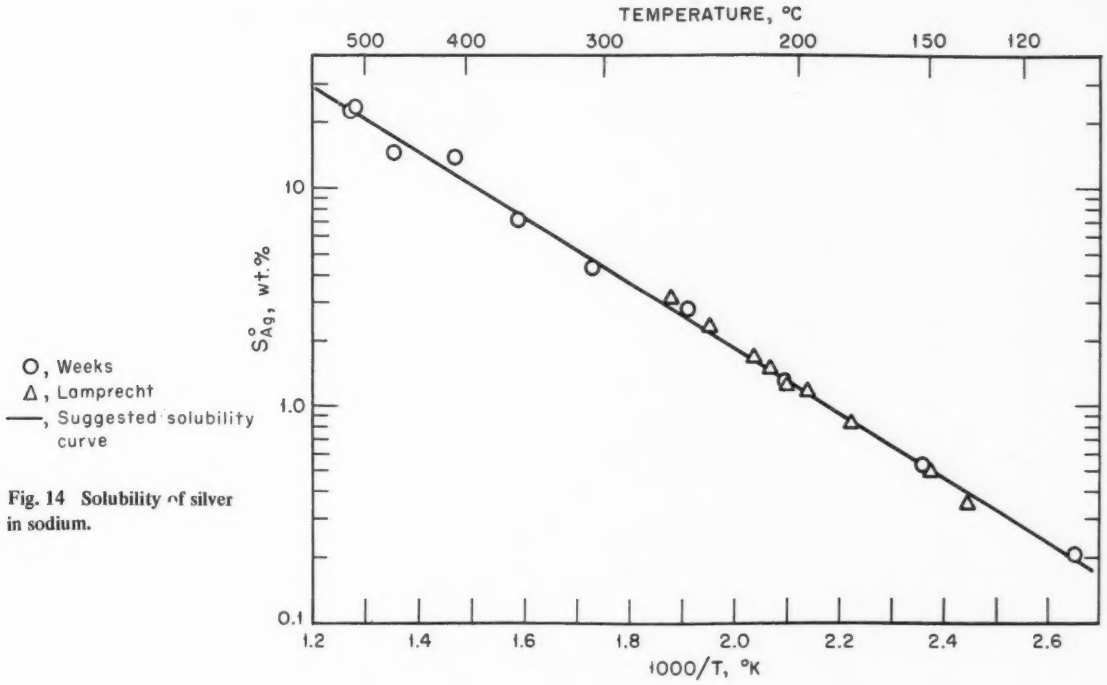

Fig. 14 Solubility of silver in sodium.

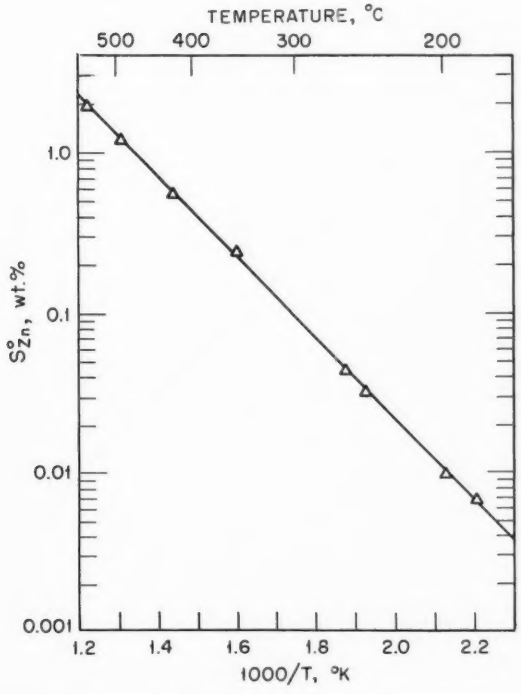

Fig. 15 Solubility of zinc in sodium. △, Lamprecht. —, suggested solubility curve.

from 67 ppM at 181°C to 2 wt.% at 543°C and can be expressed as $\log S^{\circ}_{Zn}$ (wt.%) = 3.44 – 2551/T(°K). The internal consistency of Lamprecht's work is again evident from the results of this study.

Tin

Lamprecht found that tin exists in sodium in the form of the compound Na_3Sn. Similar to the bismuth case, tin concentrations in sodium are based on the equilibrium of sodium with Na_4Sn, and the tin solubility is really the tin content of the sodium present as Na_4Sn.

Lamprecht's solubilities ranged from 0.15 wt.% tin at 120°C to 5.24 wt.% tin at 258°C. Weeks measured tin solubilities of 0.06 wt.% at 170°C to 1.70 wt.% at 391°C. The least-squares fits of Lamprecht and of Weeks were averaged to yield a recommended solubility expression of $\log S^{\circ}_{Sn}$ (wt.%) = 5.03 – 2326/T(°K). The data, shown in Fig. 16, deviate from this suggested curve at temperatures above 300°C because of the high solute concentrations at these temperatures.

Lead

Lamprecht's results for lead solubility, which varied from 0.58 wt.% at 119°C to 18.40 wt.% at

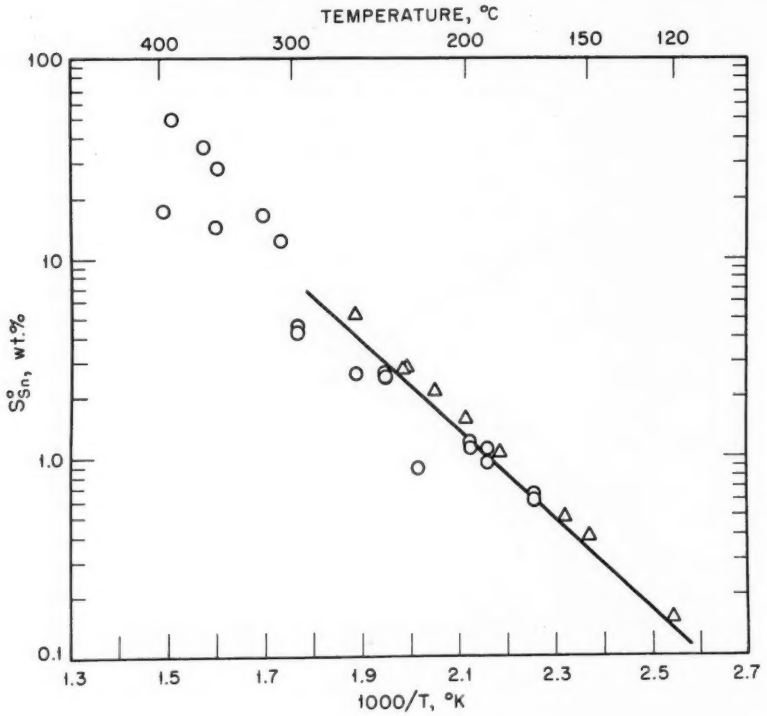

Fig. 16 Solubility of tin in sodium.

244°C, are shown in Fig. 17. The solubility was found to follow the equation log S°_{Pb} (wt.%) = 6.06 – 2465/T(°K).

Antimony

Work on this system by Lamprecht yielded values of 17 ppM at 183°C to 1082 ppM at 550°C.

Weeks[6] also investigated this system, with his results increasing from 50 ppM at 358°C to 3400 ppM at 574°C. As shown in Fig. 18, these data exhibited a considerable amount of scatter. He attributed the scatter to density differences between sodium (0.97 g/ml) and antimony (6.62 g/ml). The melts were taken through heating–cooling cycles, and, since there was little stirring, there was some problem in getting antimony back into solution after the cooling phase.

Lamprecht's data were used to obtain an antimony-solubility expression of log S°_{Sb} (ppM) = 5.28 – 1839/T(°K).

Cerium

The solubility of the rare-earth metal cerium in sodium was found by Lamprecht to vary inversely with temperature, decreasing from 0.085 ppM at 130°C to

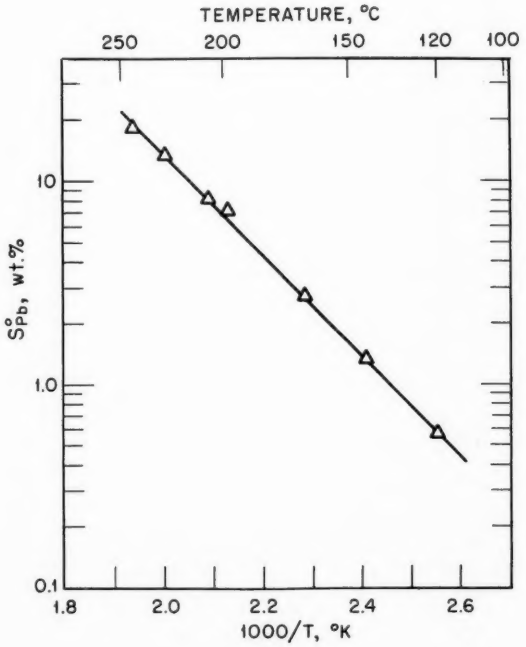

Fig. 17 Solubility of lead in sodium. △, Lamprecht. —, suggested solubility curve.

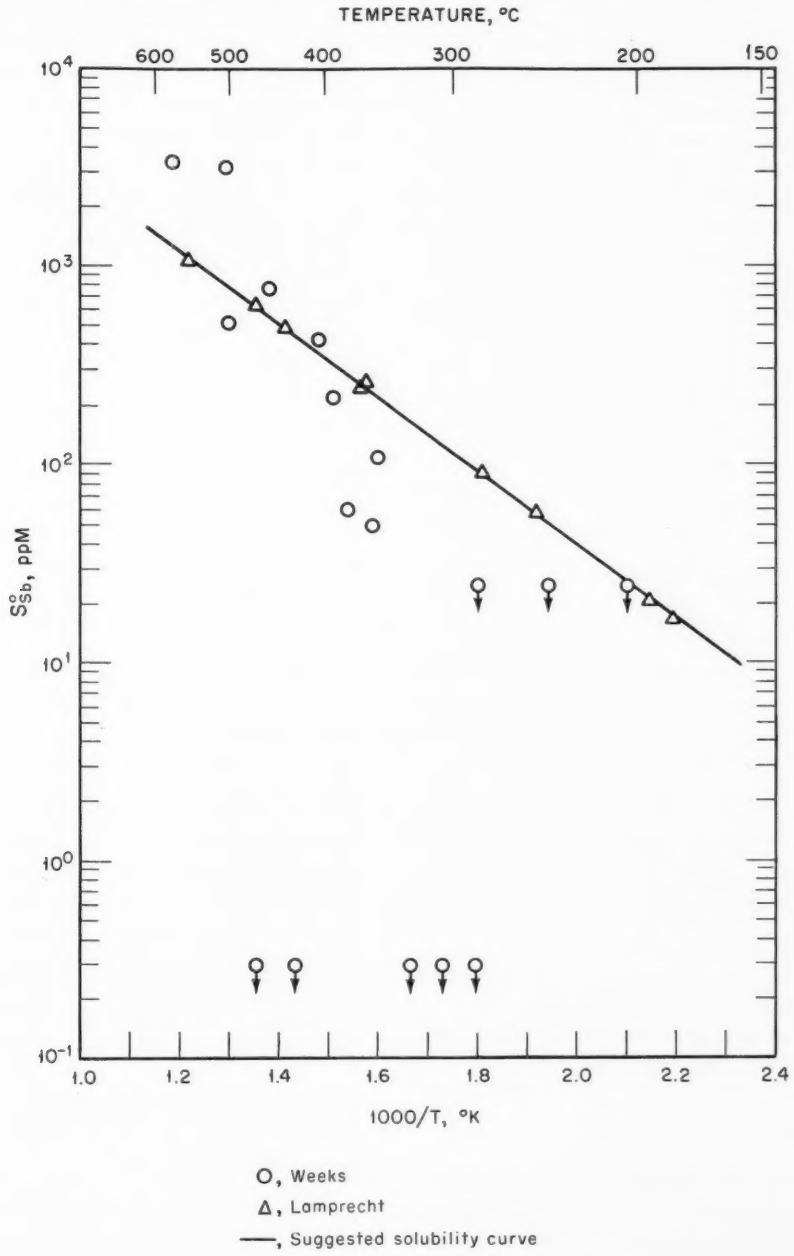

Fig. 18 Solubility of antimony in sodium.

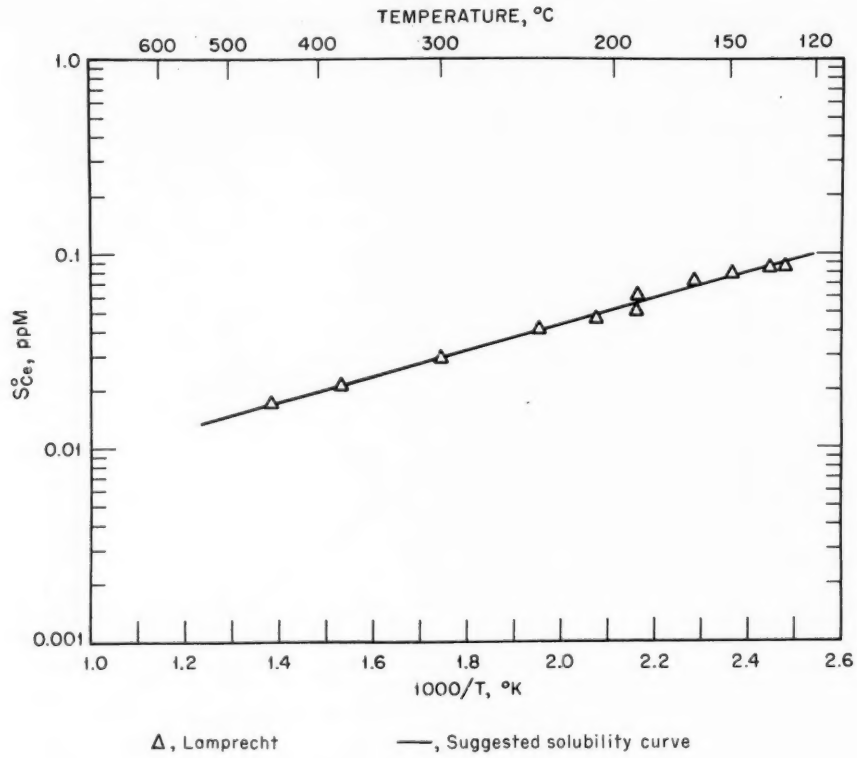

Fig. 19 Solubility of cerium in sodium.

0.017 ppM at 450°C (Fig. 19). On the basis of Ce_2O_3 and Na_2O free energies of formation, and the variation of Na_2O activity with increasing temperature, Lamprecht concluded that Ce_2O_3, not cerium, is the reference solute in this particular system containing 11 ppM oxygen. The solubility of cerium as Ce_2O_3 in sodium with 11 ppM oxygen can be expressed as log $S^{\circ}_{Ce}(\text{ppM}) = -2.68 + 658/T(^{\circ}\text{K})$. Solubility and free-energy considerations indicate that elemental cerium is less soluble than the oxide.

DISCUSSION

The work on the transition metals in sodium, especially those elements found in reactor materials, has shown encouraging improvement in the last several years. Although the solubilities of Fe, Ni, Cr, and Mn are generally low, they are important from the viewpoint of mass-transfer characteristics in reactor sodium systems and are still being studied.[38]

Some of the Group IIB metals (e.g., Zn, Cd, Sn, and Bi) have larger solubilities that have been fairly well established. These elements are of interest in reactor systems mostly from the aspects of interaction with reactor materials and possible methods of removal from the sodium (cold trapping, etc.).

The solubility data plots for several of the elements show an extreme amount of scatter. These discrepancies between the data of different investigators for the same system are best explained by considering the difficulties involved in sodium solubility work.

EXPERIMENTAL PROBLEMS

Sodium Purity

One of the major problems encountered was that of achieving and maintaining a low oxygen level in the sodium. In the earliest experiments, especially in the study of iron, the importance of the oxygen interaction with the solute being studied was not realized. After the oxygen effect was observed, attempts were made to control the oxygen level by cold-trapping the sodium. Taking advantage of the temperature de-

pendence of oxygen solubility in sodium, the cold trap would ideally maintain the oxygen level at the solubility limit at the cold-trap temperature. However, some experimenters have apparently relied solely upon the cold-trap temperature for determining the oxygen content of their system rather than actually analyzing the sodium. Such a practice may have led to erroneous results for several reasons. First, when a cold-trap temperature is decreased, the oxygen level is not immediately adjusted to the concentration at the solubility limit. Following the oxygen concentration in a recirculating cold-trapped system with an electrochemical oxygen meter, experimenters[37] found that the oxygen level was still approaching the solubility limit at the cold-trap temperature after several weeks of operation. Of course, the cleanup period depends on the characteristics of the particular system being studied. Other complications may arise when the cold-trap temperature is increased. As the oxygen level increases, oxygen may react with the iron and chromium constituents of constructional materials[12] or with metallic impurities dissolved in the sodium. In either case the cold-trap temperature alone does not control the oxygen activity of the sodium.

Purification methods have acquired a considerable degree of sophistication since the first experiments were conducted. Vacuum distillation and uranium-gettering techniques have greatly increased the purity of the sodium,[39] especially with respect to oxygen. Oxygen concentrations of <1 ppM are now being reported in solubility studies. This improvement in oxygen control has made it possible to study real effects of oxygen on the solubility of elements such as iron, nickel, and chromium.

It appears that carbon, nitrogen, and hydrogen are less influential on solubility measurements. There have been no instances reported in which the formation of solute carbides, nitrides, or hydrides has seriously hampered solubility determinations in well-controlled experiments. Thus these concentrations in sodium (typically 1 to 10 ppM) seem to be less critical than the oxygen concentration.

Equilibration and Sampling

Experimenters are becoming more aware of the phenomena that may interfere with the attainment of equilibrium within a liquid-metal system. The adsorption of dissolved metallic impurities onto dissimilar metal surfaces has made it necessary for workers to use much discretion in their choice of apparatus materials.

Because of the temperature dependence of metallic solubilities, even slight thermal cycling of the sodium bath can cause tiny metallic particles to precipitate from the solution. If these particles are allowed to form, they may interfere with equilibrium in several ways. They may remain suspended in the solution and be taken up with the sodium sample, or they may segregate at a sodium/cover-gas interface. Stringent thermal control has alleviated this problem greatly. A second approach has been to let the particles form and then allow the sodium to remain stagnant while the particles settle to the bottom of the melt.

Analysis

Since the solubility of many metals in sodium is so low even at relatively high temperatures, analysis of sodium for these trace amounts (often <1 ppM) becomes a real problem. Early experimenters used wet chemical and radiochemical methods of analysis. Wet methods often lacked the sensitivity for working in these small solute concentrations. Radioactive tracer techniques were sensitive enough to the particular element being studied, but other metallic impurities were sometimes present at much higher concentrations than the solute and interfered with the solubility measurement.

As solubility work progressed, new analytical tools were developed. Atomic absorption spectrometry and spark-source mass spectrography are now used effectively to measure solute concentrations in the sub-ppM range.

Rather than go into a detailed discussion of present analytical techniques, interested readers are referred to Appendix B for a partial list of references dealing with this subject.

ACKNOWLEDGMENTS

This work was performed under the auspices of the U. S. Atomic Energy Commission.

APPENDIX A: SOLUBILITY EXPRESSIONS

Table 1 Solubility Expressions of Individual Investigators

Element	Investigators	Expression	Experimental temperature range	Ref.
Iron	Epstein	$S^{\circ}(\text{ppM}) = -1.47 + 0.030\,t(^{\circ}\text{C})$	231–482°C	4
	Baus et al.	$S^{\circ}(\text{ppM}) = 2.28 \times 10^{-3} - 1.63 \times 10^{-5} t(^{\circ}\text{C}) + 5.63 \times 10^{-8} t^2(^{\circ}\text{C})$	230–544°C	5
	Rodgers et al.	$S^{\circ}(\text{ppM}) = 0.5 + 0.0122t(^{\circ}\text{F})$	400–1000°F	7
	Singer et al.	$\text{Log } S^{\circ}(\text{ppM}) = 5.16 - 4310/T(^{\circ}\text{K})$	486–600°C	38
Nickel	Rodgers et al.	$S^{\circ}(\text{ppM}) = -1.3 + 0.0199t(^{\circ}\text{F})$	400–1000°F	7
	Kovacina and Miller	$S^{\circ}(\text{ppM}) = 1.2 \times 10^{-3} + 1.75 \times 10^{-5} t(^{\circ}\text{C})$	200–600°C	13
	Singer et al.	$\text{Log } S^{\circ}(\text{ppM}) = 1.545 - 1230/T(^{\circ}\text{K})$	446–600°C	38
	Eichelberger and McKisson	$\text{Log } S^{\circ}(\text{ppM}) = 1.47 - 918/T(^{\circ}\text{K})$	700–914°C	8
Chromium	Singer et al.	$\text{Log } S^{\circ}(\text{ppM}) = 9.35 - 9010/T(^{\circ}\text{K})$ (combined with results of Ref. 8)	650–1000°C	38
Molybdenum	Eichelberger and McKisson	$\text{Log } S^{\circ}(\text{ppM}) = 3.142 - 3807/T(^{\circ}\text{K})$	800–1005°C	8
Copper	Koenig et al.	$\text{Log } S^{\circ}(\text{ppM}) = 1.778 - 510/T(^{\circ}\text{K})$	120–500°C	18
	Singer and Weeks	$\text{Log } S^{\circ}(\text{ppM}) = 6.91 - 4200/T(^{\circ}\text{K})$	255–547°C	12
	Humphreys	$\text{Log } S^{\circ}(\text{ppM}) = 6.59 - 4040/T(^{\circ}\text{K})$	500–700°C	20
	Walker	$\text{Log } S^{\circ}(\text{ppM}) = 4.444 - 2414.7/T(^{\circ}\text{K})$	222–640°C	21
	Eichelberger and McKisson	$\text{Log } S^{\circ}(\text{ppM}) = 5.957 - 3430/T(^{\circ}\text{K})$ (combined with results of Refs. 12, 20)	250–726°C	8
Niobium	Eichelberger and McKisson	$\text{Log } S^{\circ}(\text{ppM}) = 4.16 - 3530/T(^{\circ}\text{K})$ (combined with results of Ref. 25)	600–900°C	8
Bismuth	Walker	$\text{Log } S^{\circ}(\text{wt.\%}) = 5.888 - 4145.1/T(^{\circ}\text{K})$	253–563°C	3
	Gehri and Sullivan	$\text{Log } S^{\circ}(\text{at.\%}) = 4.900 - 4178/T(^{\circ}\text{K})$	293–649°C	21
		$\text{Log } S^{\circ}(\text{at.\%}) = 1.188 - 2100/T(^{\circ}\text{K})$	125–253°C	21
	Brown et al.	$\text{Log } S^{\circ}(\text{at.\%}) = 1.973 - 2425/T(^{\circ}\text{K})$	105–250°C	29
Indium	Weeks and Davies	$\text{Log } S^{\circ}(\text{wt.\%}) = 4.54 - 1603/T(^{\circ}\text{K})$	102–269°C	6
	Lamprecht	$\text{Log } S^{\circ}(\text{wt.\%}) = 4.34 - 1484/T(^{\circ}\text{K})$	116–221°C	33
Cadmium	Weeks and Davies	$\text{Log } S^{\circ}(\text{wt.\%}) = 3.67 - 1209/T(^{\circ}\text{K})$	102–326°C	6, 35
Silver	Weeks	$\text{Log } S^{\circ}(\text{wt.\%}) = 3.19 - 1466/T(^{\circ}\text{K})$	104–518°C	6, 36
	Lamprecht	$\text{Log } S^{\circ}(\text{wt.\%}) = 3.52 - 1621/T(^{\circ}\text{K})$	136–260°C	33
Zinc	Lamprecht	$\text{Log } S^{\circ}(\text{wt.\%}) = 3.44 - 2551/T(^{\circ}\text{K})$	181–543°C	33
Tin	Weeks	$\text{Log } S^{\circ}(\text{wt.\%}) = 5.05 - 2368/T(^{\circ}\text{K})$	170–391°C	6
	Lamprecht	$\text{Log } S^{\circ}(\text{wt.\%}) = 5.00 - 2284/T(^{\circ}\text{K})$	120–258°C	33
Lead	Lamprecht	$\text{Log } S^{\circ}(\text{wt.\%}) = 6.06 - 2465/T(^{\circ}\text{K})$	119–244°C	33
Antimony	Lamprecht	$\text{Log } S^{\circ}(\text{ppM}) = 5.28 - 1839/T(^{\circ}\text{K})$	183–550°C	33
Cerium	Lamprecht	$\text{Log } S^{\circ}(\text{ppM}) = -2.68 + 658/T(^{\circ}\text{K})$	130–450°C	33

Table 2 Recommended Solubility Expressions

Element	Expression	Element	Expression
Iron	Log S°(ppM) = 5.16 – 4310/T(°K)	Indium	Log S°(wt.%) = 4.48 – 1562/T(°K)
Nickel	Log S°(ppM) = 2.07 – 1570/T(°K)	Cadmium	Log S°(wt.%) = 3.67 – 1209/T(°K)
Molybdenum	Log S°(ppM) = 3.27 – 3962/T(°K)	Silver	Log S°(wt.%) = 3.22 – 1479/T(°K)
Copper	Log S°(ppM) = 5.45 – 3055/T(°K)	Zinc	Log S°(wt.%) = 3.44 – 2551/T(°K)
Bismuth	Log S°(ppM) = 5.67 – 4038/T(°K) (290–650°C)	Tin	Log S°(wt.%) = 5.03 – 2326/T(°K)
	Log S°(ppM) = 2.15 – 2103/T(°K) (125–290°C)	Lead	Log S°(wt.%) = 6.06 – 2465/T(°K)
		Antimony	Log S°(ppM) = 5.28 – 1839/T(°K)
		Cerium	Log S°(ppM) = –2.68 + 658/T(°K)

APPENDIX B: REFERENCES TO SODIUM-SOLUBILITY ANALYTICAL TECHNIQUES

E. Berkey, G. G. Sweeney, and W. M. Hickam, The Analysis of Sodium by Spark Source Mass Spectrography, *Nucl. Appl.*, **5**: 344 (November 1968).

C. D. Bingham, J. M. Scarborough, and M. S. Maseda, Analytical Methods for Determining Impurities in Sodium Below 10 ppM, USAEC Report ANL-7520, Part I, pp. 278-283, Argonne National Laboratory, 1968.

H. T. Carmichael et al., Determination of Iron, Nickel, and Chromium in Sodium by Atomic Absorption, Report APDA-207, Atomic Power Development Associates, Inc., July 1968.

T. P. Ramachandran and W. E. Hareland, The Determination of Trace Metallic Impurities in Reactor Sodium, presented at the 13th Conference on Analytical Chemistry in Nuclear Technology, Gatlinburg, Tenn., Sept. 30–Oct. 2, 1969.

E. B. Sandell, *Colorimetric Determination at Traces of Metals*, Interscience Publishers, a division of John Wiley & Sons, Inc., New York, 1959.

J. M. Scarborough, The Determination of Trace Level Copper in Sodium by Colorimetry and Atomic Absorption Spectrophotometry, paper presented at the 155th National Meeting of the American Chemical Society, San Francisco, Apr. 1–4, 1968.

J. M. Scarborough, C. D. Bingham, and P. F. DeVries, Determination of Trace Metallic Impurities in High Purity Sodium Using Atomic Absorption Spectrometry, *Anal. Chem.*, 39: 1394 (1967).

REFERENCES

1. Atomic Energy Commission–Department of the Navy, *Liquid-Metals Handbook: Sodium–NaK Supplement*, 3rd ed., pp. 13-19, 1955.
2. D. F. Anthrop, The Solubilities of Transition Metals in Liquid Alkali and Alkaline Earth Metals, Lanthanum, and Cerium—A Critical Review of the Literature, USAEC Report UCRL-50315, University of California Lawrence Radiation Laboratory, 1967.
3. R. A. Walker, The Solubility of Metals in Sodium, Ph.D. Thesis, University of Birmingham, United Kingdom, 1968.
4. L. F. Epstein, Preliminary Studies on the Solubility of Iron in Liquid Sodium, *Science*, **112**: 426 (1950).
5. R. A. Baus, A. D. Bogard, J. A. Grand, L. B. Lockhart, Jr., R. R. Miller, and D. D. Williams, The Solubility of Structural Materials in Sodium, in *Proceedings of the International Conference on the Peaceful Uses of Atomic Energy, Geneva, 1955*, Vol. 9, pp. 356-363, United Nations, New York, 1956.
6. J. R. Weeks, Brookhaven National Laboratory, personal communication, September 1969.
7. S. J. Rodgers, J. W. Mausteller, and E. F. Batutis, Iron and Nickel Concentrations in Sodium, Report MSA-TR-27, Mine Safety Appliances Co., 1954.
8. R. L. Eichelberger and R. L. McKisson, The Solubility of Cu, Mo, Nb, Fe, Ni, and Cr in High-Purity Sodium, USAEC Report ANL-7520, Part I, p. 319, Argonne National Laboratory, 1968.
9. R. L. McKisson, R. L. Eichelberger, R. C. Dahleen, J. M. Scarborough, and G. R. Argue, Solubility Studies in Liquid Metals, Report AI-65-210, Atomics International, 1965.
10. C. D. Bingham, J. M. Scarborough, and M. S. Maseda, Analytical Methods for Determining Impurities in Sodium Below 10 ppM, USAEC Report ANL-7520, Part I, p. 278, Argonne National Laboratory, 1968.
11. A. W. Thorley and G. Tyzack, Corrosion Behavior of Steels and Nickel Alloys in High-Temperature Sodium, in *Alkali Metal Coolants*, Symposium Proceedings, Vienna, 1967, p. 97, International Atomic Energy Agency, Vienna, 1967 (STI/PUB/143).

12. R. M. Singer and J. R. Weeks, On the Solubilities of Cu, Ni, and Fe in Liquid Sodium, USAEC Report ANL-7520, Part I, p. 309, Argonne National Laboratory, 1968.
13. T. A. Kovacina and R. R. Miller, The Solubility of Nickel in Sodium by a Tracer Technique, *Nucl. Sci. Eng.*, **10**: 163 (1961).
14. P. K. Lee and E. Berkey, Solubility of Cobalt and Nickel in Sodium, USAEC Report ANL-7520, Part I, p. 299, Argonne National Laboratory, 1968.
15. T. A. Kovacina and R. R. Miller, Solubility of Nickel in Liquid Sodium of High Oxide Content, Report NRL-6890, Naval Research Laboratory, May 1969.
16. J. K. Balkwill, Liquid Metal Engineering Center, personal communication, May 1969.
17. J. A. Grand, R. A. Baus, A. D. Bogard, D. D. Williams, L. B. Lockhart, and R. R. Miller, The Solubility of Tantalum and Cobalt in Sodium by Activation Analysis, *J. Phys. Chem.*, **63**: 1192 (1959).
18. L. F. Epstein, Argonne National Laboratory, personal communication, September 1969.
19. R. L. Eichelberger and R. L. McKisson, Solubility of Copper in Sodium, USAEC Report AI-AEC-12671, Atomics International, 1968.
20. J. R. Humphreys, Jr., Interdivisional Document K-3-774, Los Alamos Scientific Laboratory.
21. R. A. Walker and J. N. Pratt, The Solubility of Copper in Liquid Sodium, *J. Nucl. Mater.*, **32**: 340 (1969).
22. G. Kienast, Ph.D. Dissertation, Münster, 1955.
23. E. G. Brush, Aluminum Bearing Alloys in Sodium, Report No. 2 on Evaluation of the Behavior of Aluminum in Sodium, USAEC Report KAPL-M-EGB-16, Knolls Atomic Power Laboratory, 1954.
24. J. R. Humphreys, Jr., personal communication, December 1969.
25. T. A. Kovacina and R. R. Miller, The Solubility of Columbium–1% Zirconium in Sodium by Activation Analysis, Report NRL-6051, Naval Research Laboratory, 1964.
26. R. L. Klueh, The Effect of Oxygen in Sodium on the Compatibility of Sodium with Niobium, USAEC Report ANL-7520, Part I, p. 171, Argonne National Laboratory, 1968.
27. D. C. Gehri and R. J. Sullivan, Solubility of Bismuth in Liquid Sodium, USAEC Report AI-AEC-12770, Atomics International, 1969.
28. C. E. Johnson, Argonne National Laboratory, personal communication, December 1969.
29. L. E. Brown, C. H. Lewis, and K. A. Williams, Determination of the Solubility of Na_3Bi in Sodium, AUA–ANL Summer Engineering Practice School Report, 1968.
30. G. L. Lamprecht, Ph.D. Thesis, University of South Africa, Pretoria, 1966.
31. G. L. Lamprecht, P. Crowther, and D. M. Kemp, A Study of the Solubility of Metals in Liquid Sodium. I. The System Sodium–Tin, *J. Phys. Chem.*, **71**: 4209 (1967).
32. G. L. Lamprecht and P. Crowther, Solubility of Metals in Liquid Sodium: The Systems Sodium–Silver, Sodium–Zinc, and Sodium–Cerium, *Trans. AIME*, **242**: 2169 (1968).
33. R. A. Walker, Argonne National Laboratory, personal communication, September 1969.
34. H. A. Davies, The Solubility of Indium in Liquid Sodium, *Trans. AIME*, **239**: 928 (1967).
35. J. R. Weeks and H. A. Davies, Physical and Chemical Properties of Dilute Alloys of Cadmium in Sodium, in *The Alkali Metals: An International Symposium*, Chemical Society Special Publication No. 22, pp. 32-44, Nottingham, 1967.
36. J. R. Weeks, Liquidus of the Na–Ag System: 0 to 6 At.% Ag, *Trans. Amer. Soc. Metals*, **62**: 304 (1969).
37. T. F. Kassner, Argonne National Laboratory, personal communication, August 1968.
38. R. M. Singer, A. H. Fleitman, J. R. Weeks, and H. S. Isaacs, Measurements of the Solubility of Iron and Chromium in Sodium, in *Corrosion by Liquid Metals*, J. E. Draley and J. R. Weeks (Eds.), 1970.
39. H. S. Isaacs, The Determination of Oxygen Concentration and Mass-Transfer Coefficients in Sodium Using Uranium, USAEC Report ANL-7520, Part I, p. 465, Argonne National Laboratory, 1968.

A Critical Review from the American Nuclear Society

Development Potential of Zirconium Alloys for High-Temperature Applications

By C. D. Williams*

A marked improvement in the thermal efficiency of water reactors is attainable if the outlet coolant temperature can be raised to the range 450 to 500°C. With the higher efficiency of energy conversion in turbines fed with superheated steam, net station efficiencies[1] of 40% or higher may be achieved, as shown in Table 1. The U. S. Atomic Energy Commission (USAEC) nuclear superheat program was geared from its initiation to the use of enriched fuels with stainless steel as the principal structural material within the reactor core. The parasitic absorption penalty incurred by use of steels for fuel cladding and coolant channels is not acceptable in a reactor fueled with natural uranium; even allowing for some enrichment, it is evident that an economic advantage is available if an alternative material of lower neutron absorption can be used. Thus an incentive exists for development of zirconium-based alloys for use in heavy-water reactors designed to produce superheated steam.

In this article an assessment is made of the extent to which the high-temperature mechanical properties of zirconium alloys can be improved. The assessment is based on current understanding of the relation between structural and mechanical properties of alloys. The limitations of the properties of conventional alloys are examined together with information on the factors that determine these properties. The effects of neutron irradiation on mechanical properties are considered. The literature on zirconium alloys of significantly higher strength than those in service at present is reviewed, again with attention to the strengthening factors involved. The extensive titanium literature is used as an additional source of information to indicate development potential of zirconium alloys. An estimation is made of the development range of tensile and creep strength, using existing alloy-strengthening techniques. This estimation indicates that zirconium alloys having adequate strength for application at design stresses up to 20 ksi at 450°C can be developed.

Corrosion resistance has perhaps been more important than mechanical properties in the development of the Zircaloys and most of the other zirconium-based alloys developed for reactor service. Cox[2] has recently reviewed in detail the effects of neutron irradiation on oxidation of zirconium alloys in water reactors and has discussed the probable mechanisms involved. Hydriding and oxidation in aqueous environments limit the use of the Zircaloys and the Zr–2.5% Nb alloy to temperatures below ~350°C. These alloys have been used successfully[3,4] at low stresses in organic coolants at temperatures up to 460°C. Considerable effort in the United States and Canada is presently directed[4,5] to examination of the Zr–1.2% Cr alloy and Ozhennite 0.5 for cladding applications at temperatures in aqueous and organic systems at $\gtrsim$ 400°C.

For present purposes the corrosion resistance of zirconium alloys is treated as a secondary factor for two reasons:

1. Techniques are now available for cladding high-strength alloys with an alloy chosen for corrosion resistance.[6,7]

*Applied Materials Research Branch, Chalk River Nuclear Laboratories, Ontario, Canada.

2. The prospects for successful development of a high-strength alloy are greatly reduced if a compromise between strength and oxidation resistance is sought. However, the effect of aluminum on the oxidation resistance of zirconium alloys is catastrophic;[8] thus attention throughout the review is directed particularly to the potential of alloys without this addition.

BASIS FOR ALLOY DEVELOPMENT

Design of alloys for high-temperature application must be based upon information about the factors that determine the alloy's properties under the required service conditions. Although the behavior of reactor alloys is complicated by neutron-flux effects, the basic approach to development of creep-resistant alloys must be similar to that for normal structural materials.

The factors that control the high-temperature strength of a refractory-metal alloy have been included in the following empirical relation by Wilcox:[9]

$$\sigma = \sigma_0 + f\frac{Gb}{\lambda} + f\left(\left|\frac{1}{a}\frac{da}{dc}\right|\right) + f\left(\left|\frac{1}{G}\frac{dG}{dc}\right|\right) + \sigma_{SRO} + f(G\,bN^{1/2}) + f(d^{-1/2}) + f(\sigma_f V_f) \quad (1)$$

where G is the shear modulus and b is the Burgers vector for mobile dislocations.

Thus the high-temperature (creep) strength σ developed in a matrix of strength σ_0 is promoted by:

1. A small precipitate spacing λ.
2. High solution hardening due to the atomic misfit parameter[10] $\left|\frac{1}{a}\cdot\frac{da}{dc}\right|$
3. An increase in shear modulus by alloying. The Douglass[11] review of modulus effects in zirconium alloys indicates that niobium additions tend to reduce both the elastic and shear moduli at room temperature.
4. An increase in short-range order in the alloy. Such effects contribute to strengthening in numerous alloy systems but have not been identified in alpha zirconium. (Higgins and Banks[12] postulated the occurrence of solute clustering at elevated temperatures in beta zirconium in Zr–Nb alloys.)
5. An increase in (immobilized) dislocation density N. The improvement in creep strength of cold-worked Zircaloy-2 compared with annealed material[13] is a pertinent example.
6. A small grain diameter d. Weinstein's data[14] demonstrate the effect of grain size on low-temperature yield strength of zirconium, but application of this strengthening at elevated temperatures is dependent upon effective grain-boundary immobilization.
7. Introduction of a significant volume fraction of fiber reinforcement, not yet attempted in zirconium alloys.

Throughout this review, reference is made to these factors where they may be used in a development context. With specific reference to high-temperature creep, Mukherjee, Bird, and Dorn[15] have recently published an extensive correlation of creep behavior and structural parameters for a range of metals and alloys. They were interested in the temperature range above half-melting temperature (in °K) and derived the following expression for secondary creep rate $\dot{\epsilon}_s$:

$$\frac{\dot{\epsilon}_s kT}{DGb} = A\left(\frac{\sigma}{G}\right)^n \quad (2)$$

where n is the stress exponent in the expression

$$\dot{\epsilon}_s \propto \sigma^n \quad (3)$$

Table 1 Net Efficiency Values for Various Proven and Advanced Reactor Types*

	Reactor types				
		Organic		Superheat	
Reactor parameters	CANDU–PWR Douglas Point	Proved technology	Advanced system	Proved technology	Advanced system
Outlet coolant, °C	293	386	420	538	450
Pressure-tube material	Zircaloy-2	Zr–2.5% Nb	Ozhennite 0.5	Stainless steel	Zirconium alloy
Fuel	UO_2	Uranium carbide	Uranium carbide	Enriched UO_2	Enriched UO_2
Net station efficiency	29	37	39.5	38.5 to 40	38 to 42

*Data for organic and superheat systems are from Ref. 1.

The homologous temperature range considered[15] is nominally higher than that of interest here (450 to 500°C) for zirconium alloys. However, because the upper homologous temperature for zirconium (and titanium) alloys[11] is based on the phase transformation rather than the melting temperature, the secondary creep equation given above is one that allows useful comparison with other materials.

TEMPERATURE LIMITS FOR CONVENTIONAL ZIRCONIUM ALLOYS

It is not intended to review in detail the literature on mechanical properties, corrosion behavior, and neutron irradiation effects in the conventional zirconium alloys. A limited bibliography including recent detailed reviews is given in Refs. 4, 6, 12, and 16-21. For present purposes it is necessary to summarize the aspects of the alloys' mechanical properties which limit their application to a restricted temperature range, and to correlate, as far as possible, these limiting properties with the factors which control them. In this way the prospect for successful alloy development may be examined.

Since 1960, development effort in zirconium metallurgy has been divided between various dilute alloys for use in aqueous, organic, and gaseous environments, with by far the largest effort in the first category. The Zircaloys,[13,22] the Zr–2.5 Nb alloy,*[23,24] the Zr–1.2 Cr alloy,[25] and Ozhennite 0.5,[26] are in use as fuel-cladding and pressure-tube materials in numerous water- and organic-cooled reactors.[3-5] In Europe, Zr–Cu (Refs. 27 and 28), Zr–(0.5–3) Cu–(0.5–3)V (Ref. 29), and Zr–0.5 Cu–0.5 Mo (Ref. 30) alloys have been developed for application as fuel cladding in the 500 to 600°C regimes of gas-cooled reactors.

The Zr–2.5 Nb alloy in the cold-worked and stress-relieved condition has tensile and creep strength superior to that of the Zircaloys. Also, the binary alloy may be heat-treated to give significantly higher strengths than the other alloys listed above. Thus it may be conveniently used as an indicator of strength limits for these conventional alloys. Figure 1 shows design stress data for cold-worked Zircaloy-2 and the heat-treated Zr–2.5 Nb alloy.[23] The cold-worked binary alloy has properties intermediate to those shown in this figure.[31] The alloys may be used for pressure-vessel construction at stress–temperature conditions below their intersecting curves; for temperatures above 350°C, creep strength is limiting; at 400°C, the alloys may be used at a maximum design stress of ~5 ksi.

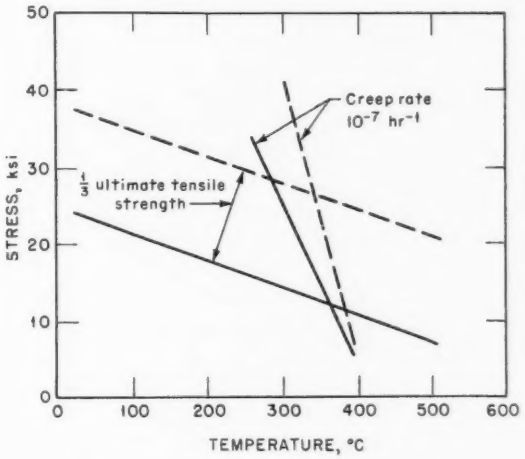

Fig. 1 Design stress data for cold-worked Zircaloy-2 (——) and the heat-treated Zr–2.5 Nb alloy (----).[23]

Strengthening Factors in These Alloys

Three materials variables have been used to control the mechanical properties of the alloys referred to above, namely, cold work, solute additions, and modification of structure by heat-treatment. The second and third variables, supplemented perhaps by deformation–annealing treatments, are the basic methods that must be more effectively exploited if the high-temperature properties of zirconium alloys are to be improved.

Figure 2 shows data reported by Winton et al.[32] and illustrates the improvements in *tensile strength* obtained by cold work and addition of niobium. The design stress data in Fig. 1 have already shown the further advantage obtained by quench–age treatment of the Zr–2.5 Nb alloy. Williams and Gilbert[33] assessed the strengthening factors in the martensitic phase obtained on beta-quenching the Zr–2.5 Nb alloy as follows: zirconium basic material, 25%; interstitial oxygen, 12%; substitutional niobium, 13%; martensitic grain size, 38%; and substructure microtwinning, 12%.

The contribution to the low-temperature tensile strength of zirconium alloys made by the common impurity oxygen is important.[34] Oxygen exists in the

*Throughout the text, alloy additions are given in weight percent with the exception of the multiple-element basis used in Figs. 9 and 11.

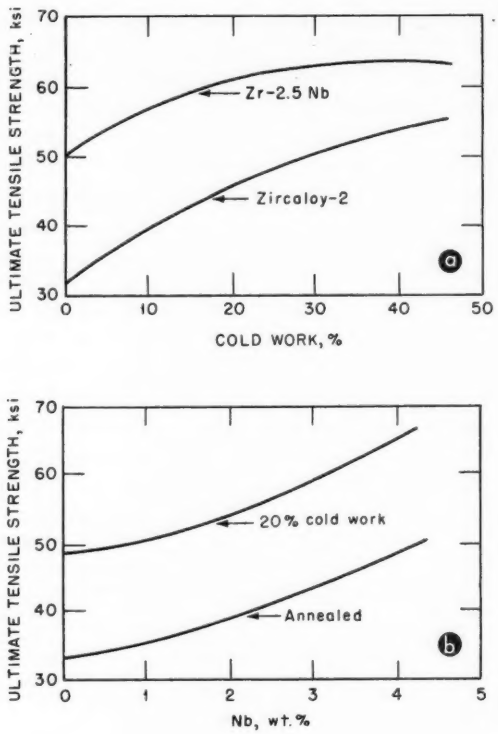

Fig. 2 Effect of (*a*) cold work on the ultimate tensile strength of Zr–2.5 Nb and Zircaloy-2, and (*b*) niobium content on annealed and cold-worked properties.[32]

zirconium lattice as an interstitial impurity, and oxygen atoms increase the lattice friction stress by interacting with the core of moving dislocations.[35] This effect is strongly temperature dependent, and oxygen (and nitrogen alike) contributes a much smaller factor to the tensile strength of zirconium alloys at 300°C or higher temperatures.[32,35] However, observations of strain-aging behavior in zirconium and Zircaloy-2 deformed under creep conditions have been interpreted[36,37] as indication of oxygen acting as a strain-aging species at ~300°C. This factor will be referred to later.

Gilbert, Doran, and Bement[38] have recently examined *creep behavior* in polycrystalline alpha zirconium over the temperature range 50 to 850°C. The mechanisms for creep deformation in five different regimes of activation energy and stress dependence were discussed, the effects being correlated where possible with other published work. Dislocation interaction, their intersection with precipitates and impurity atoms, grain-boundary diffusional creep, and nonconservative jog motion in screw dislocations were proposed as rate-controlling mechanisms.

These mechanisms are amenable to some control by alloying and deformation–thermal processing. Scott's laboratory data[13] demonstrated the improvement in creep strength obtainable by cold-working Zircaloy-2; at 400°C and a stress of 12 ksi, minimum creep rates for annealed and 15% cold-worked Zircaloy-2 were 3×10^{-6} and 4×10^{-7} hr^{-1}, respectively. This improvement is attributed to the obstacles to dislocation movement provided by the tangled networks of dislocations formed during the cold-working process, i.e., to increased N (Eq. 1). The networks are only partially relaxed by the autoclaving treatment at ~400°C, commonly used for cold-worked Zircaloy reactor components.[22,39]

Figures 3 and 4 show the decrease in creep strength at 300°C of the Zr–2.5 Nb alloy with increasing volume fraction of the equilibrium alpha phase and with increasing precipitate size in the martensitic alpha-prime phase,[40] modifications that give larger values for the parameters d and λ in Eq. 1. These data indicate the importance of selection of heat-treatment conditions to optimize creep strength.

Grain-boundary sliding experiments on crystal-bar zirconium and Zircaloy-2 have been reported by Coleman.[41] The ratio of grain-boundary sliding strain to total creep strain was ~0.1 at 500°C in zirconium of grain diameter near 150 μm. The temperature at which this effect becomes important can be raised by alloying and distribution of grain-boundary precipitates, and the effect would not be expected to restrict alloy development for temperatures up to 500°C.

The anisotropic nature of zirconium and the deformation modes obtained in its alloys were reviewed by Douglass[11] and continue to be the subject of published work. This anisotropy leads to formation of strong textures in fabricated alloys,[42] and the effects of fabrication variables on textures and mechanical properties obtained in zirconium-alloy bar, sheet, and tubing have been extensively studied, notably by Cheadle et al.[43-45] Selection of deformation conditions and fabrication route allows some control toward providing the most suitably textured material for a given application.

The effects of *fast-neutron irradiation* at 50 to 100° and 250 to 300°C on mechanical properties of zirconium alloys are well documented, the important effects being:

1. An increase in yield and ultimate tensile strength. For Zircaloy-2, the increase due to fluences $<5 \times 10^{20}$ neutrons/cm^2 ($E > 1$ MeV) at ~300°C is

larger for annealed material than 20 or 40% cold-worked material.[46] At fluences $>10^{21}$, the irradiated alloy reaches a strength that is independent of prior condition. The most recent review of this work on Zircaloy-2 is that prepared by Knecht and Pankaskie.[20] Irradiation hardening is attributed to the distribution of defect clusters and dislocation loops that develop from condensation of the lattice defects formed during neutron bombardment.[39,46] Saturation of irradiation hardening results from a saturation of this defect distribution.[47a] For Zr–2.5 Nb (and almost certainly for the other dilute heat-treatable alloys such as Zr–1.2 Cr and Zr–Cu–V), the increase in strength due to irradiation is determined by the metallurgical condition prior to irradiation.[48] This effect is associated with the phase distribution in the alloys and the influence of solutes on the damage recovery and, hence, irradiation hardening of the different phases.[49]

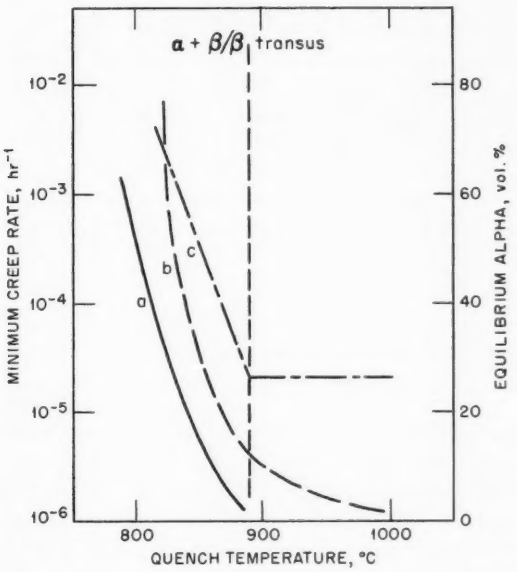

Fig. 3 Creep properties of Zr–2.5 Nb aged 24 hr at 500°C as a function of quench temperature.[41] Curve *a*, vol.% of equilibrium alpha. Curve *b*, creep rate at 300°C and 70 ksi. Curve *c*, creep rate at 450°C and 30 ksi.

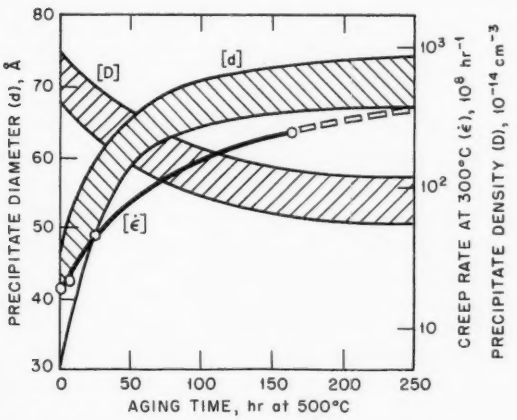

Fig. 4 Creep properties of beta-quenched Zr–2.5 Nb as a function of aging time at 500°C: $\dot{\epsilon}$ = creep rate per hour at 300°C and 70 ksi (after 200 hr); *d* = precipitate diameter, Å; and *D* = precipitate density, particles/cm^3.

2. A decrease in tensile ductility. In Zircaloy-2, ductility reaches a saturation minimum at a 290°C fluence of ~5 x 10^{20} neutrons/cm^2, with little dependence on prior condition of the material.[20,46] Heat-treatment before irradiation influences the change in ductility of the Zr–2.5 Nb alloy,[48] the beta-quenched alloy being susceptible to embrittlement by irradiation at 300°C. This susceptibility is attributed to the coincidence of high strength after irradiation with the large prior beta grain size, a combination that promotes intergranular failure in tensile tests.[50] These factors must be treated with care in the application of higher strength alloys in reactor environments.

3. An increase in creep rate at ~300°C. This aspect of zirconium alloy behavior has been given preferential attention in the past 5 years. Creep rates for cold-worked Zircaloy-2 and Zr–2.5 Nb alloy and the heat-treated binary alloy in uniaxial and biaxial stress systems are increased by a factor of 5 to 10 at 300°C in a fast flux of ~1 x 10^{13} neutrons/(cm^2)(sec).[39,51-55] Figure 5 shows the Ross-Ross plot of strain per 10^{21} neutrons/cm^2 vs. stress for

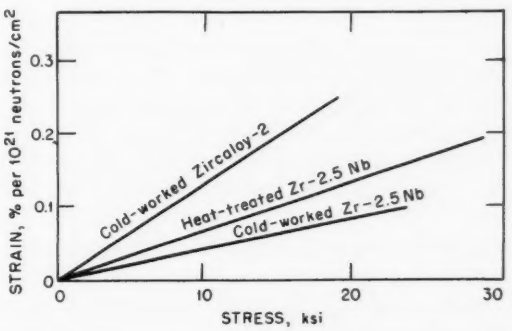

Fig. 5 Ross-Ross' data[31] for creep strain, % per 10^{21} neutrons/cm^2 fast fluence at 270°C obtained from pressure-tube gauging program.

these three materials at 300°C, these data being obtained from gauging of pressure tubes operated in reactor loop tests.[31] Ross-Ross has fitted the pressure-tube data relevant to design conditions to an equation of the form

$$\dot{\epsilon}_t = K\phi\,\sigma_t(T - 160) \qquad (4)$$

where $\dot{\epsilon}_t$ = diametral creep rate, hr^{-1}
ϕ = fast-neutron flux, neutrons/(cm^2)(sec)
σ_t = hoop stress, psi
T = temperature, °C
K = materials constant

The values obtained for the parameter K were 4×10^{-27} for cold-worked Zircaloy-2, 1.4×10^{-27} for cold-worked Zr–2.5 Nb, and 2.2×10^{-27} for heat-treated Zr–2.5 Nb; these values apply for stresses up to 20 ksi, at temperatures in the range 250 to 300°C, and in a fast-flux range of 1 to 3.5×10^{13} neutrons/(cm^2)(sec). The advantage in creep properties of the cold-worked Zr–2.5 Nb alloy has led to the selection of the alloy to replace Zircaloy-2 as the pressure-tube alloy in the CANDU–PHW reactors, Pickering III and IV.

Figures 6 and 7 show the temperature and stress dependence of in-reactor creep rate for Zircaloy-2, similar data applying to the Zr–2.5 Nb alloy.[52,56] It is useful here to refer briefly to the various interpretations placed on these data and the association of this creep information with the evidence for irradiation growth[57,58] in zirconium and Zircaloy-2. Hesketh,[57] Piercy,[56] and Nichols[59] have discussed mechanisms that may contribute to the irradiation enhancement of creep, and this discussion remains unresolved (as do explanations of various modes of creep behavior in most materials![15]). Hesketh has reported convincing evidence for irradiation growth in Zircaloy-2 and has reconciled the various uniaxial and biaxial creep data using a yielding creep model.[58] His evidence of decreasing growth coefficient with increasing fluence, and published evidence[47] for saturation of radiation damage which occurs at $\sim 5 \times 10^{20}$ neutrons/cm^2 ($E > 1$ MeV) at 300°C, suggests that the growth factor will become very small at fluences near and beyond this level.[60] Piercy's calculations[56] indicate that stress reorientation of irradiation-damage loops will not contribute significantly to creep in zirconium alloys, although Nichols[59] has invoked this mechanism to explain the irradiation enhancement at stresses below 10 ksi. Nichols proposed that, at intermediate stresses (10 to 30 ksi), enhancement was due to climb of

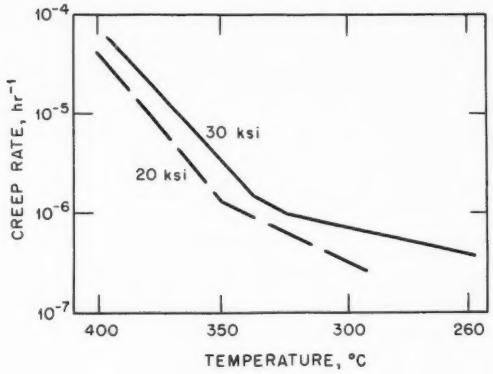

Fig. 6 Temperature dependence[52] of the steady in-reactor creep rate of cold-worked Zircaloy-2.

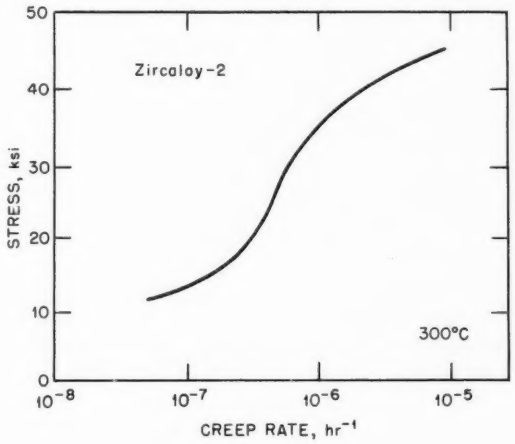

Fig. 7 Stress dependence[56] of the steady in-reactor (uniaxial) creep rate for cold-worked Zircaloy-2 at 300°C.

dislocations around obstacles at a rate increased by the vacancy–interstitial density produced by irradiation. At higher stress levels, irradiation enhancement is small, and mobile dislocations are able to cut through the obstacles without difficulty.

Veevers, Rotsey, and Snowden[61] have proposed an alternative explanation for the irradiation effect. They have suggested that peaks in activation energy[36] at ~300 and 450°C are due to strain aging by oxygen and iron, respectively. Results which showed that irradiation suppresses strain aging have led to the further suggestion that the in-reactor enhancement of creep may be due to reduced mobility of strain-aging species due to interaction with radiation damage.[37]

Recently Nichols[62] has discussed in detail the significance of the changing stress exponent (n in Eq. 3), evident in Fig. 5; at stresses near 20 ksi, this exponent takes a value close to unity,[56,59] implying that the alloys will have a capacity for resisting nonuniform elongation, leading to high ductility under these conditions. Watkins and Wood[55] have shown that, under creep conditions in reactor tests, cold-worked Zircaloy-2 exhibits a secondary creep strain several times larger than that obtained in laboratory tests. Nichols[62] postulates that a superplastic deformation mode is involved, and the alloys should be able to exhibit uniform elongation $\gtrsim 100\%$ in the stress–temperature–flux regime where the stress exponent is ~1. These experimental and theoretical observations have provided engineers with the necessary evidence[31,55] that cold-worked Zircaloy-2 is quite capable of accepting a design strain limit of 2%.

Projection of this information on irradiation creep effects into the design of alloys for higher temperature application is hazardous. Annealing experiments have shown that radiation damage formed at 300°C anneals out rapidly[47] at 450 to 500°C, but little direct information is available on damage accumulation during irradiation at these temperatures. No evidence of three-dimensional voids due to vacancy aggregation has been found in zirconium and Zircaloy-2 irradiated at 450°C in DFR and EBR-II fast fluxes.[47a,b] With high damage-recovery rates and a large thermal component of creep at ~450°C, it is likely that flux enhancement at low and intermediate stresses will be smaller than at ~300°C. Factors involved in this enhancement which can be controlled in an alloy-development program are dislocation density and mobility, as well as grain-boundary distribution and mobility.

Reference has been made to the effect of neutron irradiation on ductility of zirconium alloys. Experiments on fracture toughness[63] and critical crack propagation[64,65] in Zircaloy-2 pressure-tube material have shown that, although the material loses toughness as a result of irradiation, it does not lose its capacity for ductile failure. This change in fracture toughness follows the tensile-strength effects referred to earlier[20] in that annealed material shows a larger reduction in toughness than the cold-worked alloy at low fluences, but a saturation toughness level is reached after 3 to 6×10^{20} neutrons/cm^2 independent of prior condition. Using this ductility–fracture-toughness analogy, it is likely that large beta-grain-size high-strength materials will exhibit poor fracture toughness after irradiation,[50] and this combination should be used with caution in alloy development.

REVIEW OF LITERATURE ON HIGHER STRENGTH ZIRCONIUM ALLOYS

In a paper presented at Geneva in 1958, Adamson et al.[66] made a useful compilation of zirconium phase-equilibrium effects which provides a basis for evaluating alloy systems. They examined the electronic effects contributing to the stability of the alpha and beta phases; making an allowance for atomic size effects, a linear relation between electronic concentration and mean temperature of the alpha and beta boundaries was deduced. Figure 8 shows their arrangement of partial-phase diagrams for a number of binary systems grouped in the order of the solute elements in the periodic table. Also included in the figure are calculated values for the increase in thermal-neutron capture cross section per 1 wt.% addition for each solute.[67] The elements that combine useful effects as alloy additions with low neutron absorption are underlined. These fall into two categories with respect to alloy effects: (1) elements that are, to some extent, soluble in the close-packed hexagonal (cph) alpha phase; and (2) elements of very limited alpha solubility, but which are more soluble in the body-centered cubic (bcc) beta phase. These two groups will generally be referred to as alpha and beta stabilizers throughout the article.

In 1956 van Thyne and McPherson[68] reported results of tensile tests at room temperature, 650 and 800°C on a range of zirconium-base binary and ternary alloys containing the alpha stabilizers Al, Ti, Ta, and Sn, with restricted use of the beta stabilizers, Cr and Mo. Some of their data are included in Table 2. High strength levels were obtained, the most effective strengthening additions being aluminum and/or tin, as, for example, in the Zr–3 Al–3 Sn alloy.

Also in 1956 Chubb[69] reported on development of creep-resistant zirconium alloys, including hot-hardness, tensile, and creep data for a series of Zr–Al–Sn, Zr–Al–Mo, and Zr–Sn–Mo ternary alloys, in addition to data for a number of binary alloys containing Cr, Ta, Ti, Sn, Al, Mo, and Nb. Some of Chubb's data are summarized in Figs. 9 and 10 and Table 2. Chubb stressed the potential value of peritectoid–eutectoid hybrid alloys containing additions of alpha and beta stabilizers. However, the results of a heat-treatment survey on a Zr–4 Sn–1.5 Mo alloy at 25%, tabulated below, suggested that the beta-

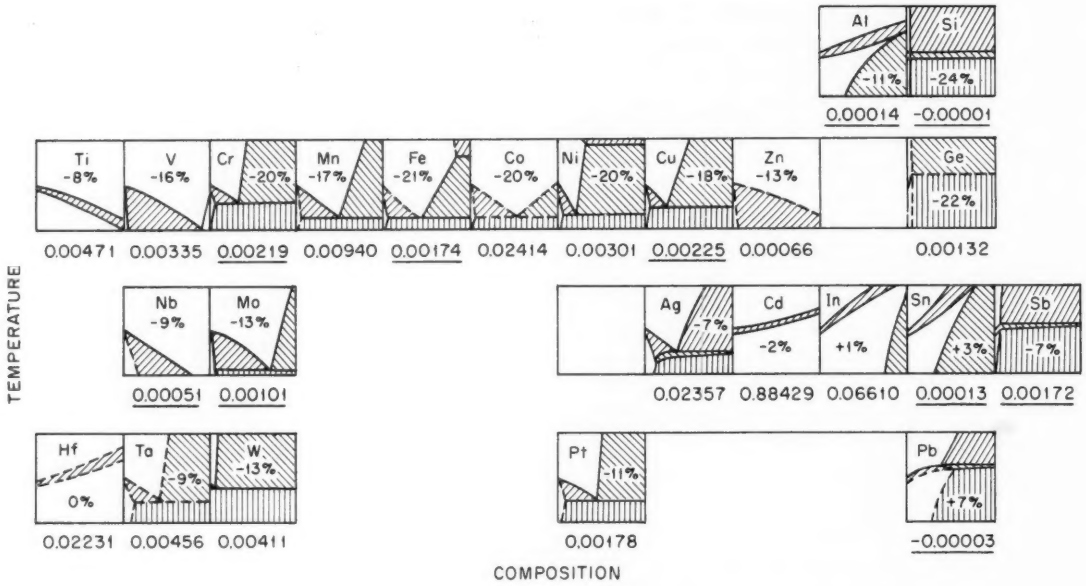

Fig. 8 Binary phase diagrams[66] for a number of zirconium-base systems for the composition range 100 to 90% zirconium and the temperature range 775 to 975°C. The numbers on the figures represent atomic size differences. The value beneath each graph represents $\Sigma_c(cm^2 \cdot cm^{-3})$, the increase in thermal-neutron capture cross section per 1 wt.% alloy addition.[67]

transformation product obtained on cooling from the high (alpha + beta) range was associated with very low ductility.

Heat-treatment	Ultimate tensile strength, ksi	Total elongation, %	Reduction of area, %
Hot rolled at 800°C; cold rolled to 30% reduction; annealed 3 hr at 700°C	90.6	20	24
1 hr at 900°C, water quenched	103.3	3	2
1 hr at 900°C, air cooled	143.3	2	1
1 hr at 900°C, furnace cooled	97.6	12	3

In 1957 Chubb[70] published a more detailed report of his work on a Zr–4 Sn–1.6 Mo alloy. In addition to having a range of tensile strength controllable by heat-treatment, the alloy showed good hot-rolling characteristics at 800°C, and, after hot working, the alloy could be cold reduced 20% without cracking. Hot-hardness tests indicated that at temperatures up to 700°C the alloy would have creep properties markedly superior to those of zirconium, but at 800°C the advantage was lost because of the introduction of the softer bcc phase in the alloy.

Domagala, Levinson, and McPherson[71] reported on transformation kinetics and mechanical properties of Zr–Mo alloys, including TTT curves and mechanical properties for a series of alloys containing up to 7.5 wt.% molybdenum. In each case a series of isothermal treatments was used, involving cooling directly from 1000°C to temperatures in the range 500 to 800°C, followed by a water quench after a prescribed interval for transformation. With the exception of the most dilute alloy, the specimens developed high tensile strength but showed very low ductility. For the Zr–1.3 Mo alloy, the highest values of ultimate tensile strength were obtained in specimens transformed at 500°C; somewhat better combinations of strength and ductility were obtained after transformation at 600 to 650°C. From X-ray studies and analogy with the Ti–Mo systems, the low ductility of the alloys was attributed to formation of a transition omega phase tentatively identified as having a tetragonal lattice.

Table 2 Mechanical Properties for Various Zirconium Alloys

Alloy addition, wt.%						Metallurgical treatment	Test temp., °C	UTS,* ksi	Elongation, %	Creep properties			Refs.
Al	Sn	Nb	Mo	Ti	Cr					Stress, ksi	Temp., °C	Minimum creep ratio, hr	
1.5						Hot rolled, annealed 25 hr at 788°C	20	99	18	25	565	1.8×10^{-3}	75
2.0						Annealed 48 hr at 650°C	20	93	16				68
3.0						30 min at 800°C, air cooled	20	123	14	45	500	7.5×10^{-6}	77
4.0						30 min at 800°C, air cooled	20	146	11	45	500	0.7×10^{-6}	77
	3					Annealed 48 hr at 650°C	20	55	32				68
1.5	3					Hot rolled, annealed 25 hr at 788°C	20	115	13	25	565	2.3×10^{-4}	75
1.1	1.6					Rolled, annealed 3 hr at 730°C	25	84	3				69
1.5			1.5			Hot rolled, annealed 25 hr at 788°C	20	122	8	25	565	1.3×10^{-4}	75
1.5	1.5		1.5			Hot rolled, annealed 25 hr at 788°C	20	127	10	25	565	1.5×10^{-4}	75
3.0	1.5		1.5			Hot rolled, annealed 25 hr at 788°C	20	133	9				75
						Hot rolled, annealed 25 hr at 788°C	565	70	30	25	565	7×10^{-5}	75
3.0	3.0					Annealed 48 hr at 650°C	20	127	10				68
1.0	3.0			5.0		Annealed 48 hr at 650°C	20	112	10				68
	3.6		1.5			Hot rolled, annealed 25 hr at 788°C	25	106	13				69
	4.2	0.6				Hot rolled, annealed 25 hr at 788°C	25	104	18				69
	2.0	5.0				Quenched from 830°C, aged 8 hr at 482°C	20	174	1				74
						Quenched from 870°C, aged 8 hr at 538°C	20	168	14				74
	2.0		5.0			Quenched from 830°C	20	153	10				74
						Quenched from 830°C, aged 8 hr at 538°C	20	172	1				74
	4.0		2.0			Quenched from 860°C, aged 24 hr at 482°C	20	141	6				74
	2.0		2.0			Beta quenched, aged 24 hr at 500°C	500	99		14	500	$< 1.8 \times 10^{-5}$	72
	1.0	5.0				Beta quenched, aged 24 hr at 500°C	500	97		14	500	$< 1.1 \times 10^{-5}$	72
		2.0			3.0	Beta quenched, aged 24 hr at 500°C	500	85		14	500	$< 1.2 \times 10^{-5}$	72

*UTS = ultimate tensile strength.

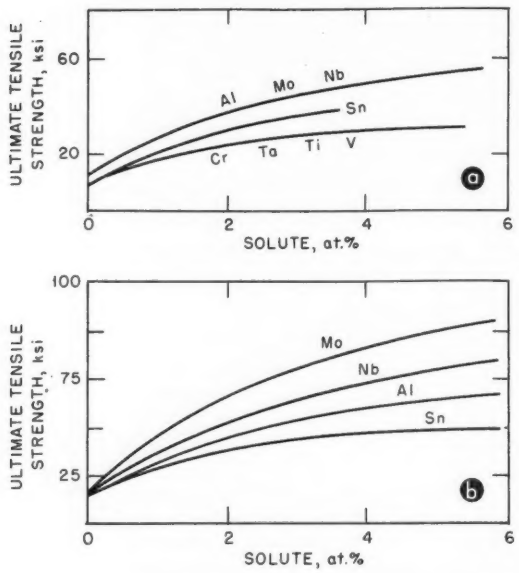

Fig. 9 Tensile strength of various binary zirconium alloys at 500°C: (*a*) annealed[69] at 730°C, and (*b*) beta quenched and aged.[72]

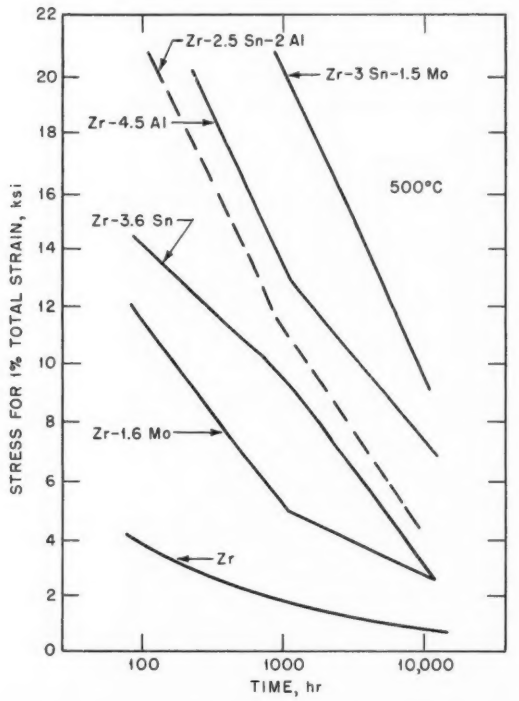

Fig. 10 Chubb's data[69] for properties of zirconium alloys at 500°C. All material annealed at 730°C prior to testing.

At the Geneva Conference of 1958, Ivanov and Grigorovich[72] reported extensive work on zirconium alloys, including tensile and creep data for (1) binary alloys with Nb (up to 75 wt.%), Be, Al, Ti (up to 20 wt.%), Sn, Mo, Fe (up to 1 wt.%), and Ta and Cr (up to 5 wt.%), and (2) ternary alloys of Zr–Cr–Nb, Zr–Cr–Sn, Zr–Nb–Mo, and Zr–Mo–Sn. Figure 9 includes tensile data for binary alloys tested at 500°C after a beta quench and aging treatment of 24 hr at 500°C, illustrating the importance of the strong beta stabilizers molybdenum and niobium in promoting high strength in dilute heat-treated alloys. Figure 11 shows the tensile properties of some of the heat-treated ternary alloys at 500°C. In these ternary alloys the highest values for tensile strength and lowest values for tensile ductility were obtained for the alloys containing a combination of an alpha-solution hardener, e.g., tin, with a strong beta stabilizer, e.g., niobium or, particularly, molybdenum.

The best combinations of high tensile and creep strengths were obtained with ternary alloys of compositions close to Zr–2 Sn–2 Nb or Zr–2 Sn–2 Mo.

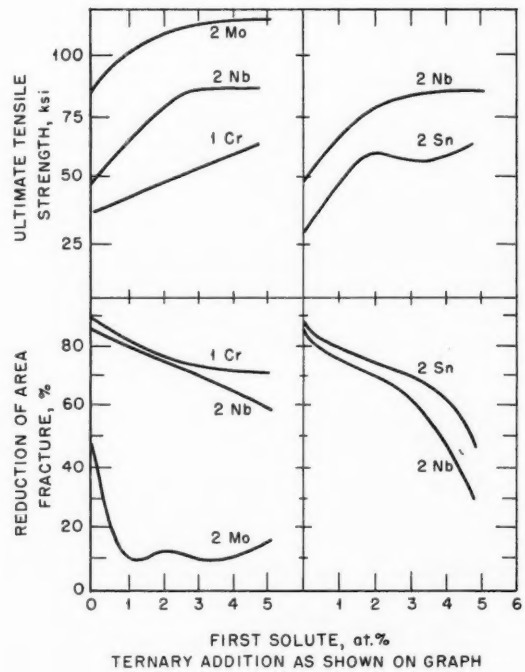

Fig. 11 Tensile properties[72] of zirconium-base ternary alloys at 500°C. All specimens beta quenched and aged 24 hr at 500°C prior to testing.

Two other papers of particular importance to zirconium-alloy development were presented at the 1958 Geneva Conference. Ambartsumyan et al.[26] reported an extensive investigation of mechanical properties and corrosion behavior of a number of dilute zirconium-base alloys. The mechanical properties examined were in the range of conventional zirconium alloys, i.e., below the range of interest in this section. However, the data for aqueous corrosion behavior at 350, 400, and 450°C are of direct interest, and typical data are shown in Fig. 12. In general, the Ambartsumyan et al. data showed that, in air and steam at these temperatures, the alloy's oxidation resistance decreased as the concentrations of Nb, Sn, Fe, or Ni were increased.

Emelyanov, Godin, and Evstyukhin[73] reported an investigation of the properties of binary and ternary zirconium-base alloys containing tantalum and niobium. Hardness and tensile tests were carried out on material in various conditions including as-cast, quenched–isothermal annealed, and hot-forged and annealed. For these alloys the major proportion of the increase in strength obtained on alloying required only ~2 wt.% total addition, although a small rate of increase was maintained with progressively larger additions. Maximum hardness in each alloy system was associated with quenching from the beta-phase region to give the martensitic beta–alpha-prime reaction.

In 1959 Robinson et al.[74] published results on heat-treatment, transformation reactions, and mechanical properties of three alloys: Zr–5 Nb–2 Sn, Zr–5 Mo–2 Sn, and Zr–4 Sn–2 Mo. Their intention was to produce a high-strength alloy with reasonable ductility, and use of aluminum as an alpha stabilizer was avoided because of its deleterious effect on oxidation resistance. Selected data are included in Table 2, the best combination of high strength and ductility being obtained for the first of the three alloys quenched from the (alpha + beta) region at 870°C and aged for 8 hr at 538°C. Robinson et al. concluded that considerable improvements in properties of the alloys could be obtained with optimization of composition and heat-treatment.

Wagner and Kline[75] made a systematic study of tensile and creep properties of ternary and quaternary alloys based on two Zr–Al binary alloys. Table 2 includes some of their data. For all these tests, specimens were machined from material vacuum annealed for 25 hr at 788°C after extrusion and hot rolling. In this condition, the strengthening effects were due to (1) solution hardening due to the alpha-soluble elements aluminum and tin, (2) grain-size refinement due to beta-zirconium phase formation during alloy fabrication in alloys containing molybdenum, and (3) formation of complex intermetallic phases including these alloying elements, precipitation of which will be largely at grain boundaries.

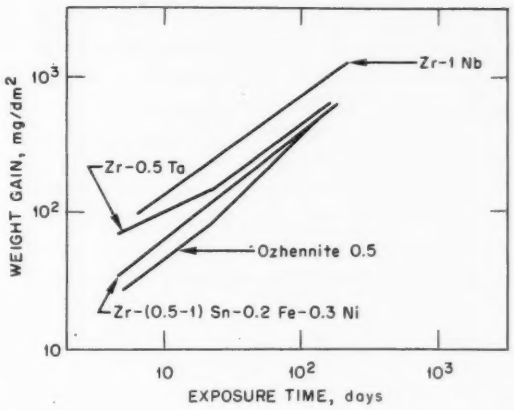

Fig. 12 Corrosion[26] of zirconium alloys in superheated steam at 450°C.

Examination of Wagner and Kline's data leads to the following conclusions:

1. The alpha hardening effects due to aluminum and tin are not simply additive, although, as seen in earlier work, these effects are quite similar for dilute binary alloys. Thus addition of 3 wt.% tin to the alloys containing 1.5 wt.% aluminum has a smaller effect on tensile properties than an increase in aluminum concentration to 3 wt.%. This discrepancy, in part, may be attributed to formation of tin-rich intermetallics.

2. The creep behavior of the alloys is not always directly proportional to the tensile properties. The substantial increase in ultimate tensile strength obtainable by increasing the complexity of the alloys is not necessarily matched by improvements in creep resistance.

The fabrication and thermal treatments used by Wagner and Kline did not exploit the alloy compositions to optimize tensile and creep properties. In particular, the alloys containing molybdenum are amenable to a quench-and-aging treatment that would raise tensile properties by refining grain structure; this treatment should also improve creep properties by refining intermetallic particle distribution.

In 1961 Beaumont[76] reported an investigation of the mechanical properties of five zirconium-base alloys containing combinations of aluminum, niobium, and

molybdenum. Tensile tests were carried out on material that had been vacuum annealed for 2 hr at 785°C, and some of the data are plotted in Figs. 13(*a*) and (*b*). No reliable creep data were obtained for the alloys. In these properties the predominant alloying factor is the alpha-solution hardening effect of aluminum, the additions of molybdenum and niobium having small influence on tensile properties of the annealed materials.

Harper[77] also reported results of tensile and creep evaluation of a number of alloys containing aluminum, tin, and niobium. Some of Harper's data are listed in Table 2. Data for creep tests on binary alloys did not show any consistent trend with increasing aluminum concentration. In the case of the Zr–3 Al alloys, the addition of 8 wt.% Nb was beneficial to creep behavior at 500°C, presumably owing to the introduction of a significant volume fraction of the beta-zirconium phase during fabrication and precipitation of intermetallic phases during final annealing and cooling. The quaternary addition of 0.2 or 0.5 wt.% tin had no significant effects in the tests reported; this is not surprising in view of the relatively large aluminum concentration that dominated alpha-solution hardening. Some advantage was apparently gained by using 800°C rather than 750°C as the preannealing temperature.

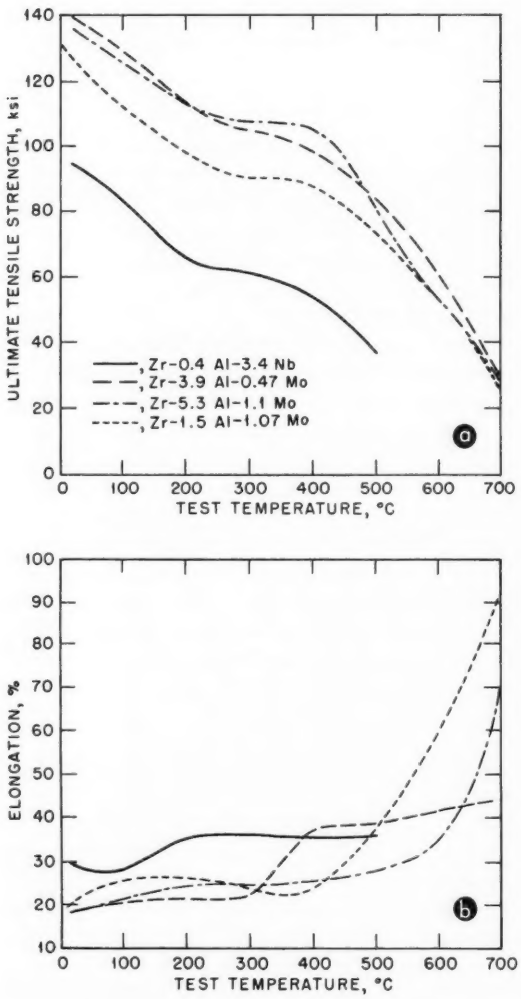

Fig. 13 Tensile properties of a number of Zr–Al-base ternary alloys.[76]

Harper suggested that the enhanced creep strength at 500°C exhibited by alloys containing aluminum was due to precipitation of Zr_3Al during deformation, although no evidence for such precipitation was presented.

Poole[78] reviewed work on zirconium-base alloys carried out at various UK laboratories, including the British Non-Ferrous Metals Research Association studies reported by Harper[77] and referred to above. He correlated tensile- and creep-test data for alloys containing Sn, Al, Mo, and Nb, using the Larson–Miller relation

$$\log \sigma \text{ vs. } T(C + \log t)$$

where σ = ultimate tensile strength or creep stress
T = test temperature, °K
C = constant, assuming values of 18 for tensile tests and 19 for creep tests
t = time of tensile test, or time to 1% deformation in creep

Figure 14 shows Poole's summary figure for the higher strength alloys including Wagner and Kline's data for the Zr–1.5 Al–1.5 Sn–1.5 Mo alloy.[75] Poole drew attention to the extrapolations made in calculating the Larson–Miller parameter for these different materials and tests, but he considered the comparison a useful guide to relative strengths. (Ibrahim[79] has found that the values of the constant C vary considerably for zirconium alloys of different composition and in different conditions.) The alloys containing aluminum showed the highest creep and tensile strength, and the advantage to be gained by increasing alloy complexity by addition of tin and molybdenum was again noted. Poole concluded that further improvements in properties for these complex alloys could be obtained by optimizing heat-treatments.

In 1964 Ito et al.[80] published results of autoclave corrosion tests at 320°C and hot-hardness measure-

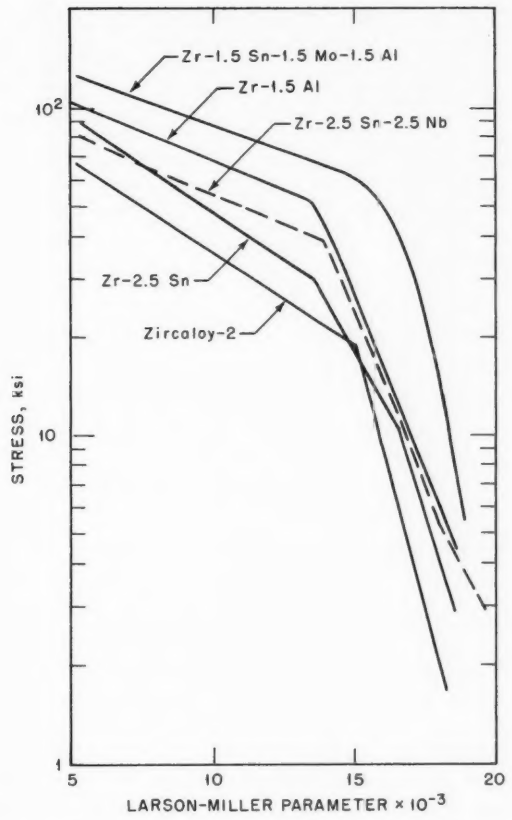

Fig. 14 Larson–Miller plot of high-temperature properties of zirconium alloys. After Poole.[78]

ments at 20 to 300°C, carried out on a range of dilute alloys containing combinations of Sn, V, Sb, Nb, P, Si, Al, Bi, Cu, Mo, and Pb. The elements conferring advantage for high-temperature strength were found to be Al, Sb, P, Mo, Fe, Bi, and Sn, the latter addition being useful in combination with other elements in improving the alloys' oxidation resistance.

Also in 1964 Aoki[81] reported the results of experiments on Zr–1 Mo–1 Cr and Zr–1 Mo–1 Ni alloys. The first of these alloys was subject to a martensitic hardening on quenching from 950°C; the Zr–Mo–Ni alloy was hardened somewhat but did not show a martensitic structure after this treatment. Recommended aging treatments to give good ductility and strength for the two alloys, respectively, were 100 min at 750°C and 100 min at 600°C. Aoki also used drop-hammer tests to evaluate the forgeability of the alloys and found them to be superior to Zircaloy-2 in this respect at 800°C.

Dicks and Bell[82] reported on an evaluation of mechanical properties of a Zr–1.5 Al–0.5 Mo alloy. Hardness and tensile tests were carried out on specimens solution treated for 2 hr at temperatures in the range 700 to 900°C and cooled at different rates. The properties fit into the pattern of behavior established by the work of Wagner and Kline[75] and Beaumont,[76] Fig. 13. Dicks and Bell pointed out that the alloy should develop higher properties than those reported if quenched from a solution-treatment temperature close to, or above, the (alpha + beta)/beta transus. Ells[83] has more recently reported the following results of tensile-property measurements on the Zr–1.5 Al–0.5 Mo alloy quenched from 900°C:

Test temp., °C	Yield strength (0.2% offset), ksi	Ultimate tensile strength, ksi	Elongation, %
20	123	147	2
400	91	119	2

With reference to the oxidation characteristics of alloys containing aluminum, Cox[8] has reported experiments made to measure rates of oxidation for various Zr–Al(–Mo) alloys in steam at temperatures in the range 300 to 650°C. Typical data for the above-mentioned Zr–1.5 Al–0.5 Mo alloy are shown in Fig. 15. The oxidation rates for all alloys tested were very high, with initial oxidation occurring predominantly around $ZrAl_3$ particles. Cox attributed the high

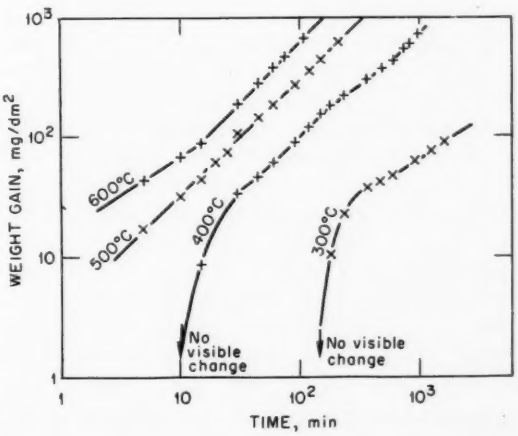

Fig. 15 Oxidation of Zr–1.5 Al–0.5 Mo in 1 atm steam.[8]

rates to aluminum in solution in the matrix zirconium, but the precise manner in which the solute influenced the oxidation process was not identified.

TITANIUM METALLURGY AS A GUIDE FOR ZIRCONIUM-ALLOY DEVELOPMENT

Intensive effort supported by the aircraft and aerospace industries has resulted in development of a wide range of titanium-base alloys. These are of varying complexity and include alloys having a high strength-to-weight ratio with good creep strength at temperatures up to 500°C. In 1963 Finlay and Lane[84] cited 80 ksi as the yield stress at 430°C for a typical commercial high-strength titanium alloy. They predicted that by 1980 development will have produced commercial alloys having a yield stress of 125 ksi at 430°C, with a 10% probability that alloys with a 156-ksi yield stress will be available. Progress toward these values has been rapid. In 1968 Imperial Metal Industries issued data sheets for the forging alloy Ti 700 that has a yield stress of ~115 ksi at 430°C in the solution-treated, air-cooled, and aged condition. Currently, development of high-strength titanium alloys is progressing more slowly because of the "rapid decline in strength of the basic structure around 500°C and by concessions which have to be made to toughness in high strength alloys."[85] Powder metallurgy is being given increased attention with the purpose of producing high-performance sintered alloys and dispersion-hardened alloys.

There are many similarities between the physical properties and metallurgy of titanium and zirconium and their alloys. Table 3 summarizes some of the important data for the two pure metals. In terms of creep strength at temperatures near 500°C, the most important parameters are probably shear moduli and self-diffusion coefficients (see Eq. 2). Alpha titanium has a higher shear modulus than alpha zirconium, the values for Young's modulus also showing a small advantage to alpha titanium. These differences indicate that titanium alloys may develop slightly higher tensile and creep strengths than zirconium alloys. Limited data are available for diffusion behavior in the close-packed hexagonal alpha-titanium and alpha-zirconium phases, and no direct measurements have been made at 500°C. The calculated diffusivities suggest that alpha zirconium may have a higher creep resistance than alpha titanium in the temperature range where steady-state creep occurs by dislocation climb, a diffusion-controlled process.

Table 3 Physical Constants for Titanium and Zirconium

Property	Zr	Ti
Atomic wt.	91.22	47.90
Density, g/cm^3	6.49	4.5
Melting temp, °C	1860	1670
Young's modulus $E \times 10^{11}$, dynes/cm^2	10.50	12.02
Shear modulus $G \times 10^{11}$, dynes/cm^2	3.04	4.56
Diffusion data:		
Frequency factor A, cm^2/sec	5.6×10^{-4}	6.4×10^{-8}
Activation energy Q, kcal/mole	45.5	29.3
$D_{calc.}$ at 500°C, cm^2/sec	7.8×10^{-17}	25.4×10^{-17}
Allotropic transformation	cph α to bcc β at ~840°C	cph α to bcc β at ~900°C
Lattice constants, Å	c/a α Zr = 1.59 β Zr a = 3.61	c/a α Ti = 1.585 β Ti a = 3.29

Obviously such comparisons are of limited value when alloying additions are made to the metals and when structural differences, i.e., grain size and dislocation distribution, are introduced by fabrication processes. However, the data support the view that zirconium alloys should be capable of providing mechanical properties similar to those of titanium alloys, and zirconium metallurgy can profit directly from experience with titanium. Further support is derived from the marked similarity that exists in the general metallurgical characteristics of the two systems. References 86 to 89 give recent compilations of the U. S., Russian, and British work on titanium metallurgy. Of particular importance to zirconium development are the analogies apparent in transformation reactions and deformation behavior as revealed in work over the past 5 years.[90-95] These analogies include the effect of heat-treatment on alpha–beta phase distribution, the range of martensitic and Widmanstätten structures obtainable in the transformed beta phases, the precipitation reactions obtained on aging the metastable phases, and the general pattern of dislocation behavior in deformed alloys.

Table 4 and Figs. 16 and 17 give[96] manufacturers' data for compositions, treatments, and properties for a selection of available complex titanium alloys. Com-

Table 4 Mechanical Properties for Various High-Strength Titanium Alloys, Taken From IMI* Data Sheets

Alloy designation	Composition, wt.%								Recommended heat-treatment	Test temp., °C	UTS, ksi	Elongation, %	Creep properties		
	Sn	Al	Mn	Mo	Cu	V	Zr	Si					Stress, ksi	Temp., °C	Minimum creep rate, hr^{-1}
(*a*) α Alloy															
Ti 317	2.5	5							Hot work in β, down through (α + β) range; recrystallize by anneal at ~850°C	20	112	12			
										500	72	18	20	500	5×10^{-6}
(*b*) (α + β) Alloys															
Ti 550	2	4		4				0.5	(1) Air cool from 900°C, age 24 hr at 500°C, air cool again	20	175	12			
										500	110	20	4	500	1×10^{-6}
									(2) Water quench from 900°C, age 24 hr at 500°C, air cool	20	210	7			
										500	130	15			
Ti 680	11	2.25		4				0.2	Solution treat in (α + β) at 800 to 840°C, air cool, age 24 hr at 500°C	20	190	16			
										500	138	16	55	450	1×10^{-5}
Ti 685		6		0.5			5	0.25	Solution treat in β region at 1050°C, oil quench, age 24 hr at 500°C	20	155	12			
										500	109	18	45	520	8×10^{-5}
Ti 700		6		4	1		5	0.2	Solution treat at 900°C, air cool, age 24 hr at 500°C	20	193	13			
										500	142	18	74	400	1×10^{-5}

*Imperial Metal Industries, Ltd., Birmingham, England.

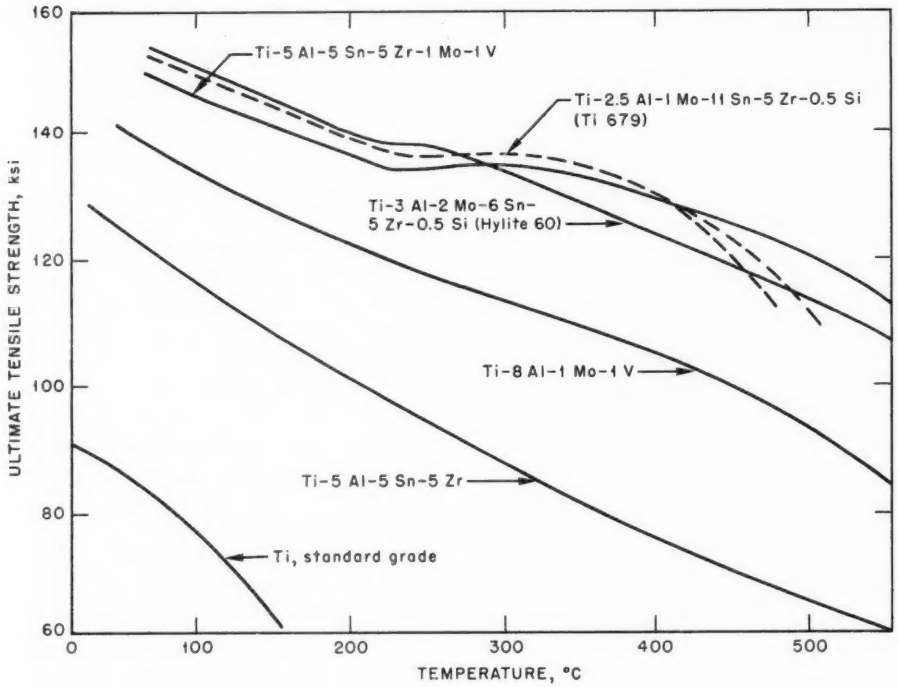

Fig. 16 Tensile properties of complex titanium alloys as a function of temperature.[96]

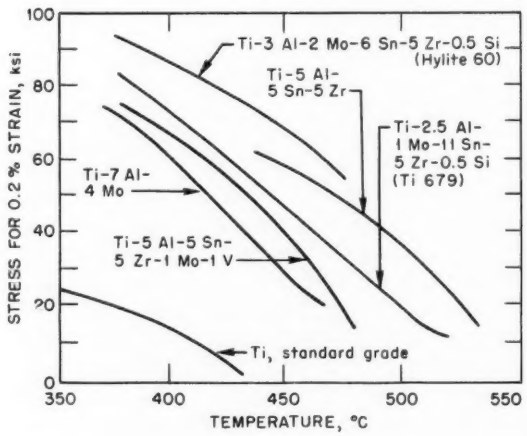

Fig. 17 Stress to give hot 0.2% strain in 1000 hr for various titanium alloys as a function of temperature.[96]

parison of these data with those for zirconium alloys given in Table 2 and Figs. 9, 11, and 13 must be made with the following points in mind:

1. Aluminum and tin are much more soluble in alpha titanium than in alpha zirconium, and more solute is required in titanium than in zirconium to provide a given hardening effect.

2. The use of solutes in titanium alloys has not been inhibited by neutron-absorption considerations, and large weight fractions have been used.

3. The titanium alloys have generally received heat-treatments that exploit solution and precipitation hardening more effectively than the treatments used for the zirconium alloys listed in Table 2, with the exception of the work of Robinson et al.[74]

The high-strength titanium alloys achieve a combination of strength and ductility that would be satisfactory in zirconium alloys for reactor applications. These properties are often obtained by a treatment that would be conveniently applied to an extruded tube, namely, air cooled from the upper (alpha + beta) region and then aged at 500°C.

Creep data for titanium alloys are not usually reported in a manner suited to prediction of behavior over the long terms considered for the operation of components in power reactors. Data plotted in Fig. 18 indicate that the stress dependence of titanium-alloy creep rates in the temperature range near 500°C may be slightly higher than for zirconium alloys. Stress-

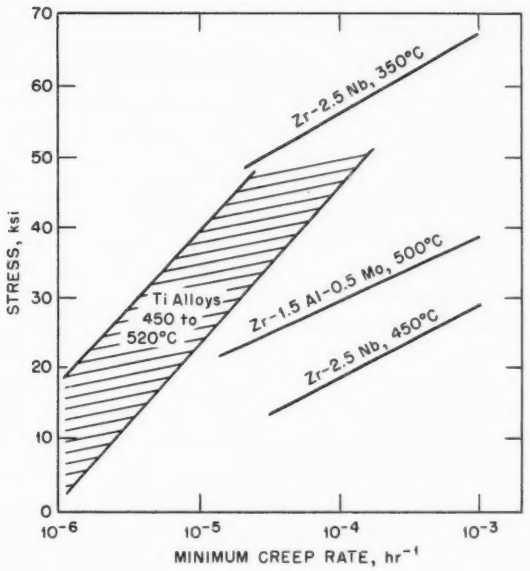

Fig. 18 Stress dependence of creep rate for various zirconium alloys[79] and titanium alloys (IMI data sheets and Refs. 96 and 97).

rupture data plotted in Fig. 19 indicate a similar stress dependence in rupture characteristics for the two alloy systems at 450°C. The data suggest that complex zirconium alloys should have creep properties at least equivalent to, and perhaps superior to, the titanium alloys, unless the stress dependence of creep rates for zirconium alloys increases significantly in the stress range below 20 ksi.

A further point gained from the data given in Table 4 is that small additions of silicon are found to be beneficial in titanium alloys. Little is known of the effect of such additions to zirconium alloys, although the solubility of silicon in zirconium is known to be very low. These additions to titanium are effective in promoting high-temperature strength, provided the silicon content remains within the soluble range; at higher concentrations, silicides may be precipitated at grain boundaries, inducing brittleness of the material.

Some problems significant in the fabrication and processing of titanium alloys should also be noted. Among these are the following:

1. The increasingly complex alloys developed for high-temperature strength have shown susceptibility to segregation of alloying elements, leading particularly to reduction in transverse properties in forging alloys. This problem has become important with an increasing demand for large forged components.

2. Beta forging is attractive in principle because it offers greater ease of production of large components. However, this technique must be used with care for alloys containing significant additions of beta-stabilizing elements (molybdenum, vanadium), because such alloys tend to show unacceptably low ductility after beta processing followed by intermediate-temperature aging. This reduction in ductility may be alleviated, for example, by effecting the final stages of processing in the (alpha + beta) range. Use of beta quenching, in general, leads to an increase in creep strength and fracture toughness, although in heavily beta-stabilized alloys this is accompanied by an unacceptable reduction in ductility.[98,99]

3. The inherent risk of distortion of large components during water quenching from solution temperatures high in the (alpha + beta) or in the beta region places importance on development of alloys that achieve high strength after air hardening. However, since maximum strength attainable is usually provided by water-quenching treatments, special quenching techniques have been devised for individual components to minimize distortion due to nonuniform cooling. Similar experience has been gained[100] with development of processing for the heat-treatable pressure-tube alloy Zr–2.5 Nb.

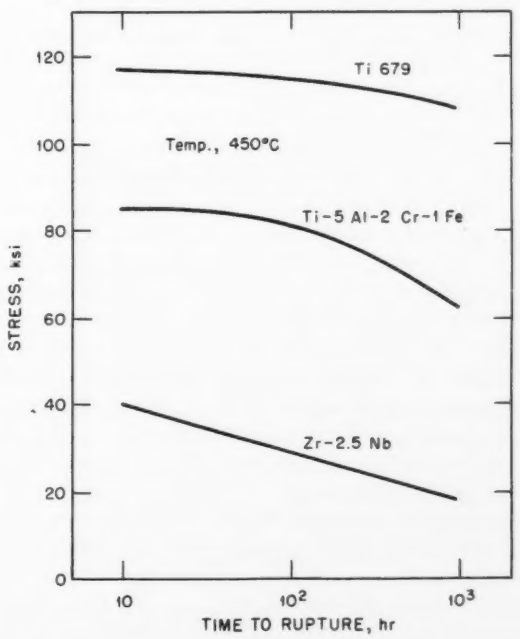

Fig. 19 Stress for rupture of the heat-treated Zr–2.5 Nb alloy[79] and two titanium alloys (IMI data sheets and Ref. 97).

The titanium-alloy data presented here indicate that zirconium alloys having reasonable ductility (near 10% elongation at 20°C), allied with ultimate tensile strength in the range 100 to 150 ksi at 450°C, should be obtainable. With an air-cooling and aging treatment, such alloys should have good creep strength at temperatures up to 500°C. The essential aspect of development which may produce zirconium alloys having these properties will be the use of the maximum solution- and precipitation-hardening potential of low-neutron-absorption addition elements.

CONCLUSIONS FROM THE LITERATURE REVIEW

It is clear that alloys having much higher tensile and creep strength than conventional zirconium alloys can be obtained by increasing alloy complexity. Increased solid-solution strengthening can be achieved by raising tin or aluminum concentrations. Creep strength can be improved by adding molybdenum and niobium to promote formation of stable precipitates in heat-treatable alloys. As stated above, solubility levels and cross-section considerations restrict alloying in zirconium to levels lower than those used in titanium metallurgy. From the reviewed work, and assuming that a 10% increase in cross section over that of Zircaloy-2 is a reasonable limit, combinations within the following range of solute additions to zirconium are considered worthy of attention: 2 to 4 wt.% tin, 0.5 to 3 wt.% aluminum, 0.5 to 1.5 wt.% molybdenum, 0.5 to 3 wt.% niobium, 0 to 0.3 wt.% silicon (solubility limit of silicon in alpha zirconium is uncertain).

The aluminum addition is not desirable if oxidation characteristics of the alloy are considered, and the combination of alloy additions, particularly of the beta stabilizers molybdenum and niobium, requires careful selection. For useful application in tubular form, the alloy must be sufficiently ductile at high temperatures for fabrication purposes and should preferably develop adequate strength by air cooling, thus obviating the necessity for difficult quenching techniques. Each of these properties requires a reasonably large volume fraction of the bcc beta phase to be present at the fabrication temperature. This phase, however, should not be enriched with solute to the point where its decomposition proceeds via the embrittling beta → omega reaction. Molybdenum is a more effective beta stabilizer than niobium (see Fig. 8) and is less soluble in alpha zirconium than niobium; thus, for a limited alloy addition, combinations of molybdenum and niobium promote higher strength levels than those obtained for Zr–Nb binary alloys. Chubb's results[70] indicate that 2 to 4 wt.% tin, in addition to a Mo–Nb combination, will provide a satisfactory solution strengthening in the alpha-zirconium phase. The titanium experience* suggests that a small addition of silicon will also be profitable, although this addition should remain within the solubility limit to avoid formation of silicides at grain boundaries.

Figure 20 gives an estimated range of strengths which should be attainable in zirconium alloys using direct alloying methods. The work of Chubb[69,70] and Robinson et al.[74] has shown that properties in this range can be achieved without use of aluminum additions. It may be anticipated that alloys having ultimate tensile strengths in the upper range will have low ductilities, <10% elongation in tensile tests at 20°C. There is little doubt that even higher strengths can be achieved in quenched–aged alloys if large alloy additions are made, but present information indicates that such alloys will have unacceptably low ductility.

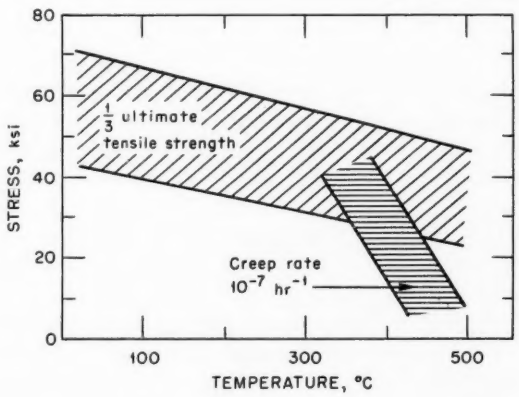

Fig. 20 Prediction of design stress range that should be attainable in complex zirconium alloys.

However, the limiting property for pressure-vessel application is likely to be creep strength, and numerous quoted examples have shown that optimum creep strength does not necessarily coincide with maximum tensile strength. Following the titanium example, development should be directed to alloys that have adequate strength after air-cooling–aging treatments.

Reference to the effects of irradiation on the properties of conventional zirconium alloys has been made. It is believed that radiation-damage accumulation at temperatures in the range 450 to 500°C will

have less influence on strength and ductility than is the case for irradiation at 300°C. Also, because of the coincident increase in thermal creep rates and radiation-defect recovery, irradiation should have a smaller effect on in-reactor creep behavior. The limited information reported for zirconium and Zircaloy-2 irradiated at 450°C has shown that small three-dimensional voids, of the type formed in steels and numerous fcc and bcc metals irradiated at similar homologous temperatures, are not formed in the cph materials at fast-neutron fluences up to 4×10^{21} neutrons/cm^2.[47a,b] It seems likely that this phenomenon, which is provoking intensive work on fast-reactor fuel-cladding materials, will not interfere with the use of zirconium alloys in water reactors at elevated temperatures.

ADVANCED TECHNIQUES FOR IMPROVING HIGH-TEMPERATURE PROPERTIES

It is appropriate here to comment on additional methods that may be available for strengthening zirconium alloys. Reed-Hill[101] has shown that the ductility of zirconium can be increased by a small prestrain (1 to 2%) introduced at liquid-nitrogen temperature, −196°C. His results show an increase in elongation from 20 to 26% at room temperature, a reduction in yield stress from 47 to 32 ksi, and no significant change in ultimate tensile strength. These changes are attributed to formation, at the low prestrain temperature, of a high density of twins in grains oriented unfavorably for slip. These grains subsequently deform with increased slip-oriented characteristics. Reed-Hill proposed that the technique could be used for tubular products of zirconium alloys, although it is likely that such processing would be costly.

Major improvements in the high-temperature properties of ferrous materials, and to a lesser extent nonferrous alloys, have been obtained using various *thermomechanical* processes.[102,103] The standard cold-working–stress-relieving treatment used in fabrication of conventional zirconium alloys is a simple process by comparison with some now used in other branches of metallurgy. These processes are designed to produce a stable dislocation substructure, often with small subgrains stabilized by precipitates. Work on Zircaloy-2 and the Zr–2.5 Nb alloy has shown that a range of such structures can be produced in zirconium alloys,[104] but the dilute alloys lack adequate precipitation capability to stabilize the structures at 450 to 500°C. It may be expected that thermomechanical processing to improve high-temperature strength and ductility may be used profitably in more complex zirconium alloys.

Various attempts have been made to improve zirconium-alloy properties by *dispersion hardening*. In principle, this technique offers improved stability of substructures in high-strength alloys at temperatures in the range 500 to 600°C. Powder-metallurgy routes with La_2O_3, ThO_2, and particularly Y_2O_3 as the dispersoids[105-107] have failed to produce materials with a sufficiently well-dispersed oxide to improve high-temperature properties significantly. Problems include difficulty in adequately mixing the powders, contamination of the matrix zirconium during the sintering–consolidation process, and interaction of zirconium with the oxide. It is possible that current attention being paid to powder-metallurgy techniques in titanium-alloy development will provide encouragement for further work on this form of strengthening in zirconium alloys.

Finally, *fiber reinforcement* is the subject of active materials research[108,109] but has not yet made a significant impression on zirconium metallurgy. As with dispersion hardening, this technique, in principle, may be applied to increase the useful temperature range of high-strength alloys, provided the economic incentive is high enough to justify the complex fabrication technology involved.

SUMMARY

More effective exploitation of zirconium can lead to development of alloys with high-temperature mechanical properties far superior to those of the conventional Zircaloys and other dilute alloys. Such exploitation involves accepting an increased neutron absorption and making adequate alloy additions to raise solution- and precipitation-hardening reactions, and also making selective use of thermal and deformation treatments. The available evidence indicates that complex zirconium alloys should have mechanical properties comparable with and perhaps superior to the high-strength titanium alloys. Concurrent development of corrosion-resistant alloys and cladding techniques should allow these strong zirconium alloys to be used in aqueous environments at temperatures up to 500°C.

ACKNOWLEDGMENTS

The author gratefully acknowledges valuable discussions with numerous colleagues, notably W. R.

Thomas, C. E. Ells, V. Fidleris, and E. F. Ibrahim. Appreciation is also expressed to E. C. W. Perryman for his interest and support throughout this work and to Atomic Energy of Canada Limited for permission to publish this article.

REFERENCES

1. D. G. Hurst, Improving the Thermal Efficiency of CANDU'S, Canadian Report AECL-3332, June 1969.
2. B. Cox, Effects of Irradiation on the Oxidation of Zirconium Alloys in High Temperature Aqueous Environments (A Review), *J. Nucl. Mater.*, **28**: 1 (1968).
3. A. J. Mooradian, R. F. S. Robertson, S. R. Hatcher, R. G. Hart, D. R. Tegart, and A. J. Summach, Present Status of Canadian Organic Cooled Reactor Technology, in *Heavy-Water Power Reactors,* Symposium Proceedings, Vienna, 1967, p. 383, International Atomic Energy Agency, Vienna, 1968 (STI/PUB/163).
4. J. Boulton, Current Knowledge of Zirconium Alloys for Reactor Usage, Canadian Report AECL-3365, June 1969.
5. R. N. Duncan, H. H. Klepfer, E. A. Pickett, R. E. Blood, and G. F. Reiger, Specific Zirconium Alloy Design Program, USAEC Report GEAP-5603, Quarterly Progress Reports Nos. 18 and 19, General Electric Company, 1968.
6. Zirconium Based Materials To Be Utilized in Nuclear Reactors, French Patent No. 1,448,044 (April 1965).
7. J. L. Baker, Fabrication of Zircaloy-4 Clad Zr–2.5% Nb Pressure Tubing, USAEC Report TID-23312, Chase Brass and Copper Co., Inc., August 1966.
8. B. Cox, Oxidation of Zirconium–Aluminum Alloys, Canadian Report AECL-2776, October 1967.
9. B. A. Wilcox, Basic Strengthening Mechanisms in Refractory Metals, in *Refractory Metal Alloys,* p. 1, Plenum Press, Inc., New York, 1968.
10. P. S. Rudman, Solution Strengthening in Refractory Metal Alloys, in *Refractory Metals and Alloys IV: Research and Development,* p. 351, Gordon and Breach, Science Publishers, Inc., New York, 1967.
11. D. L. Douglass, The Physical Metallurgy of Zirconium, *At. Energy Rev.*, **1**(4): 71 (1963).
12. G. T. Higgins and E. Banks, The Basic Features of the Isothermal Promonotectoid Transformation in a Zirconium–2.5 Wt.% Niobium Alloy, *Electrochem. Technol.*, **4**(7-8): 341 (1966).
13. D. B. Scott, Physical and Mechanical Properties of Zircaloy-2 and -4, USAEC Report WCAP-3269-41, Westinghouse Electric Corporation, May 1965.
14. D. Weinstein, Yield Point Occurrence in Polycrystalline Alpha–Zirconium, *Electrochem. Technol.*, **4**(7-8): 307 (1966)
15. A. K. Mukherjee, J. E. Bird, and J. E. Dorn, Experimental Correlations for High-Temperature Creep, *ASM (Amer. Soc. Metals), Trans. Quart.*, **62**: 155 (1969).
16. J. P. Pemsler, E. C. W. Perryman, and W. W. Smeltzer (Eds.), *Zirconium and Its Alloys,* The Electrochemical Society, 1966.
17. The In-Reactor Creep of Zirconium Alloys, *J. Nucl. Mater.*, **26**(1): 1 (1968).
18. S. H. Miller, G. J. Moyar, and C. E. Troller, Literature Survey on In-Pile Mechanical Properties: Testing and Theory, USAEC Report KAPL-3453, Knolls Atomic Power Laboratory, August 1968.
19. C. E. Ells, Hydride Precipitates in Zirconium Alloys (A Review), *J. Nucl. Mater.*, **28**: 129 (1968).
20. R. L. Knecht and P. J. Pankaskie, Zircaloy-2 Pressure Tubing, USAEC Report BNWL-746, Battelle–Northwest, December 1968.
21. *Applications-Related Phenomena in Zirconium and Its Alloys,* American Society for Testing and Materials, Special Technical Publication No. 458, 1970.
22. C. R. Woods (Ed.), Properties of Zircaloy-4 Tubing, USAEC Report WAPD-TM-585, Bettis Atomic Power Laboratory, 1965.
23. C. E. Ells, S. B. Dalgaard, W. Evans, and W. R. Thomas, Development of Zirconium–Niobium Alloys, in *Proceedings of the Third International Conference on the Peaceful Uses of Atomic Energy, Geneva, 1964,* Vol. 9, p. 91, United Nations, New York, 1965.
24. J. Winton and R. A. Murgatroyd, The Effect of Variations in Composition and Heat-Treatment on the Properties of Zr–Nb Alloys, *Electrochem. Technol.*, **4**(7-8): 358 (1966).
25. H. H. Klepfer, Zirconium Base Nuclear Reactor Alloy, U. S. Patent No. 3,287,111 (November 1966).
26. R. S. Ambartsumyan, A. A. Kiselev, R. V. Grebennikov, V. A. Myshkin, L. J. Tsuprun, and A. F. Nikulina, Mechanical Properties and Corrosion Resistance of Zirconium and Its Alloys in Water, Steam, and Gas at High Temperatures, in *Proceedings of the Second United Nations International Conference on the Peaceful Uses of Atomic Energy, Geneva, 1958,* Vol. 5, p. 12, New York, 1958.
27. M. Armand, H. Demars, and J. P. Givard, Influence of Precipitates on Mechanical Properties of Zr–Cu Alloys, *Revue Met. (Paris)*, **64**(3): 249 (1967).
28. J. M. Frenkel and M. Weisz, Study of Deformation and Oxidation of Zr–Cu Alloys in CO_2, International Conference on Use of Zirconium Alloys in Nuclear Reactors, Marianske Lazne, October 1968.
29. P. Baque and R. Darras, Ternary Alloy of Zirconium, Canadian Patent No. 750,318 (January 1967).
30. Associated Electrical Industries, Zirconium Alloys Used for Construction of Fuel Elements in Nuclear Reactors, French Patent No. 1,281,191 (November 1961).
31. P. A. Ross-Ross, The In-Reactor Creep of Zirconium Alloy Pressure Tubes, Symposium on Creep Rate vs. Total Creep, U. S. National Materials Exposition, Philadelphia, October 1969.
32. J. Winton, R. A. Murgatroyd, B. Watkins, and R. W. Nichols, The Strength of Zr–2.5% Nb Alloy in the Annealed and Cold-Worked Condition, *Trans. Jap. Inst. Metals, Suppl.*, **9**: 630 (1968).
33. C. D. Williams and R. W. Gilbert, On Structural Factors Influencing the Strength of Martensitic α' in Quenched Zr–2.5% Nb., *Trans. Jap. Inst. Metals, Suppl.*, **9**: 625 (1968).
34. B. Lustman and F. Kerze, *The Metallurgy of Zirconium,* McGraw-Hill Book Co., Inc., New York, 1955.

35. W. R. Tyson, Strengthening of hcp Zr, Ti, and Hf by Interstitial Solutes—A Review, *Can. Met. Quart.*, 6(4): 301 (1966).

36. V. Fidleris, Effect of Strain Aging and Texture on Creep of Zirconium Alloys, *Applications-Related Phenomena in Zirconium and Its Alloys*, American Society for Testing and Materials, Special Technical Publication No. 458, 1970.

37. R. Smith, Discussion to paper by C. D. Williams and R. W. Gilbert, Fast Neutron Damage in Zirconium Based Structural Alloys, in *Radiation Damage in Reactor Materials*, Symposium Proceedings, Vienna, 1969, Vol. 1, p. 379, International Atomic Energy Agency, Vienna, 1969 (STI/PUB/230).

38. E. R. Gilbert, S. A. Doran, and A. L. Bement, Creep of Zirconium from 50 to 850°C, in *Applications-Related Phenomena in Zirconium and Its Alloys*, American Society for Testing and Materials, Special Technical Publication No. 458, 1970.

39. V. Fidleris and C. D. Williams, Influence of Neutron Irradiation on the Creep of Zircaloy-2 at 300°C, *Electrochem. Technol.*, 4(5-6): 258 (1966).

40. C. D. Williams, V. Fidleris, and L. G. Bell, A Correlation of Creep Behavior at 300°C and 450°C with Structure of Zr–2.5 Wt.% Nb Alloy, Canadian Report AECL-2615. Presented at Conference of Metallurgists, Toronto, 1965.

41. C. E. Coleman, Grain Boundary Sliding in Zirconium, presented at Conference of Metallurgists, Windsor, Ontario, August 1969.

42. M. L. Picklesimer, A Preliminary Examination of the Formation and Utilization of Texture and Anisotropy in Zircaloy-2, in Proceedings of the USAEC Symposium on Zirconium Alloy Development—Castlewood, Pleasanton, California, November 12–14, 1962, H. H. Klepfer (Comp.), USAEC Report GEAP-4089(Vol. 1), Vallecitos Atomic Laboratory, 1962.

43. B. A. Cheadle and C. E. Ells, The Effect of Heat-Treatment on the Texture of Fabricated Zirconium-Rich Alloys, *Electrochem. Technol.*, 4(7-8): 329 (1966).

44. B. A. Cheadle, C. E. Ells, and W. Evans, The Development of Texture in Zirconium Alloy Tubes, *J. Nucl. Mater.*, 23: 199 (1967).

45. B. A. Cheadle and C. E. Ells, The Effect of Rolling Temperature on the Texture Developed in Rolled Zirconium-Rich Alloys, *J. Nucl. Mater.*, 24: 240 (1967).

46. A. L. Bement, Jr., Radiation Damage in Hexagonal Close-Packed Metals and Alloys, in *Radiation Effects*, p. 671, Gordon and Breach, Science Publishers, New York, 1965.

47. *a*. C. D. Williams and R. W. Gilbert, Fast Neutron Damage in Zirconium Based Structural Alloys, in *Radiation Damage in Reactor Materials*, Symposium Proceedings, Vienna, 1969, Vol. 1, p. 235, International Atomic Energy Agency, Vienna, 1969 (STI/PUB/230).

b. G. L. Kulchinski, Discussion to C. D. Williams and R. W. Gilbert, Fast Neutron Damage in Zirconium Based Structural Alloys, in *Radiation Damage in Reactor Materials*, Symposium Proceedings, Vienna, 1969, Vol. 1, p. 247, International Atomic Energy Agency, Vienna, 1969 (STI/PUB/230).

48. C. E. Ells and V. Fidleris, Effect of Neutron Irradiation on Tensile Properties of the Zirconium–2.5 Wt.% Niobium Alloy, *Electrochem. Technol.*, 4(5-6): 268 (1966).

49. C. D. Williams and C. E. Ells, The Influence of Niobium in Irradiation Strengthening of Dilute Zr–Nb Alloys, *Phil. Mag.*, 18(154): 763 (1968).

50. C. E. Ells and C. D. Williams, Beta Embrittlement of the Zr–2.5 Wt.% Nb Alloy, *Trans. Met. Soc. AIME*, 245: 1321 (1969).

51. P. A. Ross-Ross and C. E. L. Hunt, The In-Reactor Creep of Cold-Worked Zircaloy-2 and Zr–2.5 Wt.% Niobium Pressure Tubes, *J. Nucl. Mater.*, 26: 2 (1968).

52. V. Fidleris, Uniaxial In-Reactor Creep of Zirconium Alloys, *J. Nucl. Mater.*, 26: 51 (1968).

53. P. H. Kreyns and M. W. Burkart, Radiation Enhanced Relaxation in Zircaloy-4 and Zr/2.5 Wt.% Nb/0.5 Wt.% Cu Alloys, *J. Nucl. Mater.*, 26: 87 (1968).

54. E. R. Gilbert, In-Reactor Creep of Zr–2.5 At.% Nb, *J. Nucl. Mater.*, 26: 105 (1968).

55. B. Watkins and D. S. Wood, The Significance of Irradiation-Induced Creep on Reactor Performance of a Zircaloy-2 Pressure Tube, in *Applications-Related Phenomena in Zirconium and Its Alloys*, American Society for Testing and Materials, Special Technical Publication No. 458, 1970.

56. G. R. Piercy, Mechanisms for the In-Reactor Creep of Zirconium Alloys, *J. Nucl. Mater.*, 26: 18 (1968).

57. R. V. Hesketh, Applications of the Generalized Theory of Yielding Creep of Irradiation Creep in Zirconium Alloys, *J. Nucl. Mater.*, 26: 77 (1968).

58. R. V. Hesketh, J. E. Harbottle, N. A. Waterman, and R. C. Lobb, Irradiation Growth and Creep in Zircaloy-2, in *Radiation Damage in Reactor Materials*, Symposium Proceedings, Vienna, 1969, Vol. 1, p. 365, International Atomic Energy Agency, Vienna, 1969 (STI/PUB/230).

59. F. A. Nichols, Theory of the Creep of Zircaloy During Neutron Irradiation, *J. Nucl. Mater.*, 30: 249 (1969).

60. C. D. Williams, Discussion to R. V. Hesketh, J. E. Harbottle, N. A. Waterman, and R. C. Lobb, Irradiation Growth and Creep in Zircaloy-2, in *Radiation Damage in Reactor Materials*, Symposium Proceedings, Vienna, 1969, Vol. 1, p. 378, International Atomic Energy Agency, Vienna, 1969 (STI/PUB/230).

61. K. Veevers, W. B. Rotsey, and K. U. Snowden, The Effect of Neutron Irradiation and Cold Work on the Strain Ageing Behavior of Zircaloy-2, Australian Report AAEC/TM-491, 1968, reported by R. Smith, Ref. 37.

62. F. A. Nichols, Evidences for Superplasticity During Irradiation Creep, presented at AIME Meeting, Philadelphia, 1969. Submitted for publication to *Trans. Met. Soc. AIME*.

63. R. G. Hoagland and R. G. Rowe, Fracture of Irradiated Zircaloy-2, *J. Nucl. Mater.*, 30: 179 (1969).

64. A. Cowan and W. J. Langford, Effect of Hydrogen and Neutron Irradiation on the Failure of Flawed Zircaloy-2 Pressure Tubes, *J. Nucl. Mater.*, 30: 271 (1969).

65. W. J. Langford, The Metallurgical Examination of a Cold-Worked Zircaloy-2 Pressure Tube Irradiated in the U-2 Loop, Canadian Report AECL-3457, October 1969.

66. G. M. Adamson, Jr., J. O. Betterton, Jr., J. H. Frye, Jr., and M. L. Picklesimer, Jr., Recent Advances in the

Metallurgy of Zirconium and Titanium Alloys of Special Interest in Reactor Technology, in *Proceedings of the Second United Nations International Conference on the Peaceful Uses of Atomic Energy, Geneva, 1958,* Vol. 5, p. 3, New York, 1958.

67. E. F. Ibrahim, private communication.
68. R. J. van Thyne and D. J. McPherson, Elevated Temperature Strength of Selected Zirconium-Based Alloys, *ASM (Amer. Soc. Metals), Trans. Quart.*, **48**: 795 (1956).
69. W. Chubb, Progress in the Development of Creep Resistant Zirconium Alloys, *ASM(Amer. Soc. Metals), Trans. Quart.*, **48**: 804 (1956).
70. W. Chubb, High Strength Zirconium Alloy: Zr–4 Wt.% Sn–1.6 Wt.% Mo, *Trans. Met. Soc. AIME*, **209**: 461 (1957).
71. R. F. Domagala, D. W. Levinson, and D. J. McPherson, Transformation Kinetics and Mechanical Properties of Zr–Mo Alloys, *Trans. Met. Soc. AIME*, **209**: 1191(1957).
72. O. S. Ivanov and V. K. Grigorovich, Structure and Properties of Zirconium Alloys, in *Proceedings of the Second United Nations International Conference on the Peaceful Uses of Atomic Energy, Geneva, 1958,* Vol. 5, p. 11, United Nations, New York, 1958.
73. V. S. Emelyanov, Y. G. Godin, and A. I. Evstyukhin, Mechanical Properties of Zirconium Binary and Ternary Alloys with Tantalum and Niobium at Room and Elevated Temperatures, in *Proceedings of the Second United Nations International Conference on the Peaceful Uses of Atomic Energy, Geneva, 1958,* Vol. 5, p. 69, 1958.
74. H. A. Robinson, J. R. Doig, M. W. Mote, and P. D. Frost, Heat-Treatment, Transformation Reactions, and Mechanical Properties of Some High-Strength Zirconium-Base Alloys, *Trans. Met. Soc. AIME*, **215**: 237 (1959).
75. R. K. Wagner and H. E. Kline, High Strength Zirconium Alloys, *ASM (Amer. Soc. Metals), Trans. Quart.*, **52**: 713 (1960).
76. F. V. Beaumont, Orenda Ltd., private communication.
77. S. Harper, Creep Properties of Zirconium Alloys, Report S144/11, British Non-Ferrous Metals Research Association, 1961.
78. D. M. Poole, Creep Resistant Zirconium Alloys. A Survey, British Report AERE-M-886, 1961.
79. E. F. Ibrahim, The Stress Rupture Properties of Heat-Treated Zirconium–2.5% Niobium Alloy, Canadian Report AECL-3361, May 1969.
80. G. Ito, R. Hasiguti, M. Hasegawa, Y. Mishima, F. Sawayanagi, and Y. Shimizu, A Study on the Zirconium Alloys for Nuclear Reactors with High Strength at Elevated Temperatures, *Trans. Jap. Inst. Metals*, **6**: 173 (1964).
81. S. Aoki, Studies on Workability, Heat-Treatment Characteristics and Corrosion Resistance for Pressurized Water of Zr–1% Mo–1% Cr and Zr–1% Mo–1% Ni Alloys, *J. Jap. Inst. Metals*, **28**: 22 (1964).
82. T. S. Dicks and L. G. Bell, Hawker Siddeley Laboratory, unpublished, 1964.
83. C. E. Ells, Atomic Energy of Canada Limited, personal communication.
84. W. L. Finlay and J. R. Lane, Closing the Metal Gap, *Metal Progr.*, **84**(3): 78 (1963).
85. Allen G. Gray, A Look at Worldwide Titanium Technology: A Report on the International Conference on Titanium, London, 1968, *Metal Progr.*, **94**(3): 60-71 (see Gray's discussion of P. Hodgkinson's paper on page 62).
86. Foreign Technology Division, Air Force Systems Command, The Physical Metallurgy of Titanium (translations from Russian), Report AD-655033, December 1966.
87. A. W. Hodge and D. J. Maykuth, Properties of New High-Temperature Titanium Alloys, Report AD-667533, Defense Metals Information Center, February 1968.
88. Defence Documentation Center Bibliography, Titanium: Titanium Alloys, Report AD-689850, Vol. 1, June 1969.
89. Proceedings of an International Conference on Titanium, London, 1968.
90. Z. Nishiyama, M. Oka, and H. Nakagawa, The Electron Microscopic Structure and Lattice Defects of the Martensite in Commercially Pure Titanium, *Trans. Jap. Inst. Metals*, **3**: 168 (1966).
91. M. J. Blackburn, Relationship of Microstructure to Some Mechanical Properties of Ti–8 Al–1 V–1 Mo, *ASM (Amer. Soc. Metals), Trans. Quart.*, **59**: 695 (1966).
92. J. C. Williams and M. J. Blackburn, Comparison of Phase Transformations in Three Commercial Titanium Alloys, *ASM (Amer. Soc. Metals), Trans. Quart.*, **60**: 373 (1967).
93. K. R. Evans, Deformation Mechanisms in Titanium and Titanium-Aluminum Alloys, *Trans. Met. Soc. AIME*, **242**: 648 (1968).
94. M. J. Blackburn and J. C. Williams, Phase Transformations in Ti–Mo and Ti–V Alloys, *Trans. Met. Soc. AIME*, **242**: 2461 (1968).
95. A. A. Adair, Influence of Processing Variables on the Microstructure of Extruded Titanium 5 Al–2.5 Sn Alloy, *ASM (Amer. Soc. Metals), Trans. Quart.*, **62**: 345 (1969).
96. M. G. Manzone, Titanium Alloys with Molybdenum—the 1966 Picture, Climax Molybdenum Co. Publication, 1966.
97. Z. Takao, H. Kusamichi, S. Tokuda, K. Miyamoto, and Y. Fukuhara, Properties and Application of Ti–5 Al–2 Cr–1 Fe Alloy (KS150B), in Proceedings of an International Conference on Titanium, London, 1968.
98. T. E. Green and C. D. Minton, The Effect of Beta Processing on the Properties of Titanium Alloys, in Proceedings of an International Conference on Titanium, London, 1968.
99. J. E. Coyne, The Beta Forging of Titanium Alloys, in Proceedings of an International Conference on Titanium, London, 1968.
100. W. Evans, J. E. LeSurf, and W. R. Thomas, Heat-Treated Zr–2.5% Nb Pressure Tubes for Water-Cooled Power Reactors, Canadian Report AECL-2890, May 1967.
101. R. E. Reed-Hill, Process for Improving Properties of Zirconium Metal, Canadian Patent No. 746,589 (October 1967).
102. V. S. Ivanov and L. K. Gordienko, New Ways of Increasing the Strength of Metals, Translation published by the Iron and Steel Institute, Publication No. 109, London, 1968.
103. T. J. Koppenaal, The Current Status of Thermomechanical Treatment of Steel in the Soviet Union, *ASM (Amer. Soc. Metals), Trans. Quart.*, **62**: 24 (1969).
104. C. D. Williams and R. W. Gilbert, Effects of Thermomechanical Treatments on Structures and Properties of Zirconium Alloys, presented at ASTM Symposium on

Applications Related Phenomena in Zirconium and Its Alloys, Philadelphia, 1968, to be published.
105. D. Weinstein and F. C. Holtz, Dispersion Strengthened Zirconium Alloys, Report ARF-2234-7, Illinois Institute of Technology, September 1962.
106. K. C. Anthony and H. H. Klepfer, Dispersion Strengthened Zirconium Alloys, *J. Less-Common Metals*, 8: 36 (1965).
107. J. Rezek and B. G. Childs, Structure and Properties of Yttria–Zirconium Dispersions, *J. Nucl. Mater.*, 26: 285 (1968).
108. A. Kelly, *Strong Solids*, Clarendon Press, Oxford, England, 1966.
109. B. A. Wilcox and A. H. Clauer, Tensile and Creep Deformation of a Fiber Reinforced Mg–Li Alloy, *Trans. Met. Soc. AIME*, 245: 935 (1969).

[End of the American Nuclear Society's

Critical Reviews,

which began on page 123]

Sodium-Cooled Reactors: EBR-II Physics Aspects

By Myrna L. Steele*

Core kinetic and neutronic parameters are presented below on a per-run basis for Runs 25 to 35 of the EBR-II. This approach was chosen so that changes in core loadings could be correlated with measurements made under those very specific reactor conditions. The role of the EBR-II as a research reactor dictates that core loadings will be continuously changing; consequently it is recommended that the reader pay particular attention to the run number that is associated with any given measurement or set of measurements.

I also want to point out that the documents[1-2 3] from which the material for this article is taken are progress reports; this means that the data are subject to revision and should be used for information only. Those wishing parameters for experiment design should check with the EBR-II personnel or consult the EBR-II Irradiation Guide, July 1969.

The basic intent is to include the results of reactivity-worth, power-coefficient, and transfer-function measurements; activation ratios, fission ratios, and capture ratios; neutron-flux measurements; and control-, shim-, and safety-rod calibrations. Few, if any, correction factors and data and error analyses are included.

As results of physics measurements in runs subsequent to No. 35 become publicly available, they will be summarized in this journal as an effort to keep the information updated.

RUN 25: CORE LOADING

The increase[1] of the EBR-II core size from 81 to 91 subassemblies occurred between Runs 24 and 25. The core changes were made in three incremental steps with subcriticality determined between steps. The final core configuration consisted of 2 safety rods, 11 normal control rods, 1 special stainless-steel control rod for rod-drop tests in control-rod position No. 1, 12 experimental irradiation subassemblies, 33 normal driver core-type subassemblies, 28 enriched inner-blanket subassemblies, and 4 special half-worth subassemblies.

Temperatures and sodium-flow values for the hottest fuel element in each core row were calculated from a SNARG computation of relative fission rates for a nominal 91-subassembly core; these values are compared in Table 1 for 73- and 91-subassembly cores.[1] However, in Run 25 the 91-subassembly core was never operated above 500 kW(t), and in this run at power the core contained only 88 subassemblies, two rows of stainless-steel reflectors (rows 7 and 8), and no oscillator rod.

RUN 25: CONTROL-ROD CALIBRATION

Results[2] of period calibration of control rods subsequent to loading for Run 25 and prior to stainless-steel substitutions are shown in Table 2.

RUN 25: NEUTRON FLUX AND REACTION RATES

A program for characterizing the EBR-II neutron spectra[2] was begun in the latter part of 1966. During the shutdown prior to Run 25 at power, four low-power runs (25A to 25D) were made for flux-distribution measurements. The core configurations for these runs were: 25A, core with depleted uranium blanket; 25B, same as 25A but with the flux-wire-

*U. S. Atomic Energy Commission, Division of Technical Information Extension, Oak Ridge, Tenn. 37830.

Table 1 Comparison of Calculated Temperatures[1] for 73- and 91-Subassembly Cores* at 45 MW(t)

Run No.	1		2		3		4		5		6	
Subassemblies	73	91	73	91	73	91	73	91	73	91	73	91
Sodium flow, gal/min, per subassembly	134	133	132	131	119	118	90	89	75	74	70	69
Flow velocity, ft/sec	22.7	22.5	22.3	22.1	20.0	19.9	15.2	15.2	12.6	12.5	11.8	11.7
	Temperatures, °F											
Fuel center (max.)	1074	1022	1066	1012	1056	1022	1064	1041	1088	1051	961	1001
Fuel surface (max.)	975	937	970	931	970	955	994	976	981	993	919	953
Sodium at channel outlet (max.)	901	874	898	870	904	885	934	920	931	941	882	911
Sodium at subassembly outlet (mixed mean)	867	844	865	841	869	853	895	882	892	900	951	875
Sodium channel ΔT (max.)	201	174	198	170	204	185	234	220	231	241	182	211
Sodium subassembly ΔT (mixed mean)	167	144	165	141	169	153	195	182	192	200	181	175
Sodium at point of max. fuel temp.	872	849	870	845	874	859	934	920	931	941	882	911
Cladding ID (max.)	956	921	951	915	954	930	979	963	969	980	911	943
Cladding OD (max.)	926	895	922	890	927	905	956	940	950	960	896	943

*Calculations are based on a 91-subassembly loading. Actual loading during Run 25 was 88 subassemblies.

Table 2 Control-Rod Period Calibration[2] for Run 25

Control rod No.	Total worth, inhours
1	Stainless Steel
2	153
3	142
4	163
5	147
6	159
7*	126
8	Oscillator
9	135
10	153
11	136
12	150

*Mark I fuel.

loaded subassemblies in different locations; 25C, flux-wire-loaded subassemblies distributed for measurements in the depleted-uranium blanket; and 25D, core with stainless-steel-blanket subassemblies in rows 7 and 8. The results of the fission-rate-distribution measurements, using both depleted- and enriched-uranium wire detectors in rows 7 to 15 of the depleted-uranium blanket (no stainless steel), are shown in Fig. 1. The calculated values shown in Fig. 1 were obtained using the SNARG code. The depleted-uranium wire data are corrected for 0.22% ^{235}U content.[3]

RUN 25: POWER-COEFFICIENT DATA

Since rows 7 and 8 in the core blanket region had been changed from depleted-uranium to stainless-steel subassemblies, the approach to power was made slowly with power-coefficient and kinetic-performance measurements being made at small increments. The differential power coefficient was normal at low power levels but decreased with increasing power.[4] At about 22 MW(t) the power coefficient was at the operating limit of 1 inhour/MW. The reactor was shut down until a temporary waiver for this limit was received from the AEC.

On Apr. 24, 1967, the reactor was restarted, and power-coefficient measurements were made in small increments to determine, precisely, the differential power coefficient and to obtain the magnitude and sign of the prompt-power-coefficient component. Subsequently the reactor was recycled through two addi-

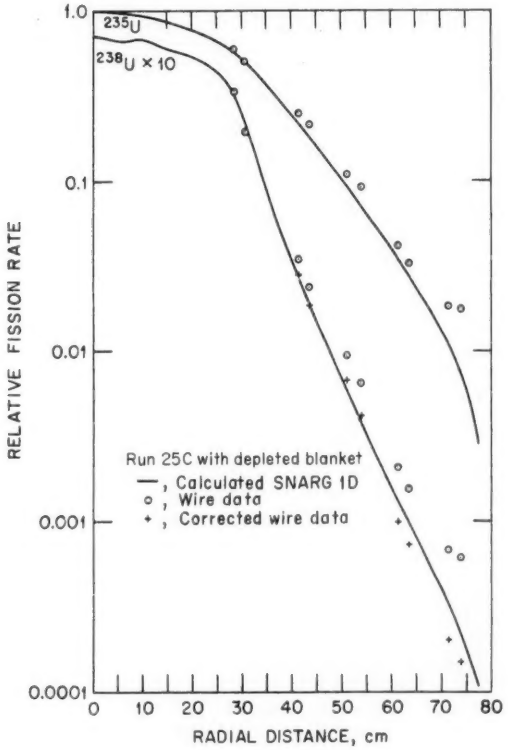

Fig. 1 Fission-rate distribution.[3]

tional power operations from 0 to 45 MW(t); the results are shown in Table 3.

The isothermal temperature coefficient of reactivity was determined[4] to be −1.04 inhour/°F from control-rod-position changes at 50 kW(t) when the bulk-sodium temperature was reduced from 700 to 650°F.

The overall average power coefficient, as a result of the blanket changes, was reported[5] as 0.87 inhour/MW.

A series of reactivity feedback tests was run to separate the thermal contributions to the power coefficient. This series consisted of tests at reduced flow, rod-drop tests, constant ΔT experiments, forced perturbations of reactor power by the trapezoidal insertion of reactivity, and observations of low-frequency power oscillations. Reduced-flow tests with the stainless-steel-blanket subassemblies showed an overall (net) loss of 4.1 inhours when coolant flow was reduced from 100 to 54% of full-rated value of 9000 gal/min. The flow coefficient showed a reversal[5] in sign, proving to be negative at 22.5 MW(t) and positive at 42.5 MW(t). This is shown[8] in Fig. 2.

Table 3 EBR-II Power Coefficient[4] for Run 25

Power,* MW(t)	$\Delta k/k$,* inhours	$\left(\frac{\Delta k/k}{MW}\right)$ overall average, inhours/MW	$\left(\frac{\Delta k/k}{\Delta MW}\right)$ incremental, inhours/MW
0	0		
10.0	16.2	1.62	1.62
12.5	18.2	1.46	0.80
15.0	19.6	1.31	0.56
17.5	21.0	1.20	0.56
20.5	22.5	1.10	0.50
22.5	23.6	1.05	0.55
25.0	24.8	0.99	0.48
28.0	27.0	0.96	0.88
30.5	28.3	0.93	0.52
33.0	29.6	0.90	0.52
36.0	30.0	0.89	0.80
37.5	34.5	0.92	1.00
40.0	37.0	0.93	1.00
42.5	40.2	0.95	1.28
45.0	43.2	0.96	1.20
Repeat 1			
37.5	30.3	0.81	
45.0	38.4	0.85	1.08
Repeat 2			
37.5	31.0	0.83	
45.0	39.0	0.87	1.07

*The power level has a reproducibility of ±0.5 MW(t) and the reactivity an uncertainty of ±0.5 inhour.

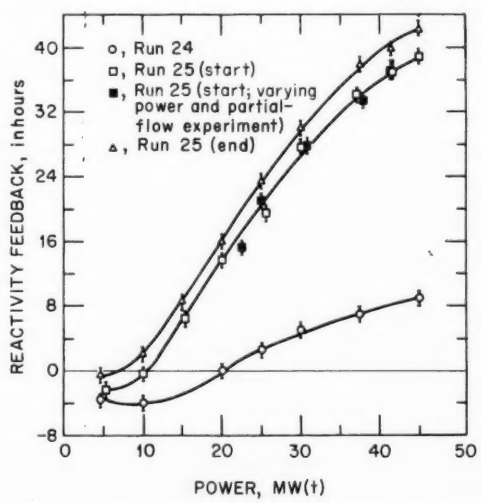

Fig. 2 The nonlinear "bowing" component of the total reactivity feedback for Run 25 vs. reactor power.[8]

On July 21, 1967, the reactor was restarted after being shut down for the loading of two new experimental fuel subassemblies.[6] During the approach to 30 MW(t), which was the irradiation power level for the test assemblies, it was noted that 12.5 inhours of reactivity was required to bring the reactor from hot critical to 10 MW(t) and that only 0.3 inhour was necessary to go from 10 MW(t) to 20 MW(t). Later that day (July 21), the power was raised incrementally. The results[6] of the differential power-coefficient measurements are shown in Fig. 3.

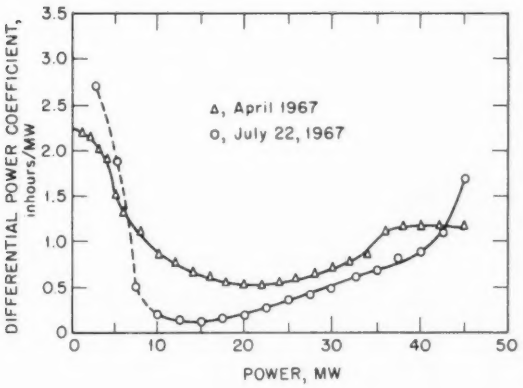

Fig. 3 Differential power coefficient[6] in Run 25.

In an attempt to analyze the change in power-reactivity decrement (PRD) which appeared to occur between Runs 24 and 25, data from Run 25 were compared with data from earlier runs; Table 4 is a summary of these results.[7] The suspected cause for the change in the PRD was the inverse bowing in row 8 of the stainless-steel reflector pieces.[2,4]

Efforts to understand and describe the physical occurrences associated with the power-coefficient anomaly[8] continued into September 1967. Effects of core size and composition on the power coefficient were analyzed by one-group diffusion-theory calculations assuming 71 fuel elements with (1) a depleted-uranium blanket and (2) a stainless-steel blanket and by multigroup two-dimensional diffusion calculations. Results of the two-dimensional calculations are summarized in Table 5.

Additional experimental data on the power-coefficient anomaly were taken during Run 26A (prior to power-operation Run 26). Table 6 shows the results of PRD measurements as a function of power level for a nine-rod bank at 13 in. Analyses of power-coefficient data led EBR-II personnel to the conclusion that attempts at reorientation of the core and blanket subassemblies had little significant effect on the reactivity feedback.[8]

RUN 26: TRANSFER-FUNCTION MEASUREMENTS

During Run 26A the EBR-II was operated for 90 MWd with a core loading similar to that of Run 25 so that reactor performance and kinetic behavior could be checked. The reactor was then shut down for installation of an oscillator rod and for loading adjustments that had been previously planned.

During Run 26B, reactor kinetic behavior was assessed by a series of transfer-function measurements in terms of the feedback component H. Results[9] of these measurements are shown in Figs. 4 to 6. The amplitudes and phases of the transfer functions shown in the figures were normalized[9] to corresponding zero-power data at approximately 8.8 Hz. The oscillator tests at high reactor power levels were limited to a minimum frequency of 0.1 Hz at 30 MW(t) and 0.3 Hz at 41.5 MW(t) because the oscillator rod "rubbed" below these frequencies. Oscillator measurements[10] were made from 0.0025 to 8.8 Hz at the lower reactor power levels of 500 kW(t) and 22.5 MW(t).

RUN 26: ROD-DROP MEASUREMENTS

Data from rod-drop experiments are shown in Fig. 7 for measured feedback recovery[9] and in Fig. 8 for a typical stainless-steel-rod calibration taken from five sets of measurements.[10] The short-time behavior, illustrated by the data in Fig. 7, is tentatively attributed to either a small, prompt positive-feedback component or to drifts in power or coolant-inlet temperature.[9]

RUNS 26A AND 26B: REDUCED-FLOW EXPERIMENTS

Data from reduced-flow experiments in Run 26A and at the beginning and end of Run 26B are given in Table 7. In Run 26A the reactor power was leveled carefully at each point, but no averaging procedure was used. In Run 26B the procedure included leveling the power, holding the power level constant by control-rod movement, taking readings at 1-min intervals over at least a 20-min period, and averaging the results. The averages so determined are given in Table 7 for ΔT, rod

Table 4 PRD[7] Between 0 and 45 MW(t)

Date (1967)	4/26	4/28	4/28	5/17	5/19	5/22	7/5	7/7	7/10	7/14	7/18	7/19	7/23	8/18
						Run 25								
Raw data,* inhours	42.3	38.4	38.0	37.4	39.1	33.3	39.6	32.5	34.8	35.9	25.9	21.5	32.7	32.0
Corrections														
Initial power					+0.8	0.0	+1.0	0.0	0.0	+1.00	1.0	0.0	0.0	+1.00
Temperature	+2.0	0	0	+1.0	+0.0	0.0	2.0	−1.0	0.0	−2.00	0.0	+2.00	0.4	−0.8
Burnup	−6.0	0	0	−2.2	−1.1	0.0	−3.0	−2.0	0.0	0.0	0.0	0.0	−0.8	−0.6
Rod bank†	0.0	0	0	0.0		+1.0	+1.0	+2.1	+2.1	+4.7	+4.7	+4.7	+4.7	+4.7
Corrected data, inhours	38.3	38.4‡	38.0	36.2	38.8	34.3	40.6	31.6	36.9	34.9	31.6	28.2	37.0	36.3
MWd	0	40	60	250	306	450	960	975	1096	1270	1425	1481	1543	1552
Rod-bank position, in.	11.0	11.0	11.0	11.0	11.0	11.4	11.4	12.0	12.0	13.00	13.00	13.00	13.00	13.00

	Run 24			Run 22		Run 16		
Raw data, inhours	64.3	64.0	56.5	69.7	72.2	77.0	77.8	73.0
Corrections								
Initial power	0	0		0.0	0.0	0.0		0.0
Temperature	0	0		0.0	0.0	0.0		0.0
Burnup	0	0		0.0	0.0	0.0		0.0
Rod bank	2.4	2.4	8.1	2.4	0.9	0.4	0.4	2.4
Corrected data, inhours	66.7	66.4	64.6	72.1	73.1	77.4	78.2	75.4
MWd	0	500	555	0	220	0	350	695
Rod-bank position, in.	12.0	12.0	14.0	12.0	11.4	11.2	11.2	12.0

*Raw data give the difference in control-rod position as determined from "book" value times the period-calibration correction.

†Rod-bank correction is normalized to the 11.0-in. rod-bank position.

‡Corrected data enclosed in blocks are reactivity decrement obtained under controlled conditions in which a proper zero-power datum point was obtained using a calibrated control rod.

Table 5 Calculated Effect of Core Size and Composition on Power Coefficient[8] (Multigroup Two-Dimensional Calculation)

Principal components	Power coefficient, inhours/MW	
	Run 16 (75 sub-assemblies	Run 24 (81 sub-assemblies)
Core sodium	−0.425	−0.425
Upper axial gap and reflector sodium	−0.310	−0.326
Radial blanket sodium	−0.075	−0.070
Axial fuel expansion	−0.510	−0.495
Radial fuel displacement of sodium	−0.95	−0.95
Total	−1.415	−1.411
Measured	−1.50	−1.27

Table 6 PRD Data[8] for the 13.00-in. Rod-Bank Position in Run 26A

Power level, MW(t)	PRD, inhours		
	9/25/67	9/27/67	9/29/67
0.05	0	0	0
0.50	1.0		
10.0	16.0	18.4	17.3
15.0	17.6	20.4	19.4
20.0	19.3		20.9
25.0	21.6	24.0	22.5
30.0	23.3		23.9
35.0	27.0	27.3	28.0
39.0	31.5		32.1
45.0	37.0	39.5	38.3

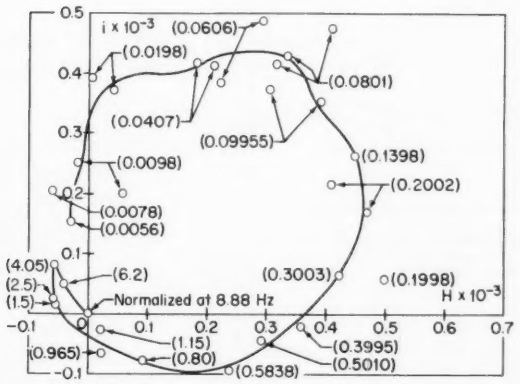

Fig. 4 Transfer-function data[9] in terms of feedback component H at 22.5 MW(t) and 100% flow, Run 26B, Oct 23, 1967. (Values in parentheses are in hertz.)

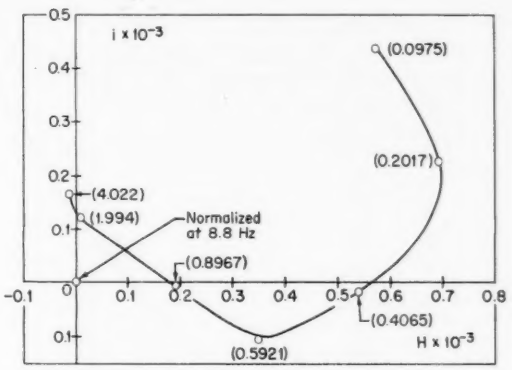

Fig. 5 Transfer-function data[9] in terms of feedback component H at 30.0 MW(t) and 100% flow, Run 26B, Oct. 17, 1967. (Values in parentheses are in hertz.)

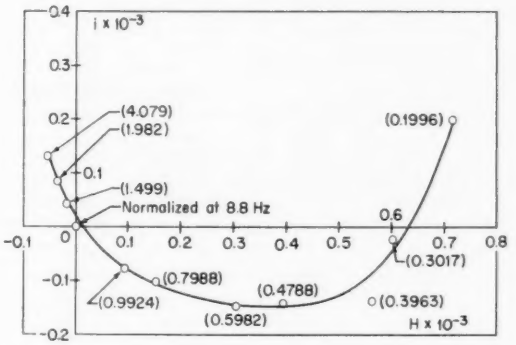

Fig. 6 Transfer-function data[9] in terms of feedback component H at 41.5 MW(t) and 100% flow, Run 26B, Oct. 18, 1967. (Values in parentheses are in hertz.)

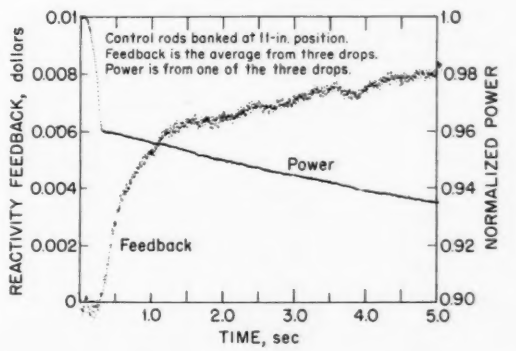

Fig. 7 Results of rod-drop experiment[9] at 45 MW(t).

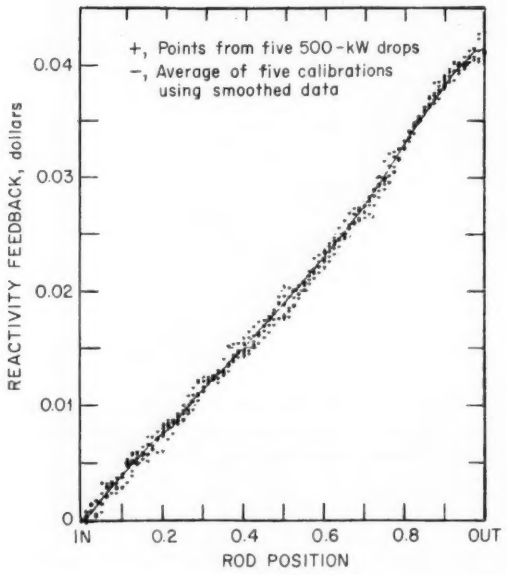

Fig. 8 Stainless-steel-rod calibration in rod-drop experiments.[10]

Table 7 Data from Reduced-Flow Experiments[10]

Approximate clock time	ΔT, °F	Reactor power (Q), MW(t)	Percent flow (R)	Reactivity rod worth, inhours	Bulk-sodium temp. correction, inhours	Burnup correction, inhours	Excess reactivity,* inhours
			Run 26A, Sept. 27, 1967				
1025	121.8	41.5	100	52.6	0	0	52.6
1200	66.0	22.5	100	63.2	0.5	0.3	64.0
1350	69.5	22.5	95	64.6	0	0.45	65.0
1425	73.5	22.6	90	65.8	0	0.6	66.4
1550	88.0	22.5	75	65.6	0.3	0.75	66.6
1742	122.8	22.6	54	← (Scrammed—no reading) →			
2208	122.0	22.5	54	59.3	0.5	1.35	61.1
			Start of Run 26B, Oct. 19, 1967				
0915	122.8	41.9	100	36.4	0.3	0	36.7
1700	65.9	22.5	100	55.2	0.3	0.4	55.9
1800	74.2	22.8	90	55.3	0.2	0.6	56.1
1900	93.1	23.8	75	53.0	0.16	0.8	54.0
2000	117.5	24.1	60	46.2	0.08	0.9	47.2
2100	131.6	24.2	54	42.1	−0.02	1.1	43.2
2235	123.6	30.7	73	40.1	0.14	1.4	41.6
2330	97.8	30.0	90	44.1	0.4	1.5	46.0
			End of Run 26B, Nov. 6, 1967,				
1700	120.9	41.2	100	54.0	0.1	0	54.1
1845	121.6	29.9	72	58.6	0.6	0.3	59.5
2100	66.2	22.6	100	67.7	−1.2	0.6	67.1
2200	73.1	22.4	90	68.7	0.5	0.8	70.0
2330	88.7	22.7	75	68.6	0.4	0.9	69.9
0115	111.5	22.8	60	64.8	0.6	1.2	66.6
0215	122.9	22.6	54	63.2	0.4	1.2	64.8
0415	121.7	14.9	36.2	67.0	−0.6	1.5	67.9

*Corrections for rod-bank expansion have not been applied.

reactivity worth, and bulk-sodium corrections. The percent flow (flow rate is read directly) is an average of readings from the two high-pressure flowmeters. The reactor power level,[10] Q, is then computed from the average ΔT and percent flow, R, using $Q = 34.1\ \Delta T/R$.

RUN 26C: REACTOR BEHAVIOR

The stability[11] of the EBR-II at power was determined by operation for 2½ hr at 45 MW(t) with no adjustment in control-rod position or sodium flow in the secondary system and with the control rods banked at 12.75 in. The reactor showed a slow power oscillation with a maximum amplitude of 10.6 MW(t) and an oscillation period of 17 min. The test was repeated on the following day with rods banked at 14 in.; the maximum amplitude was 10.7 MW(t), and the oscillation period was unchanged.

RUN 26C: REACTIVITY HYSTERESIS TESTS

For the hysteresis tests, the reactor power level, which had been at 45 MW(t) with 48.8 inhours of excess reactivity in control rod 5, was dropped[11] to 22.5 MW(t) at 1100 hours on Nov. 7, 1967. After 7½ hr at 22.5 MW(t), the power level was returned to 45 MW(t), and the excess reactivity in control rod 5, corrected for burnup to 1100 hours, was 55.6 inhours. The excess reactivity in control rod 5 gradually returned to its earlier value during continued operation at 45 MW(t). The sequence of measurements[11] is shown in Table 8. Similar results had been obtained in previous operation (Table 9).

RUN 27: POWER-COEFFICIENT MEASUREMENT[12] AND ANALYSIS[13]

Core changes[12] between Runs 26C and 27A consisted of replacements for 21 driver subassemblies, 5 control rods, and 1 safety rod.

PRD measurements were made during an ascent to 45 MW(t), during a descent to 50 kW(t), and during the second ascent to 45 MW(t). These data[12] are shown in Tables 10 to 12.

Calculations for the linear component of the power coefficient were performed using the Run 27A data and for a similar core loading surrounded by a depleted-uranium blanket (referred to as Run 27-BNKT). For the Run 27-BNKT calculations, four half-loaded subassemblies in the 27A configuration

Table 8 Excess Reactivity[11] (Nov. 7 and 8, 1967)

Time	Power level, MW(t)	Excess reactivity* in control rod 5, inhours
0800	45.0	48.2
1100	45.0	48.8
1130	22.5	
1825	22.5	
1902	45.0	55.6
2400	45.0	51.6
0800	45.0	49.9

*Corrected to 1100 hours. Nov. 7, 1967.

Table 9 Excess Reactivity[11] (Oct. 22–24, 1967)

Time	Power level, MW(t)	Excess reactivity* in control rod 5, inhours
2400	45.0	48.0
0800	45.0	49.1
1000	22.5	
2325	45.0	54.8
2400	45.0	53.3
0800	45.0	51.0
1600	45.0	51.2

*Corrected to 0800 hours, Oct. 23, 1967.

Table 10 PRD Data,[12] Ascending Mode, Run 27A, Feb. 5 and 6, 1968

Power level,* MW(t)	Time	PRD (rods banked at 12.00 in.), inhours	PRD (normalized to 11.00-in. rod bank), inhours
0.05	0800, 2/5	0.0	0.0
2.5	1630, 2/5	5.4	5.5
5.9	1945, 2/5	12.3	12.5
11.5	0200, 2/6	20.1	20.6
16.7	0430, 2/6	23.3	24.0
21.7	0700, 2/6	23.8	24.7
26.4	0930, 2/6	25.5	26.6
31.6	1130, 2/6	27.0	28.4
37.5	1330, 2/6	30.2	31.8
41.5	1544, 2/6	35.8	37.6
46.5	1915, 2/6	41.8	43.8

*Power-level values based on heat balance, Feb. 6, 1968.

were replaced with fully loaded subassemblies, and the steel reflectors in rings 7 and 8 were replaced with blanket subassemblies. Table 13 (page 180) shows the measured and calculated values.[13]

RUN 27: FEEDBACK ANALYSIS

Two rod-drop experiments[13] were conducted at reduced sodium flow in Run 27, and Figs. 9 and 10 show the results of the feedback measurements for operating conditions of 30 MW(t) with 75% flow and 22.5 MW(t) with 54% flow, respectively.

RUN 27: PHYSICS MEASUREMENTS

Analyses of PRD's[13] measured during the various startups in Run 27 showed no significant trends; however, the many loading changes that were made throughout Run 27 could have obscured any small trends.

The results[13] of the routine physics measurements in Runs 27D to 27G are listed in Table 14.

Table 11 PRD Data,[12] Descending Mode, Run 27A, Feb. 7 and 8, 1968

Power level, MW(t)	Time	PRD* (rods banked at 12.00 in.), inhours	PRD (normalized to 11.00-in. rod bank), inhours
45.0	1040, 2/7	40.0	42.0
40.0	1300, 2/7	35.6	37.4
30.0	1514, 2/7	28.1	29.5
20.0	1800, 2/7	23.5	24.4
10.0	2035, 2/7	19.0	19.5
0.5	2240, 2/7	−2.5	−2.5
0.05	0005, 2/8	−4.6	−4.6

*Reactivity value at 45.0 MW normalized to the data of Table 10.

RUN 28: PHYSICS TESTS AND MEASUREMENTS[14]

Since all the experimental ceramic fuel elements had been removed from the core by the end of Run 27I because of fission-gas-leakage problems, a series of tests was conducted in Run 28 to establish a no-ceramic-fuel reference core. The series[14,15] included power-coefficient (PRD) measurements in both ascending and descending modes; coolant-flow tests with 100% flow at 41.5 MW(t) and 58% flow at 22.5 MW(t); and rod-drop tests under the following conditions: 100% flow at 500 kW(t); 58% flow at 500 kW(t); 100% flow at 41.5 MW(t); 100% flow at 22.5 MW(t); and 58% flow at 22.5 MW(t).

Estimates[14] of reactivity worths of the drop rods in Run 28A are summarized in Table 15 for various power and flow conditions.

Results[15] of the PRD measurements for Runs 28A to 28C are summarized in Table 16. All PRD values are normalized to an 11.00-inch rod-bank position; PRD values for the descending mode are normalized to those for the ascending mode at 45 MW(t).

RUN 29: PHYSICS EXPERIMENTS AND MEASUREMENTS

Physics experiments related to the exchange of depleted uranium for stainless steel in the blanket[16]

Table 12 PRD Data,[12] Ascending Mode, Run 27A, Feb. 8, 1968

Power level, MW(t)	Time	PRD (rods banked at 12.00 in.), inhours	PRD (normalized to 11.00-in. rod bank), inhours	PRD in Run 26B 10/15/67 (rods banked at 11.00 in.), inhours
0.05	0210	0.0	0.0	0.0
5.0	0230	14.2	14.4	
10.0	0450	22.2	22.7	17.8
15.0	0600	24.0	24.7	20.5
20.0	0700	25.2	26.1	22.5
25.0	0740	26.4	27.5	24.3
30.0	0915	28.1	29.5	27.0
35.0	1130	32.7	34.3	30.2
40.0	1235	36.8	38.6	36.0
45.0	1425	42.7	44.7	43.0

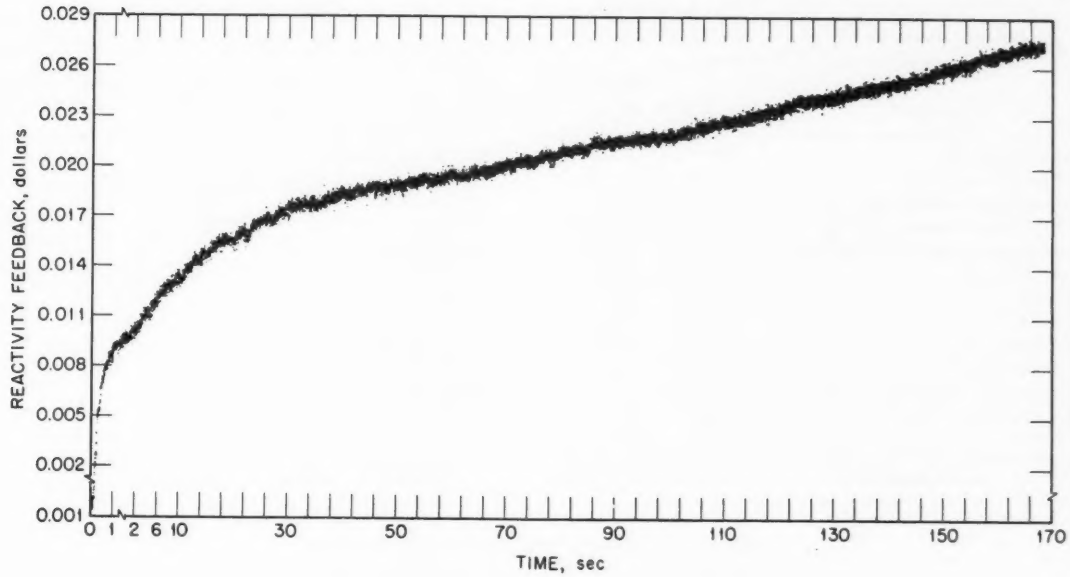

Fig. 9 Feedback[13] at 30 MW(t) and 75% flow for Run 27.

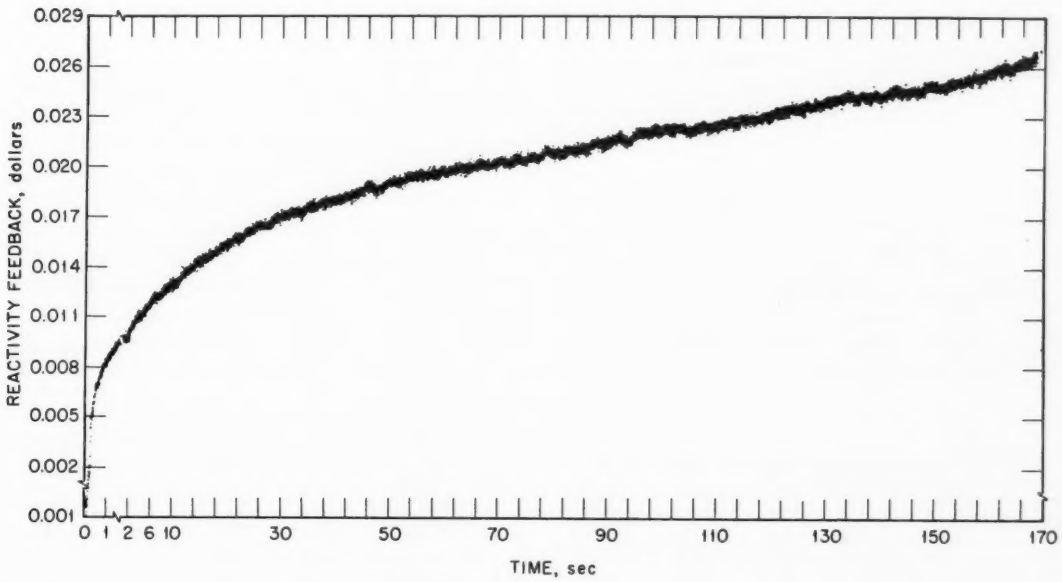

Fig. 10 Feedback[13] at 22.5 MW(t) and 54% flow for Run 27.

Table 13 Components[13] of the Power Coefficient in Units of Δk ($\times 10^5$) or $\Delta k/\Delta T$ ($\times 10^5$)

Component	Run 27A	Run 27-BNKT
Sodium (core) Δk	−41.7	−39.3
Sodium (core) $\Delta k/\Delta T$	−0.453	−0.451
Sodium (upper reflector) Δk	−41.3	−37.5
Sodium (upper reflector) $\Delta k/\Delta T$	−0.225	−0.214
Sodium (inner reflector/blanket) Δk	−3.4	−5.6
Sodium (total)	−86.7	−82.4
Fuel Δk	−42.0	−44.0
Fuel $\Delta k/\Delta T$	−0.199	−0.218
Steel (axial) Δk	−17.3	−10.9
Steel (radial) Δk	−115.4	−88.7
Steel (radial) $\Delta k/\Delta k$, inhours/mil	−3.42	−3.59
45-MW(t) Δk (no radial)	−148.1	−141.3
45-MW(t) Δk	−265.9	−244.0

Table 14 Results of Physics Measurements for Runs 27D–27G

	Run 27D	Run 27E	Run 27F	Run 27G
PRD* at 45 MW(t), inhours	44.1	47.2	40.4	41.9
Estimated Δk, inhours		+7	−34	+73
Measured Δk, inhours		+24	−60	+90
Control-rod bank, in.	11.0	11.25	12.25	11.0
Total control-rod worth, inhours	1390	1414	1383	
Safety-rod worth, % $\Delta k/k$			1.05	

*Corrected to 11-in. control-rod-bank condition.

Table 15 Rod-Drop[14] Measurements in Run 28A

Power and flow	Reactivity, inhours			
	Rod drop 1	Rod drop 2	Rod drop 3	Rod drop 4
500 kW(t), 100%	13.12	13.06	13.19	
22.5 MW(t), 100%	12.24	12.28	12.22	12.24
22.5 MW(t), 58%	12.09	12.14	12.21	
41.5 MW(t), 100%	11.51	11.73	11.93	11.98

Table 16 PRD Data[15] for Runs 28A–28C

Run 28A				Run 28B				Run 28C			
Ascending		Descending		Ascending		Descending		Ascending		Descending	
Power, MW(t)	PRD, inhours	Power, MW(t)	PRD, inhours	Power, MW(t)	PRD, inhours	Power, MW(t)	PRD, inhours	Power, MW(t)	PRD, inhours	Power, MW(t)	PRD, inhours
0	0	0	−7.0	0	0	0	−1.8	0	0	0	−5.5
6.3	13.5	0.5		5.0	16.5	0.5		5.8	16.9	0.5	
11.3	22.7			9.0	25.0	9.0	24.5	9.1	25.2	9.0	22.8
16.3	26.3	16.0	24.8	16.2	28.6			16.3	27.9		
21.2	27.3	23.0	29.7	21.0	31.0	20.7	33.9	21.4	29.5	21.4	29.9
26.1	29.3			25.9	32.1			25.9	30.4		
30.8	32.0	30.0	32.9	31.0	34.4	31.0	36.9	31.5	32.7	31.2	33.3
36.2	35.0	36.0	36.6	36.5	38.1			36.4	37.2		
40.2	38.9	39.5	40.2	40.0	41.1	39.8	43.9	40.4	41.0	40.4	42.3
45.0	43.5	45.0	43.5	45.0	47.1	45.0	47.1	45.0	47.2	45.0	47.2

were begun with Run 29A. This run was performed with all the stainless steel in place, but nearly all the stainless-steel subassemblies in blanket row 7 were removed for Run 29B. Run 29C was conducted with *all* the stainless-steel subassemblies of rows 7 and 8 replaced by depleted uranium, and Run 29D was a continuation of power operation with the depleted-uranium blanket.

Information on reactivity hysteresis effects was obtained from PRD measurements during Runs 29A and 29C (Table 17). Table 17 also shows the results of cycling from 0 to 45 MW(t) in Runs 29A to 29C.[16]

Table 17 Summary of PRD Values[16] for Runs 29A–29C*

Power range, MW(t)	PRD, inhours		
	Run 29A	Run 29B	Run 29C
0 to 25	34.0		48.0
25 to 0	−37.3		−51.6
0 to 41.5	48.5		79.0
41.5 to 0	−51.2		−79.2
0 to 45	51.5	57.5	84.4
45 to 0	−53.5	−59.7	−83.7

*All values normalized to an 11.00-in. rod-bank position.

When the stainless steel was replaced by depleted uranium in blanket rows 7 and 8, a corresponding total reactivity loss of 580 inhours was noted. This loss with depleted uranium agrees rather well with the reactivity gain of 580 to 610 inhours which had been estimated before operation with the stainless-steel blanket. The plutonium content of the uranium blanket had been taken into account in that estimate.[16]

RUN 29D: CORE FLUX MAPS

Flux wire detectors were mounted in fuel assemblies during Run 29D to measure the ^{235}U fission-rate distribution. The 67 detectors were distributed over 12 core and blanket positions and were exposed for 1 hr at 50 kW(t). Relative fission rates were determined by counting fission-product gamma activity in the 0.5- to 0.85-MeV energy range,[18] and the results of the measurements are shown in Figs. 11 and 12.

A comparison of Figs. 11 and 12 shows that the ^{235}U fission-rate maximum is displaced very slightly toward the blanket region for Run 25D. The reader

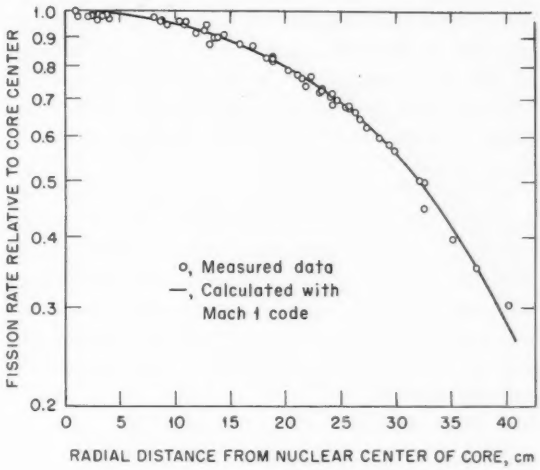

Fig. 11 ^{235}U fission rate vs. distance[18] from nuclear center for Run 29D (uranium blanket, 91-subassembly core).

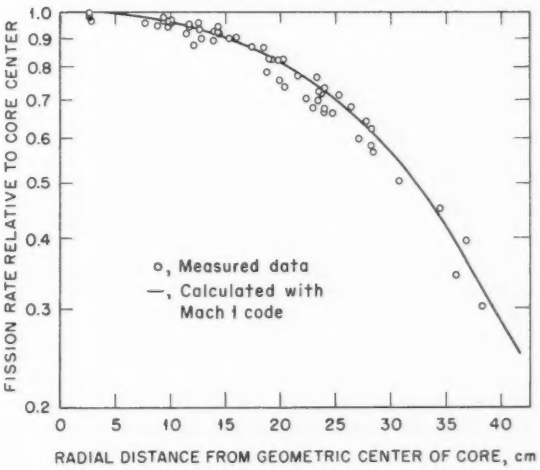

Fig. 12 ^{235}U fission rate vs. distance[18] from geometric center for Run 29D (uranium blanket, 91-subassembly core).

should be aware that environmental characteristics in a test-reactor core are dependent not only on basic design parameters of the core but on the core loading which may, and often does, vary from run to run.

RUN 29: ROD-DROP MEASUREMENTS

The effects of stainless steel on reactivity feedback were studied[16] in a series of rod-drop measurements

during Runs 29A and 29C. A stainless-steel reflector was used in Run 29A and a depleted-uranium blanket in 29C. The results[17] are shown in Figs. 13 and 14. The time-dependent[20] feedback functions were then fitted to a six-term mathematical feedback model as shown in Figs. 15 and 16.

These studies led to the conclusions that the prompt feedback term was unaffected by the stainless-steel reflector; the stainless-steel reflector affected the feedback in the midpower region by either decreasing the magnitude of the delayed negative components or increasing the magnitude of the positive components; and, in the region above 35 MW(t), the feedback is strongly negative.[22]

RUN 30: POWER COEFFICIENT

Results[17] of PRD measurements subsequent to the reinsertion of the depleted-uranium blanket (in Run 29C) are shown in Fig. 17. Included are measurements from Runs 29C and 30A to 30D. All data are corrected for variations in bulk-sodium temperature, for burnup, and for differences in control-rod-bank positions. Core configurations for all these runs except 30D were essentially the same. The configuration was considerably different for 30D because 11 experimental subassemblies were removed prior to that run. Run 30C was carried out at a power level[17] of 30 MW(t).

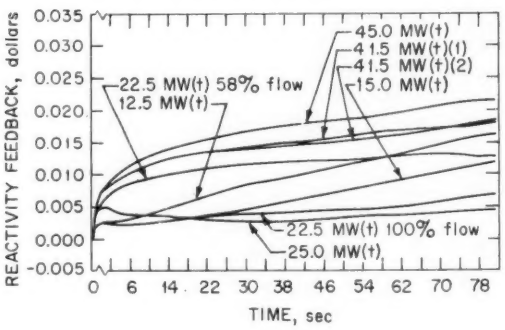

Fig. 13 Reactivity feedback[17] for Run 29A.

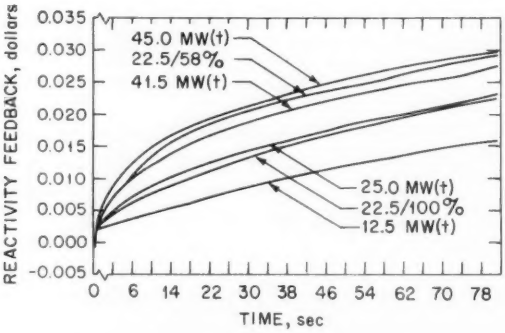

Fig. 14 Reactivity feedback[17] for Run 29C.

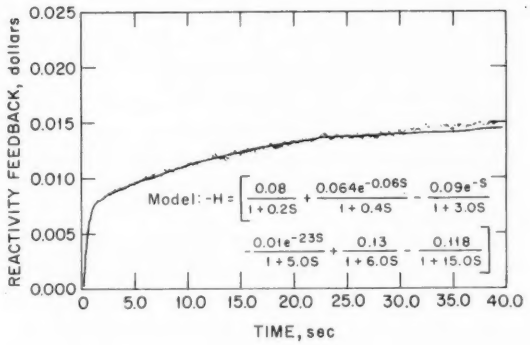

Fig. 15 Comparison of time-dependent feedback[20] function from Run 29A rod-drop studies with values calculated with mathematical feedback model (stainless-steel reflector in rows 7 and 8; 41.5 MW(t); 100% coolant flow).

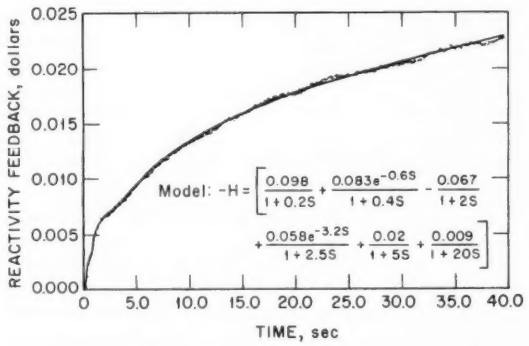

Fig. 16 Comparison of time-dependent feedback[20] function from Run 29C rod-drop studies with values calculated with mathematical feedback model (depleted-uranium reflector; 41.5 MW(t); 100% coolant flow).

RUN 31: CORE DOSIMETRY

An experimental dosimetry subassembly[19] was irradiated for 1 hr at 50 kW(t) in Run 31E, and four other experimental dosimetry subassemblies were irra-

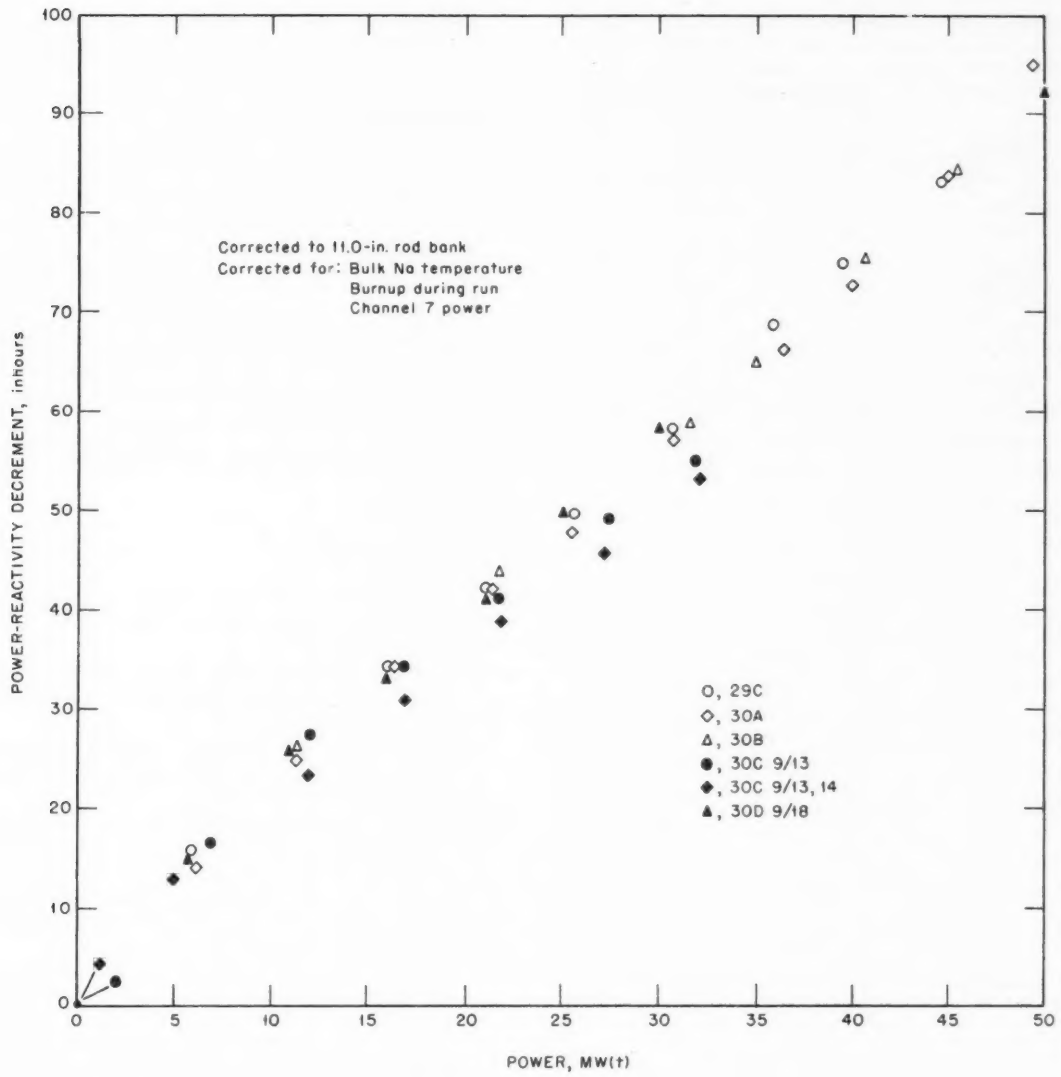

Fig. 17 PRD data[17] since restoration of depleted blanket.

diated for 8 days at 50 MW(t) in Run 31F. Spectrum-averaged reaction[21] rates for the measured reactions in these runs are summarized in Table 18. The reaction rates are expressed as the number of atoms produced in the reaction per 10^9 atoms of target material per megawatt-day and are listed as a function of in-core radial position.

Conversion of the reaction-rate data to neutron fluxes and spectrum-averaged cross sections for the EBR-II will be published later. If the reader needs more specific information, he should contact EBR-II personnel.

RUN 35: STAINLESS-STEEL DROP ROD

A special stainless-steel drop rod was installed[23] in control-rod location No. 1 between Runs 34B and 35 to provide a small, prompt reactivity step for kinetic studies. Standard rod-drop techniques were used for preliminary calibration of the new rod. Results of the

Table 18 EBR-II Spectrum-Averaged Reaction Rates[21]

Reaction	Reaction rate at indicated radial position, ppB/MWd			
	5.9 cm	15.6 cm	27.0 cm	31.2 cm
$^{54}Fe(n,\gamma)^{55}Fe$	30.3	28.2	18.6	16.2
$^{62}Ni(n,\gamma)^{63}Ni$	27.8	27.3	22.5	19.4
$^{45}Sc(n,\gamma)^{46}Sc$	51.1	51.9	44.1	30.3
$^{58}Fe(n,\gamma)^{59}Fe$	14.1	13.6	11.0	9.1
$^{59}Co(n,\gamma)^{60}Co$	52.9	48.0	42.0	35.2
$^{63}Cu(n,\gamma)^{64}Cu$		64.0	59.7	
$^{197}Au(n,\gamma)^{198}Au$	809	786	606	567
$^{54}Fe(n,p)^{54}Mn$	57.1	56.5	30.0	11.7
$^{58}Ni(n,p)^{58}Co$	84.3	76.0	45.2	15.7
$^{46}Ti(n,p)^{46}Sc$	7.4	7.0	3.9	1.4
$^{47}Ti(n,p)^{47}Sc$	16.0	14.7	8.7	3.2
$^{48}Ti(n,p)^{48}Sc$	0.19	0.17	0.10	0.03
$^{59}Co(n,p)^{59}Fe$	0.99	0.93	0.56	0.17
$^{63}Cu(n,p)^{63}Ni$	18.0	15.9	9.9	3.6
$^{32}S(n,p)^{32}P$	12.8	11.6	6.9	2.52
$^{54}Fe(n,a)^{51}Cr$	0.62	0.61	0.34	0.11
$^{58}Ni(n,a)^{55}Fe$	3.3	2.8	3.8	0.6
$^{50}V(n,a)^{47}Sc$	0.78	0.32	0.23	0.11
$^{51}V(n,a)^{48}Sc$	0.02	0.014	0.008	0.003
$^{63}Cu(n,a)^{60}Co$	0.37	0.31	0.20	0.07

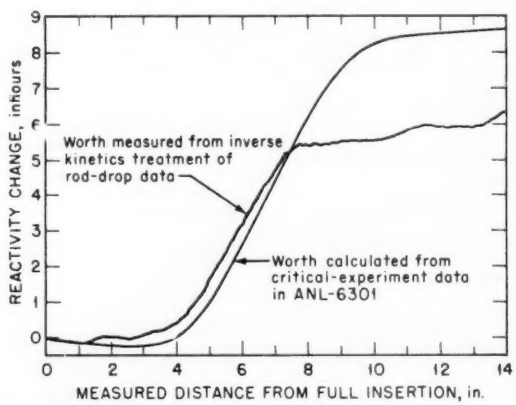

Fig. 18 Measured and calculated worths of redesigned stainless-steel drop rod[23] as a function of distance from full insertion.

in-core calibration are shown in Fig. 18, together with calculated values from critical-experiment data.

SUMMARY

The data and very brief discussions included in this article are an attempt to gather reasonably descriptive and, where possible, measured EBR-II core-physics parameters in one place. This article does not present detailed data, but the information given here on characteristics of past core configurations and environment should enable the reader to make his own comparisons between fast and thermal reactors. For detailed core and experiment-irradiation conditions, which reflect core-loading changes as they occur, prospective experimenters should contact EBR-II personnel.

REFERENCES

1. Argonne National Laboratory, Reactor Development Program Progress Report, January 1967, USAEC Report ANL-7302, p 2.
2. Argonne National Laboratory, Reactor Development Program Progress Report, February 1967, USAEC Report ANL-7308, pp. 2-3 and 61-62.
3. Argonne National Laboratory, Reactor Development Program Progress Report, March 1967, USAEC Report ANL-7317, pp. 3 and 24.
4. Argonne National Laboratory, Reactor Development Program Progress Report, April 1967, USAEC Report ANL-7329, pp. 2-4.
5. Argonne National Laboratory, Reactor Development Program Progress Report, May 1967, USAEC Report ANL-7342, pp. 3-5 and 17.
6. Argonne National Laboratory, Reactor Development Program Progress Report, July 1967, USAEC Report ANL-7357, pp. 3 and 24.
7. Argonne National Laboratory, Reactor Development Program Progress Report, August 1967, USAEC Report ANL-7371, pp. 3 and 11.
8. Argonne National Laboratory, Reactor Development Program Progress Report, September 1967, USAEC Report ANL-7382, pp. 2, 15, and 21.
9. Argonne National Laboratory, Reactor Development Program Progress Report, October 1967, USAEC Report ANL-7391, pp. 51-111.
10. Argonne National Laboratory, Reactor Development Program Progress Report, November 1967, USAEC Report ANL-7399, pp. 48-94.
11. Argonne National Laboratory, Reactor Development Program Progress Report, December 1967, USAEC Report ANL-7403, pp. 44 and 87-89.
12. Argonne National Laboratory, Reactor Development Program Progress Report, February 1968, USAEC Report ANL-7427, pp. 40 and 82-83.

13. Argonne National Laboratory, Reactor Development Program Progress Report, April 1968, USAEC Report ANL-7445, pp. 41 and 90-91.
14. Argonne National Laboratory, Reactor Development Program Progress Report, May 1968, USAEC Report ANL-7457, pp. 48 and 87-88.
15. Argonne National Laboratory, Reactor Development Program Progress Report, June 1968, USAEC Report ANL-7460, pp. 40 and 75-76.
16. Argonne National Laboratory, Reactor Development Program Progress Report, July 1968, USAEC Report ANL-7478, pp. 47 and 75-76.
17. Argonne National Laboratory, Reactor Development Program Progress Report, September 1968, USAEC Report ANL-7500, pp. 47-56.
18. Argonne National Laboratory, Reactor Development Program Progress Report, October 1968, USAEC Report ANL-7513, pp. 79-83.
19. Argonne National Laboratory, Reactor Development Program Progress Report, November 1968, USAEC Report ANL-7518, p. 66.
20. Argonne National Laboratory, Reactor Development Program Progress Report, February 1969, USAEC Report ANL-7553, pp. 31-32.
21. Argonne National Laboratory, Reactor Development Program Progress Report, March 1969, USAEC Report ANL-7561, p. 63.
22. Argonne National Laboratory, Reactor Development Program Progress Report, April–May 1969, USAEC Report ANL-7577, p. 135.
23. Argonne National Laboratory, Reactor Development Program Progress Report, June 1969, USAEC Report ANL-7581, pp. 36 and 62.
24. R. R. Smith, T. R. Bump, R. A. Cushman, R. W. Hyndman, F. S. Kirn, W. B. Loewenstein, J. K. Long, J. T. Madell, P. J. Persiani, and W. R. Wallin, The Effects of an Overcooled Stainless Steel Reflector on the EBR-II Power Coefficient, USAEC Report ANL-7544, Argonne National Laboratory, May 1969.

Sodium-Cooled Reactors: Current Status

By Myrna L. Steele*

Plant-systems operating experience is summarized below for the EBR-II (July–December 1969)[1-6] and for the Fermi Fast Breeder Reactor (May–September 1969).[7-13] This summary updates the reviews that appeared in Vol. 12, No. 3, pages 279–292, and Vol. 12, No. 4, pages 335–337.

EBR-II

Unscheduled Scrams. Indicated fast periods on nuclear channels 4 to 6 initiated an unscheduled reactor scram before the end of Run 36A. Since analysis of operations instrumentation charts showed no apparent parameter changes, a power-supply perturbation was considered to be the most likely cause of the scram. A special recorder was installed to monitor the voltage of the continuous power supply to the nuclear channels. Reactor restart gave no indication of anomalous behavior.[2]

Early in Run 36B a manual scram was necessitated by failure of one of the sight-glass segments in the steam drum. The sight glass was isolated, and reactor power was returned to 50 MW(t). Run 36 was completed on July 31 with no other interruptions.

Run 37 was begun[2] on August 2, and, after rod-drop experiments were performed at 0.5 and 50 MW(t), steady-power operation continued until August 14 when a voltage dip on the 138-kV incoming line caused the breakers to open. Voltage perturbations caused false scram and off-normal annunciations, and the reactor was manually scrammed. Emergency power for both nuclear and process systems was lost temporarily; the plant was placed in standby while the occurrence was evaluated. Low battery voltage had caused the emergency-power loss at the time of the reactor scram. The batteries were charged, load tested, and recharged. Normal 50-MW(t) operation for Run 37 was then resumed.[2] Run 37 was completed[3] on August 30.

Rated Nominal Power Increase. Beginning with Run 38A the reactor power level was increased[3] from a nominal 50 MW(t) to 62.5 MW(t). This power-level increase necessitated extensive fuel-handling operations to remove or relocate experimental subassemblies. Several plant changes also had to be made to accommodate this increase: The cooling-tower-fan pitches were adjusted to optimum; three Annubar flow sensors were installed in the steam line to the turbine-driven condensate pump; and the pressure in the secondary sodium surge tank was increased to allow increased flow rates with the existing pump.

Prior to startup for the power run, the response times of selected shutdown-circuit trips were checked, and startups for a criticality check and control-rod calibration were conducted.[3]

During the ascent to 50 MW(t), vibration and condensate flow rates were measured in the components of the sodium boiler plant. An abnormally high condensate flow rate was indicated in the desuperheater system. After rod-drop tests at 0.5 and 50 MW(t), the reactor was shut down temporarily for changing the temperature compensation of the coolant-outlet-flow indicator and for checking the desuperheater system. Replacement of eroded superheater nozzles restored normal flow to the desuperheater system, and the reactor was returned to 50 MW(t). The data base for the power increase was established; then the reactor power was slowly raised to 56 MW(t). The final increase to 62.5 MW(t) was made almost 2 days

*U. S. Atomic Energy Commission, Division of Technical Information Extension, Oak Ridge, Tenn. 37830.

after the 56-MW(t) level was reached. When the rod-bank level had stabilized at 62.5 MW(t), rod-drop tests were again performed, and the operation of all systems was rechecked.[3] Run 38A, the initial 62.5-MW(t) run of the EBR-II, was completed September 28 after 517 MWd of operation. On October 16, after 600 MWd of operation at 50 MW(t) in Run 38B, the reactor was shut down for extended maintenance.[4]

The reactor was restarted December 15 for Run 39A. Reactivity was adjusted, rods were calibrated, rod-drop experiments were performed at 0.5 MW(t), and reactor power was raised slowly. At each 5-MW(t) step between 10 and 50 MW(t), reactor operation was carefully monitored. Operation during Run 39A (through December 20) amounted to 170 MWd, which brought the EBR-II cumulative total[5] to 30,120 MWd.

Primary Sodium System. The unsatisfactory commutation and short life of brushes in the exciter for the main turbine generator and in the exciters and slip rings for the primary-pump motor-generator sets led to reliability studies on the brushes.[1] Test results on brushes of the only type that performed satisfactorily under the EBR-II environmental conditions[3] are shown in Table 1.

Unscheduled reactor scrams caused by problems related to primary sodium pumps had been reported as early as March 1969. The recurring problems and unscheduled scrams resulted in a primary-system stability analysis with the primary pumps operating in open-loop mode. Both manually variable-speed and fixed-speed control modes were considered. Analyses showed that a 10% variation in line voltage to the drive motors of the motor generators produced a calculated 3-rpm change in pump speed and that a 20% variation produced a calculated 7-rpm change in pump speed. The calculated change in reactor power resulting from pump-speed variations was ±47 kW/rpm. From these analyses it was determined that two reactor scrams during July 1969 could be attributed to dips in line voltage.[1] Overall conclusions resulting from the analyses were that:

1. With either the variable- or fixed-speed mode of open-loop operation of the primary system, unscheduled scrams would probably continue to be caused by a high rate of change of coolant flow resulting from the variations in line voltage to the primary pumps.

2. With the closed-loop control system that is now used for the EBR-II, a temperature gradient of ±0.5°F (in ΔT) across the core is maintained by jogging a control rod about every half hour. An open-loop fixed-speed control system would require the operator to make more frequent adjustments in rod position to maintain the ΔT within the nominal limits; an open-loop variable-speed control system would likewise require more frequent rod adjustments by the operator to hold ΔT within the limits.

3. The advantages of the simpler circuitry of the open-loop control system are mitigated by the resultant less-stable sodium pumping system.[1]

Table 1 Results of Performance Tests[3] on National Carbon No. 258 Electrical Brushes*

Electrical machine used for testing	Hours operated	Brush wear, in.	Estimated obtainable averaged brush life, hr
Exciter of main turbine generator	1616	1, worn from original 2¾	2500 to 3000
Exciter of No. 1 primary-pump motor-generator set	2976	⅜, worn from original 1½	5000
Slip rings of No. 1 primary-pump motor-generator set	3286	5/16, worn from original 2	6000
Exciter of No. 2 primary-pump motor-generator set	3022	½, worn from original 1½	4500
Slip rings of No. 2 primary-pump motor-generator set	2924	½, worn from original 2	5000

*One or more repeat tests were run with comparable results.

Secondary Sodium Systems. Heat-transfer-coefficient[1] measurements for the outside heat-transfer area of the EBR-II intermediate heat exchanger (IHX), evaporators, and superheaters were reported in July 1969. The comparison of design and measured heat-transfer coefficients at 50 MW(t) is shown in Table 2.

Table 2 Design and Measured Overall EBR-II Heat-Transfer Coefficients[1] (Based on Outside Area)

	Heat-transfer coefficients, Btu/(hr)(ft^2)($^\circ$F)	
	Design	Measured
Intermediate heat exchanger	1120	1070
Evaporators	610	470
Superheaters	430 to 220	71% of design

Expected system conditions[1] calculated for 62.5-MW(t) operation are shown in Table 3; the heat-transfer computer-code input data are based on the fraction of design performance of the EBR-II systems at 50 MW(t).

The main turbine with a throttle steam flow of about 170,000 lb/hr generated[4] about 18.6 MW(e) while the reactor was at 62.5 MW(t). Although the steam consumption of the feedwater-pump turbine was higher than indicated from the manufacturer's data for the rated 62.5-MW(t) operation, no control problems were experienced. Accelerometers mounted in each of the two superheaters were used to determine frequency spectra. No appreciable change in either amplitude or shape of the frequency spectrum was noted as reactor power was increased from 20 MW(t) to 62.5 MW(t).

Table 3 Predicted EBR-II System Conditions[1] at 62.5 MW(t) [Based on Values for 50-MW(t) Operation]

Primary System	
Core flow, gal/min	9000
IHX inlet temperature, $^\circ$F	883
IHX outlet temperature, $^\circ$F	700
Secondary System	
Flow, gal/min	5420
IHX outlet temperature, $^\circ$F	874
IHX inlet temperature, $^\circ$F	583
Superheater outlet temperature, $^\circ$F	802
Steam System	
Flow, lb/hr	2.54×10^5
Superheater outlet temperature, $^\circ$F	819
Feedwater temperature, $^\circ$F	540
Blowdown, lb/hr	2.0×10^4

The steam-bypass-system performance was also tested at 62.5 MW(t). Two transient tests were conducted:

1. With the reactor at 62.5 MW(t) and the turbine on initial-pressure regulator, breakers on the incoming line were tripped open.
2. With the reactor at 62.5 MW(t) and the turbine on initial-pressure regulator, the turbine was tripped off.

In the first test, the turbine autotransfer system operated as it should, but the large steam-bypass valve did not open fast enough to avert high steam pressure and subsequent relief-valve opening. About 15 sec after the transient was initiated, the steam-bypass valve was opened manually.

Satisfactory operation of the condenser and cooling tower under maximum heat load was noted during the second test; however, the large steam-bypass valve once again failed to respond fast enough to avoid high steam pressure. The relief valve again opened automatically, but the large steam-bypass valve had to be opened manually. Although the latter valve had failed to respond during the transients, it handled plant steam generated up to 61 MW(t); however, while power was being increased to 62.5 MW(t), the valve started vibrating and the result was an oscillating steam-plant pressure. The steam flow through the large steam-bypass valve was increased by closing the small steam-bypass valve. This steam-flow increase sufficiently loaded the large valve to damp the oscillations.[4]

A fast scram was required at the beginning of Run 39A when the steam seal regulator apparently failed to function normally. The regulator problem was corrected, and the reactor[6] was returned to 50 MW(t).

Rotating Plugs. In August the fast and slow speeds of the large and small rotating plugs were measured[2] at the outside diameters of the blades. The fast speeds were 87 and 53 in./min for the large and small plugs, respectively; the slow speeds were 24 and 20 in./min, respectively. Inspection of the freeze seals of both the large and small plugs revealed only a small amount of fine, powdery dross in the freeze-seal troughs.[2] In September the large-plug seal trough was brush cleaned, and new Bi–Sn eutectic alloy was placed in the trough. The previous brush cleaning of the trough

had taken place on May 24, 1969; between that cleaning and the September cleaning, 171 round-trip rotations (for fuel transfers) had been accomplished.[3]

During the maintenance shutdown in November, a new freeze-seal temperature-control system was installed. The blade thermocouples of the large and small plugs were removed and replaced with iron–constantan thermocouples that were vertically positioned by Swagelok fittings. During the dismantling of the freeze-plug heating system, 13 faulty blade heaters were located and repaired.[5]

Fuel-Unloading Machine (FUM). A new type of filter[6] was installed in the argon cooling system of the FUM. The original filter became plugged frequently, and replacement was necessary long before the capacity of the filter was reached. The original filter element was stainless-steel mesh, but the new one is made of sintered stainless-steel tubes with a flow area approximately 25 times that of the original element. The newly installed filter element was operated[6] in the vapor trap for the first time in December.

FERMI FAST BREEDER REACTOR

The Fermi Fast Breeder Reactor remained shut down through September, but preparations for restarting the reactor were still under way.

Primary Sodium System. The primary sodium system remained partially drained[7–11] through July. During May[7,8] and June,[9,10] photographic studies of the fingers on the hold-down mechanism were conducted. Detailed analyses of the photographs showed no damage to the hold-down mechanism resulting from the fuel-meltdown incident and postincident activities.[9]

A trial run[12] of the handling of the newly designed flow-guarded subassembly was conducted on August 8 through the new fuel-transport facility and the reactor fuel-handling cycle. General procedures required that the offset handling mechanism be raised about 3 in. higher than normal for handling the flow-guarded subassembly, but no difficulties were encountered.

On August 19 the primary system was refilled with sodium.[12] Subsequent to refill, the core sweep mechanism was returned to the reactor vessel, sweep controls were assembled, and the unit was tested.

Because of the open, low-pressure-drop condition of the core, the pony-motor drive was used for initial sodium-pump operation.[12] Before the main sodium-pump motor drives could be restarted, it was necessary to begin fuel-element reloading so that sufficient coolant-pressure drop could be established across the core.

The sodium temperature during shutdown was maintained at 365°F until September 1, when sodium heating and cleaning (cold trapping) were begun.[13] By September 30 the sodium temperature was up to 550°F. A preliminary evaluation of the new strip heater–heat transfer block plugging-meter modifications showed that there were well-defined "knees" on the readout chart and left little doubt as to plugging temperatures. Results of plugging-loop modifications are that the initial sodium-flow settings can now be achieved by pump voltage control and that the insoluble particulate matter can now be controlled by reverse flushing of the orifice. The newly modified plugging loop was operated about 420 hr in September.

Secondary Sodium Systems. During May all three of the secondary sodium loops remained filled with sodium[7,8] at about 350°F.

Feedwater-flow pressure-drop tests[7] were performed on the water sides of the No. 1 and No. 2 steam generators to determine whether all the newly installed poppet-type pressure-drop orifices had reseated following the isolation tests. The No. 3 steam generator was also scheduled for feedwater pressure-drop tests, but, when it was filled with water at 600 psig, a leak developed at the steam-manifold cover-plate. Then the water side of the No. 3 unit had to be vented, purged, filled with nitrogen, and capped.

The feedwater pressure-drop tests that were performed in May indicated that not all the poppet-type orifices had reseated.[9] On June 20 the No. 1 secondary sodium loop was drained and the steam generator allowed to cool; on June 23 the water-manifold cover was removed, and the poppet-type orifices were inspected. Small particles of scale had lodged between six of the orifices and downcomer tubes.

The water- and steam-manifold tube sheets of the No. 1 steam generator were bubble tested[11] in July while the unit was dismantled. No tube-to-shell-side leaks were discovered. Ultrasonic tests[12] on 11 of the steam-generator tubes gave no indication of tube-metal wastage. By the end of August, the No. 1 steam generator had been reassembled, and the loop was filled with sodium. The steam generator[13] was pressurized to 600 psig on September 10, and no indication of leaks was noted.

The No. 2 steam generator[9] remained inerted with nitrogen at 20 psig on the tube side and filled with 350°F sodium on the shell side throughout June.

On June 4 the No. 3 steam generator[9] was refilled with water at 600 psig to determine whether retorquing of the head bolts on the steam-manifold coverplate had eliminated the gasket leak. Again steam leakage occurred, and the water side was vented, purged, and inerted until the gasket seal could be replaced.

REFERENCES

1. Argonne National Laboratory, Reactor Development Program Progress Report, July 1969, USAEC Report ANL-7595, Aug. 25, 1969.
2. Argonne National Laboratory, Reactor Development Program Progress Report, August 1969, USAEC Report ANL-7606, Sept. 26, 1969.
3. Argonne National Laboratory, Reactor Development Program Progress Report, September 1969, USAEC Report ANL-7618, Oct. 27, 1969.
4. Argonne National Laboratory, Reactor Development Program Progress Report, October 1969, USAEC Report ANL-7632, Nov. 25, 1969.
5. Argonne National Laboratory, Reactor Development Program Progress Report, November 1969, USAEC Report ANL-7640, Dec. 31, 1969.
6. Argonne National Laboratory, Reactor Development Program Progress Report, December 1969, USAEC Report ANL-7655, Jan. 29, 1970.
7. R. E. Mueller, Compilation of Current Technical Experience at Enrico Fermi Atomic Power Plant, May 1969, USAEC Report APDA-CFE-33, Atomic Power Development Associates, Inc., October 1969.
8. Power Reactor Development Company, Enrico Fermi Atomic Power Plant Report for May 1969, Report DOCKET-50016-5.
9. R. E. Mueller, Compilation of Current Technical Experience at Enrico Fermi Atomic Power Plant, June 1969, USAEC Report APDA-CFE-34, Atomic Power Development Associates, Inc., October 1969.
10. Power Reactor Development Company, Enrico Fermi Atomic Power Plant Report for June 1969, USAEC Report DOCKET-50016-6.
11. Power Reactor Development Company, Enrico Fermi Atomic Power Plant Report for July 1969, USAEC Report DOCKET-50016-26.
12. Power Reactor Development Company, Enrico Fermi Atomic Power Plant Report for August 1969, USAEC Report DOCKET-50016-28.
13. Power Reactor Development Company, Enrico Fermi Atomic Power Plant Report for September 1969, USAEC Report DOCKET-50016-29.

Nuclear Science Abstracts

The U. S. Atomic Energy Commission, Division of Technical Information, publishes *Nuclear Science Abstracts (NSA)*, a semimonthly journal containing abstracts of the literature of nuclear science and engineering.

NSA covers (1) research reports of the U. S. Atomic Energy Commission and its contractors; (2) research reports of government agencies, universities, and industrial research organizations on a worldwide basis; and (3) translations, patents, books, and articles appearing in technical and scientific journals.

Complete indexes covering subject, author, source, and report number are included in each issue. These indexes are cumulated and sold separately.

Availability of NSA

SALE *NSA* is available on subscription from the Superintendent of Documents, U. S. Government Printing Office, Washington, D. C. 20402, at $42.00 per year for the semimonthly abstract issues and $38.00 per year for the cumulated-index issues. Subscriptions are postpaid within the United States, Canada, Mexico, and all Central and South American countries, except Argentina, Brazil, Guyana, French Guiana, Surinam, and British Honduras. Subscribers in these Central and South American countries, and in all other countries throughout the world, should remit $52.50 per year for subscriptions to semimonthly abstract issues and $47.50 per year for the cumulated-index issues. The single-copy price for the abstract issues is $1.75 postpaid, with this exception: Add one-fourth of $1.75 for mailing to the countries to which the $52.50 subscription rate applies.

EXCHANGE *NSA* is also available on an exchange basis to universities, research institutions, industrial firms, and publishers of scientific information. Inquiries should be directed to the Division of Technical Information Extension, U. S. Atomic Energy Commission, P. O. Box 62, Oak Ridge, Tennessee 37830.

TECHNICAL PROGRESS REVIEWS may be purchased from Superintendent of Documents, U. S. Government Printing Office, Washington, D. C. 20402. *Nuclear Safety* at $3.50 per year (six issues) for each subscription or $0.60 per issue; *Reactor Technology* at $3.00 per year (four issues) for each subscription or $0.75 per issue; *Isotopes and Radiation Technology* at $2.50 per year (four issues) or $0.70 per issue. The use of the order form below will facilitate the handling of your order.

POSTAGE AND REMITTANCE: Postpaid within the United States, Canada, Mexico, and all Central and South American countries except Argentina, Brazil, Guyana, French Guiana, Surinam, and British Honduras. For these Central and South American countries and all other countries: add, for each annual subscription, $1.00 for *Nuclear Safety* and $0.75 for each of the other journals; for single issues, add one-fourth of the single-issue price. Payment should be by check, money order, or document coupons, and MUST accompany order. Remittances from foreign countries should be made by international money order or draft on an American bank payable to the Superintendent of Documents or by UNESCO book coupons.

order form

SUPERINTENDENT OF DOCUMENTS
U. S. GOVERNMENT PRINTING OFFICE
WASHINGTON, D. C. 20402

Please send — 1, 2, or 3 years

- ☐ Isotopes and Radiation Technology _____
- ☐ Nuclear Safety _____
- ☐ Reactor Technology _____

Enclosed: document coupons ☐ check ☐ money order ☐

Charge: Superintendent of Documents No._____

SUPERINTENDENT OF DOCUMENTS
U. S. GOVERNMENT PRINTING OFFICE
WASHINGTON, D. C. 20402

(Print clearly)

_____
Name

_____
Street

_____
City, State, ZIP Code